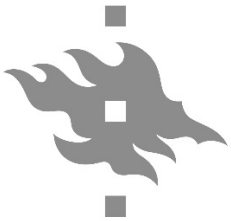

SUITABILITY OF KUUSIVAARA, SODANKYLÄ, CENTRAL FINNISH LAPLAND FOR HOSTING MINING INFRASTRUCTURE BASED ON ITS STRATIGRAPHY

Markus Valkama

03.12.2018

Master's thesis

Department of Geosciences and Geography

University of Helsinki

HELSINGIN YLIOPISTO
HELSINGFORS UNIVERSITET
UNIVERSITY OF HELSINKI

Tiedekunta/Osasto Fakultet/Sektion – Faculty Faculty of Science		Osasto/Institution– Department Department of Geosciences and Geography
Tekijä/Författare – Author Markus Timo Oskari Valkama		
Työn nimi / Arbetets titel – Title Suitability of Kuusivaara, Sodankylä, central Finnish Lapland for hosting mining infrastructure based on its stratigraphy		
Oppiaine /Läroämne – Subject Geology		
Työn laji/Arbetets art – Level Master's thesis	Aika/Datum – Month and year 12/2018	Sivumäärä/ Sidoantal – Number of pages 82

Tiivistelmä/Referat – Abstract

AA Sakatti Mining Oy is planning on utilising the Cu-Ni-PGE deposit discovered in 2009 in Sodankylä, central Finnish Lapland. Sediments of Kuusivaara hill and Porokodanjänkä mire were studied to find out their feasibility in regards to hosting mining infrastructure. Six test pits were excavated, fourteen soil samples analysed, and fifteen kilometres of ground penetrating radar profile was acquired. A GIS-based bedrock elevation model, a sediment thickness model and a peat thickness model were created. The bedrock and sediment thickness models were supplemented with data gathered in other relevant studies in the area to extend these models to cover Kenttäaapa mire north of Kuusivaara.

Local stratigraphy corresponds with typical stratigraphy of central Finnish Lapland. Two till beds with occasional, thin interlayers of sand blanket the central and eastern parts of the area. Their hydraulic conductivity is poor. Till thickness ranges from two to six metres. The flanks of the river Kitinen are covered with thick and permeable fluvial sediments. Peat thickness at Porokodanjänkä mire ranges from less than 0.5 metres to 5.4 metres. Mean sediment thickness, including peat thickness, is 5.5 metres. The mean peat thickness under Porokodanjänkä is 1.3 metres. The bedrock surface, especially under Porokodanjänkä mire shows frequent weathering. This is a typical phenomenon under the low-erosion regime of the ice divide zone. Maximum weathering depths were not clarified by this study.

The study area is mostly suitable for hosting mining infrastructure. Except under the old channel of river Kitinen, sedimentary units demonstrate poor hydraulic conductivity. There are no significant acquifers in the area. Full extent and depth of weathered bedrock must however be mapped before initiating construction of mining infrastructure. Weathered and fractured bedrock is significantly more permeable than crystalline bedrock. Such units must therefore be identified to understand local hydrology.

Avainsanat – Nyckelord – Keywords

EIA, GIS, GPR, Lapland, mine tailings, Sakatti, saprolite, stratigraphy, weathering

Säilytyspaikka – Förvaringställe – Where deposited

Muita tietoja – Övriga uppgifter – Additional information

3 Appendices

HELSINGIN YLIOPISTO
HELSINGFORS UNIVERSITET
UNIVERSITY OF HELSINKI

Tiedekunta/Osasto Fakultet/Sektion – Faculty Matemaattis-luonnontieteellinen tiedekunta	Osasto/Institution– Department Geotieteiden ja maantieteen osasto	
Tekijä/Författare – Author Markus Timo Oskari Valkama		
Työn nimi / Arbetets titel – Title Suitability of Kuusivaara, Sodankylä, central Finnish Lapland for hosting mining infrastructure based on its stratigraphy		
Oppiaine /Läroämne – Subject Geologia		
Työn laji/Arbetets art – Level Pro gradu	Aika/Datum – Month and year 12/2018	Sivumäärä/ Sidoantal – Number of pages 82

Tiivistelmä/Referat – Abstract

AA Sakatti Mining OY suunnittelee vuonna 2009 löytämänsä Cu-Ni-PGE-esiintymän hyödyntämistä Sodankylässä. Kitisen itäpuolisen Kuusivaaran ja Porokodanjängän maaperän soveltuvuutta kaivosinfrastruktuurin tarpeisiin tutkittiin. Maaperän rakenteen selvittämiseksi alueelle kaivettiin 6 koekuoppaa, otettiin 14 maanäytettä ja kerättiin 15 km maatutka-aineistoa. Kallion pinnan syvyydestä sekä sedimenttien ja suoalueen turpeen paksuudesta tehtiin GIS-pohjaiset mallit. Kallion syvyyden ja sedimenttien paksuuden malleja täydennettiin muissa tutkimuksissa kerätyllä aineistolla ja siten laajennettiin kattamaan Kuusivaaran pohjoispuoleinen Kenttäaapa.

Alueen maaperän kerrosjärjestys noudattaa Keski-Lapille tyypillistä stratigrafiaa. Kaksi moreenipatjaa satunnaisine ohuine välihiekkoineen peittävät alueen keski- ja itäosia. Niiden vedenjohtokyky on huono. Moreenin paksuus alueella on 2–6 metriä. Kitisen lähiympäristö on hyvin vettä läpäisevien, fluviaalisten sedimenttien peitossa. Porokodanjängällä turpeen paksuus vaihtelee alle 0,5 metristä 5,4 metriin. Keskimääräinen sedimenttien paksuus on 5,5 metriä sisältäen turpeen paksuuden. Turpeen keskimääräinen paksuus suoalueella on 1,3 metriä. Kallion pinta, etenkin suon alla, vaikuttaa suurilta osin rapautuneelta. Tämä on tyypillinen ilmiö jäänjakaja-alueen heikon kulutuksen vyöhykkeellä. Rapautuman syvyyttä ei tässä tutkimuksessa saatu selville.

Alue soveltuu pääosin kaivosinfrastruktuurin sijoittamiseen. Maaperän yksiköt Kitisen vanhaa uomaa lukuun ottamatta ovat heikosti vettä johtavia, eikä alueella ole merkittäviä pohjavesiesiintymiä. Rapautuneen kallioperän syvyys ja levinneisyys on kuitenkin selvitettävä ennen rakentamisen aloittamista. Rapautunut ja rakoileva kallioperä johtavat vettä huomattavasti kiteistä kallioperää paremmin, ja nämä yksiköt on tunnistettava alueen hydrologian ymmärtämiseksi.

Avainsanat – Nyckelord – Keywords

GIS, maatutka, rapauma, rikastushiekka, Sakatti, saproliitti, stratigrafia, YVA

Säilytyspaikka – Förvaringställe – Where deposited

Muita tietoja – Övriga uppgifter – Additional information

3 Liitettä.

Contents

1. INTRODUCTION

Mining operations have inevitable consequences on the environment. These effects begin at the ore exploration phase and continue through the mine construction and its ore production, and remain even after the mine's closure (Kauppila et al. eds. 2011). Influence stems not only from the ore deposit itself, transformation of land at the mining site, and explosives used in blasting, but also from the processing of the ore, its transport, and the storage of waste rock and mine tailings. These effects may have long-lasting consequences on local ecosystems and societies. The environmental impact assessment (EIA, Act 277/2017) is a legislative procedure aimed at promoting diligent mine planning and mining practices, proper informing of stakeholders during the founding of a mine, and mitigating the environmental impacts of a mine during every phase of its life cycle. In the course of the EIA all relevant aspects of natural and human environments are brought up, discussed and evaluated (Räisänen et al. 2015).

The major Ni-Cu-PGE sulphide deposit named Sakatti ore was found by AA Sakatti Mining Oy in 2009 in Sodankylä, central Finnish Lapland (Brownscombe et al. 2015). As the ore body is situated under the Natura 2000 designated and protected Viiankiaapa mire, special care is required in order to ensure the protected values of the mire system during exploration, evaluation and possible utilisation of the discovery. Mining refuse, such as tailings pose a well-known environmental risk in metal ore mining (e.g. Yuval and Oldenburg 1996, Kauppila et al., eds. 2011, Räisänen et al. 2015).

Quaternary development and sediments of the mine prospecting area have been studied and mapped (A. Åberg et al. 2017a) together with a baseline description of its hydrology and hydrogeology (S. Åberg et al. 2017). The purpose of this study is to extend the existing sedimentological model (A. Åberg et al. 2017a) southwards to cover the Kuusivaara area, which hosts one of the twelve possible sites for tailing disposal and other mining infrastructure of the planned future mine (Pöyry Finland Oy 2018). The aim is to provide up-to-date background information on thickness and quality of Quaternary sediments and their properties to support environmental assessment, evaluating and permitting procedures in the area. Fundamental understanding of local strata is essential before mining related construction begins. Important factors to consider are sediment permeability, bearing capacity, and their suitability for construction. Local watersheds and aquifers are closely connected with these factors. The bedrock in the region is known to be variably weathered (Hirvas 1991, Islam et al. 2002, Hall et al. 2015) and up to 100

metres in places (Rask & Lintinen 2001). Therefore, knowledge of bedrock weathering depth and intensity is a key element in understanding and evaluating local stratigraphy.

2. STUDY AREA AND GEOLOGICAL SETTING

The study area is located in Sodankylä municipality, central Finnish Lapland. It covers an area of approximately 20 km^2 at and around Kuusivaara hill, including the mires Porokodanjänkä to its south and Kenttäaapa to its north. It is delimited by Kitinen river in the west and Eliasaavankummut mound in the south. The eastern edge of the study area is delimited by Viiankiaapa mire and the southeastern edge by the northernmost reaches of Eliasaapa mire. Elevation ranges between 231 and 181 m a.s.l. The highest point is atop Kuusivaara hill and the lowest point is the water level of Kitinen river. An index map of the study area is presented in Figure 1, and a map of Kuusivaara and its surroundings are presented in Figure 2.

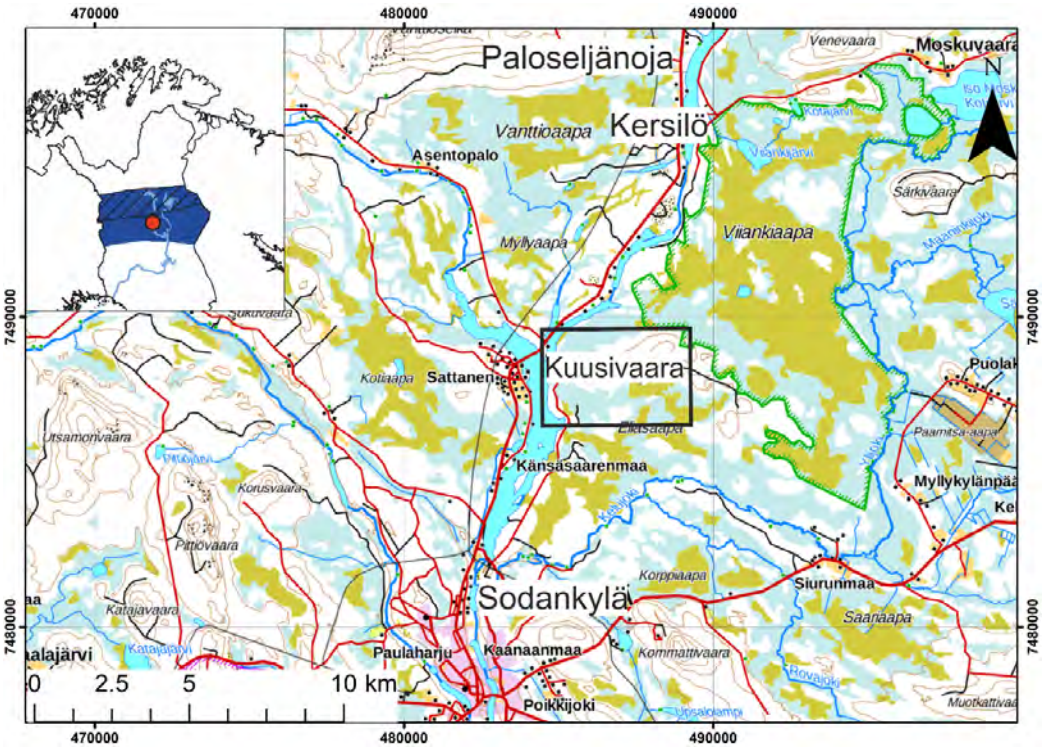

Figure 1. An index map of the study area. Limits of the study area are marked with the black rectangle. Location of Sodankylä within the ice divide zone (blue) is marked with a red spot in the embedded map of Lapland in the northwest corner. The bigger map © National Land Survey of Finland. Ice divide zone after Hirvas (1991) and Johansson et al. (2011), blue and hatched areas respectively. Country borders from gadm.org.

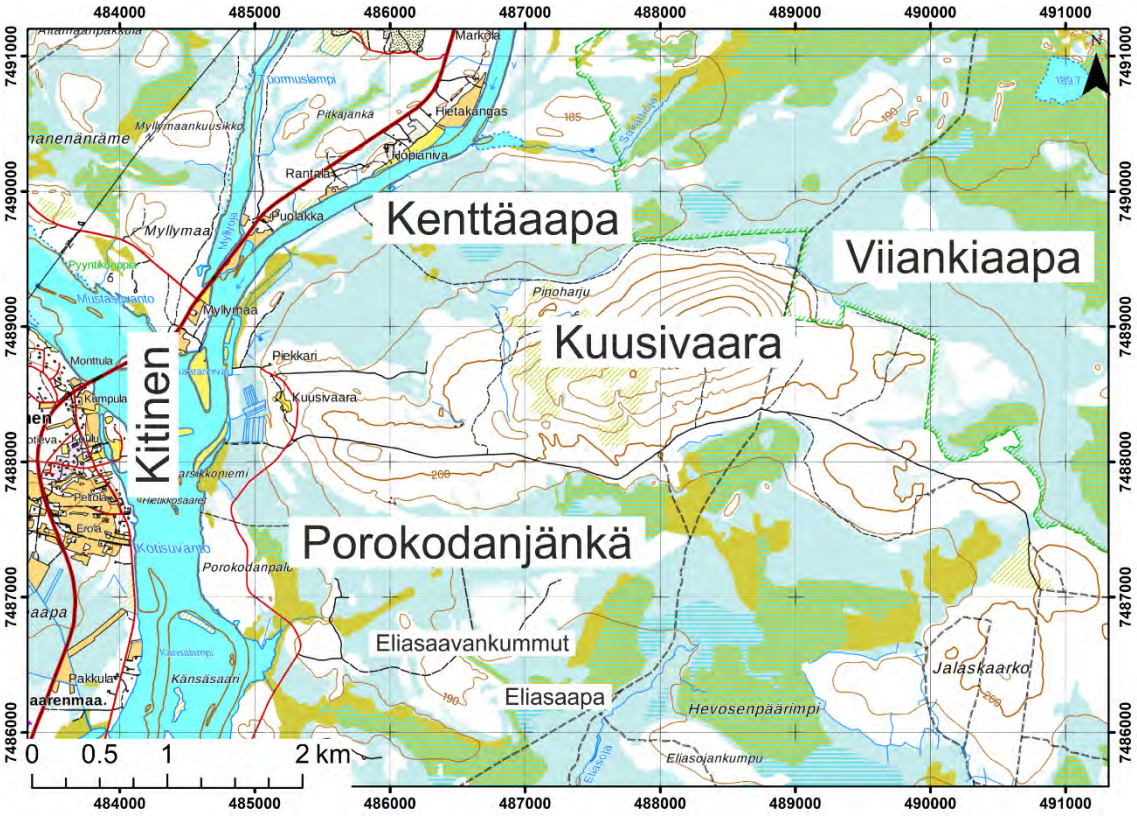

Figure 2. Location of the study area. © National Land Survey of Finland.

The study area is situated in the Central Lapland Greenstone Belt, characterised by Palaeoproterozoic metasediments (Hanski & Huhma 2005) and basic and ultrabasic volcanics (Hölttä et al. 2007, Brownscombe et al. 2015) with mafic and ultramafic intrusions (Lehtonen et al. 1998, Hölttä et al. 2007) as well as quartzites (Lehtonen et al. 1998). The Palaeoproterozoic evolution of the Central Lapland Greenstone Belt spans 600 Ma from circa 2.5 Ga BP to 1.9 Ga BP (Lehtonen et al. 1998). The Matarakoski formation surrounding the study area is characterised by phyllites and black schists (Törmänen et al. 2016). The summit of Kuusivaara hill is composed of picritic volcanic rock. Other, unspecified mafic volcanics and black schists dominate the rest of the area (Lehtonen et al. 1985).

Final deglaciation of the Scandinavian Ice Sheet began at the end moraines of the Younger Dryas circa 11.6 ka BP (Saarnisto and Saarinen 2001). In northern Finland ice retreated towards the south-southwest in the north, and towards northwest in the south (Johansson 2007). Retreating ice margin from the end moraines in Norway (Andersen et al. 1995) reached the area surrounding present day lake Inari by 10.8 ka BP (Kujansuu et

al. 1998) and Sodankylä by 10.4 ka BP (Johansson 2007). Glacial meltwaters filled the basin northeast of Sodankylä creating the Moskuvaara ice lake. The ice dammed lake covered more than 400 km^2, draining first towards Luiro valley in the northeast and later towards Orajärvi lake in the south through the Hirviäkuru gorge. As the glacier melted, draining direction shifted, and the water level altitude decreased gradually from its highest stand of 207 m a.s.l. to 195 m a.s.l. As ice margin withdrew from Kitinen valley, Moskujärvi ice lake was finally connected to the Ancylus lake. By this time water level had dropped to 186 m a.s.l. (Johansson 2005).

Quaternary deposits from the nearby Paloseljänoja 10 km to the north-northwest and Kersilö 10 km to the north have been described by Hirvas (1991) and A. Åberg et al. (2017a), respectively. Three till beds from different ice advances were identified at both locations. The topmost and middle tills of Paloseljänoja have been correlated with till beds II and III of Hirvas (1991), respectively. They have been extensively described from central Finnish Lapland (e.g. Hirvas et al. 1977, Aalto et al. 1992 Hirvas et al. 1994). The lowest till of Kersilö has been correlated with the till bed III. Till beds III and II were initially thought to represent Early and Middle Weichselian glaciations (Hirvas 1991, Aalto et al. 1992). Recent dating suggests, however, that they might represent different glaciations in different areas (Lunkka et al. 2015). Weathering of bedrock up to more than 100 metres have been described from several nearby sites (e.g. Rask & Lintinen 2001, Hall et al. 2015).

Maps of superficial deposits from the study area have been compiled by Väisänen & Maunu (2004) and later updated from LiDAR data by Räisänen (2014). The Kuusivaara hill and its vicinity is mostly covered by till and the surrounding lowlands by peat. Relatively small sand and gravel deposits are present in the Kitinen river valley to the west and northwest. Local bedrock outcrops are visible on the southern slope of Kuusivaara hill. An overview of the surficial deposits is presented in Figure 3.

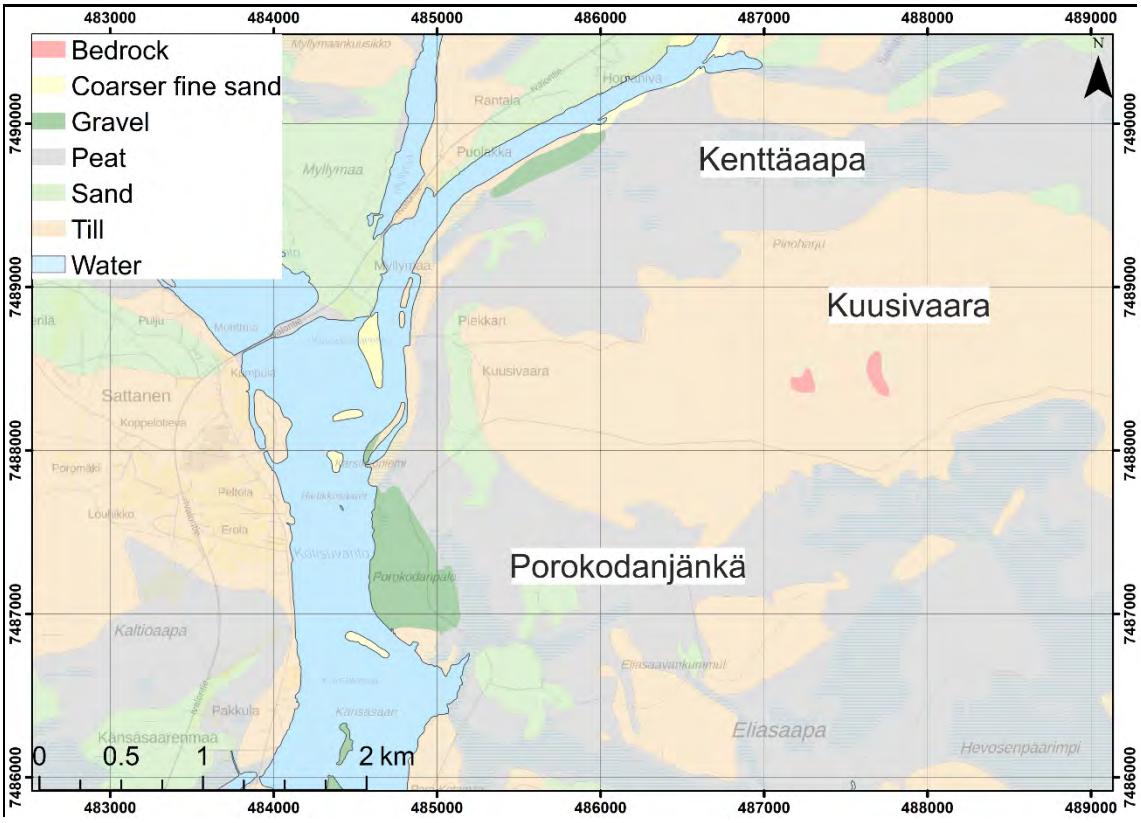

Figure 3. Superficial sediment map of Kuusivaara and its surroundings. © Geological Survey of Finland.

Over 25 % of Sodankylä municipality is covered by peat (Maunu and Virtanen 2005). Viiankiaapa mire directly adjacent to the study area has been largely protected by the national Mire Conservation Programme since 1988 and has later been included in the Natura 2000 conservation network.

3. MATERIALS AND METHODS

More than 15 km of GPR profile was acquired, and 6 test pits as well as 15 peat cores were examined in the vicinity of Kuusivaara hill 12.–22.9.2017. From the test pits, 14 sediment samples were gathered and their granulometric properties analysed. Additionally, over 5 km of GPR data from a third party expedition (Geofcon), 921 base of till (BOT) samples provided by AA Sakatti Mining Oy , nine targeting till geochemistry samples (Gustavsson 1979), eight boreholes and two groundwater monitoring wells (Anne Rautio, pers. comm. 2018) were utilised in this study. Data point locations are expressed in Figure 4.

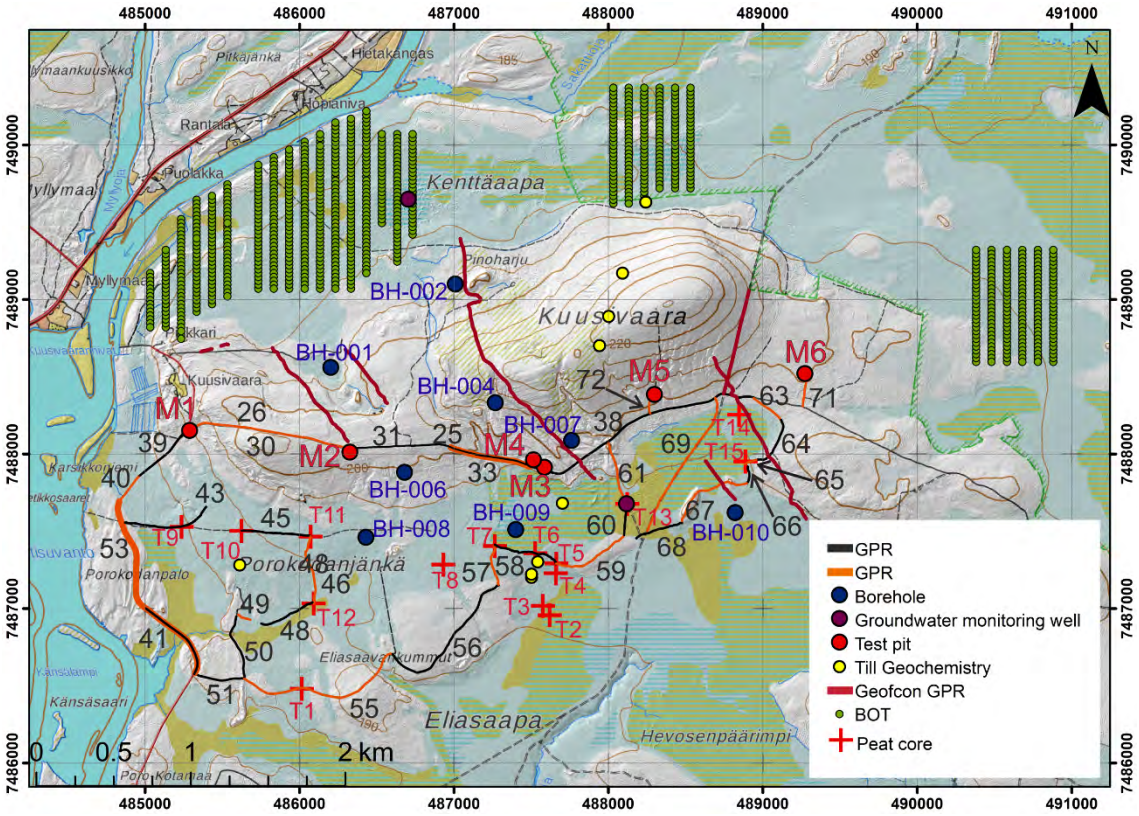

Figure 4. All data point locations used in this study. GPR profiles of this study are in both black and orange for better visibility. Thick orange lines indicate multiple GPR profiles over the same area. Base map © National Land Survey of Finland.

3.1. Peat Coring

Peat thickness was determined at fifteen coring sites. Peat cores were obtained with a Russian peat corer, three cm in diameter. This information was used as a reference in the processing and interpretation of GPR profiles. Coring locations were deliberately chosen to directly overlap with GPR acquisition whenever practical. Peat coring also served as reference for peat stratigraphy and identification of underlying clastic sediment. An example of peat cored at Porokodanjänkä mire is shown in Figure 5.

Figure 5. Russian peat corer with a sample of peat and underlying sediment at the eastern part of Porokodanjänkä mire. Photo by Markus Valkama.

3.2. Ground Penetrating Radar

15 kilometres and 59 profiles of GPR data was acquired on foot at Porokodanjänkä mire and surrounding gravel roads. The apparatus used was a manually operated Malå ProEx GPR system. Antennae with three frequencies were used: 50 MHz, 100 MHz and 250MHz. The first two were unshielded, and the third was a shielded antenna. The 50 MHz antenna was used to obtain bedrock contact data and sediment thickness whereas the 100 MHz and 250 MHz antennae were used to obtain bedrock contact data and stratigraphic data of sediments, as well as their thicknesses. Two antennae were used simultaneously for all GPR acquisition. Parameters used for the GPR acquisition are listed in Table 1.

Table 1. Parameters used in GPR acquisition.

Antenna Frequency (MHz)	Distance measurement	Sampling Frequency (MHz)	Time window (ns)	Point interval (m)	Time Interval (s)
50	Hipchain	500	1000	0.15	
100	Hipchain	1000	800	0.15	
250	Hipchain	2500	400	0.05	
50	Time triggering	500	1000		0.15
100	Time triggering	1000	800		0.15
250	Time triggering	2500	400		0.05

Five profiles were acquired using the hipchain option for distance measuring. The rest were acquired using time triggering. All GPR profiles were processed with Reflex-Win 7.5 software using the following steps:

1. Removing DC shift
2. Dewowing the data
3. Moving the start time
4. Adding a manual gain function in the vertical direction
5. Adding a bandpass filter
6. Using migration
7. Topographic correction when possible
8. Time-depth conversion

A velocity of 0.1 mns^{-1} was estimated for the radar signal for inorganic sediment (Neal 2004) and 0.034–0.4 mns^{-1} for peat. Velocity for peat was calculated from peat thickness, which was obtained from peat cores. Bedrock contact was identified from all GPR profiles if possible. Estimated bedrock contacts, overlying sediment and peat thickness were used to create a bedrock digital elevation model, a sediment thickness map and a peat thickness map, respectively. GPR acquisition in action is shown in Figure 6.

Figure 6. GPR acquisition with the 50 MHz and 100 MHz antennas at the west basin of Porokodanjänkä mire. Photo by Emilia Koivisto.

Sources of error are present in the acquisition, processing and interpretation stages of GPR data (Neal 2004). In this study, two major sources for error are identified. Time triggering assumes constant velocity from the GPR operator for data to be plotted correctly when it is being processed. A constant velocity could not be kept at all times. As velocities for other sediment than peat was a rough estimation, their thicknesses in GPR profiles are not always accurate.

3.3. Sedimentological Observations

Six test pits were excavated with a tractor to reconstruct a sedimentological model of the area and to support GPR interpretation. Lithofacies properties and structural features of the test pits were observed and sedimentological logs were compiled accordingly.

Fourteen sediment samples were collected for particle size analysis and one sample was collected for optically stimulated luminescence (OSL) dating.

3.4. Particle Size Analysis

Sediment samples were analysed for their hydraulic conductivity. Coarse (>0.063 mm) fraction and fine (<0.063 mm) fraction were analysed separately. Sorted sediments were dry sieved. Unsorted sediments were wet sieved to remove fine fraction and the remaining coarse fraction was then dry sieved. The mesh sizes used in sieving were: 8 mm, 4 mm, 2 mm, 1 mm, 0.5 mm, 0.250 mm, 0.125 mm, and 0.063 mm. The fine fractions from unsorted sediment samples were analysed with Malvern Mastersizer 2000 laser diffractometer.

The samples were soaked in 0.0134M sodium pyrophosphate ($Na_4P_2O_7$) prior to measurements and treated with the diffractometer's ultrasound probe for 30 seconds to avoid flocculation of grains. The medium used to transfer samples to be measured was water. The measurement settings were as follows: general purpose calculation model, measurement time 30 s, background time 15 s., pump speed 2100 revolutions per minute (rpm) and stirrer speed 550 rpm. The average values of three measurements per sample were used for further analyses.

The laser diffractometer downplays the proportion of clay fraction in samples. Therefore, one sample (M5N9) was also analysed with an areometer to find out its more accurate fines distribution. A calibration curve was plotted with particle sizes from the aerometer results on the x-axis and particle sizes from the diffractometer results on the y-axis. The equation for the curve is:

$$y = 0.7795x - 0.8275$$

where (y) is the estimated particle size for any given diffractometer percentage value and (x) is the particle size given by the diffractometer for said value. This graph is plotted in Figure 7.

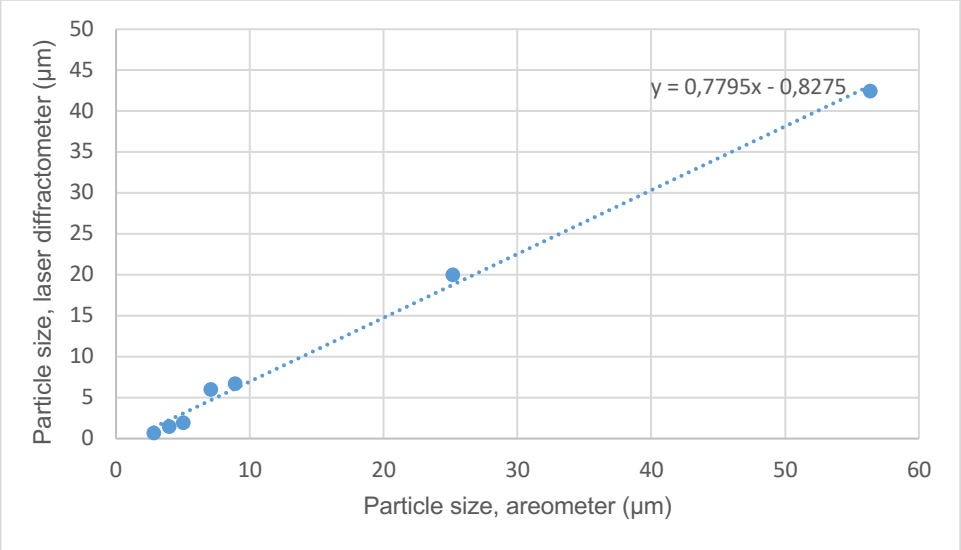

Figure 7. Corresponding particle size for equal, arbitrary percentage values at the particle size distribution curve for the aerometer (x-axis) and laser diffractometer (y-axis) are plotted. The trendline equation y = 0.7795x – 0.8275 *is used to convert all 14 laser diffractometer samples' results to better describe the real particle size distribution of these samples.*

As the diffractometer results use the same particle sizes for all samples, this equation was used to estimate the particle size for any given percentage of any given sample.

A cumulative particle size distribution (PSD) curve was compiled for each sediment sample. The Sauerbrei method (Vukovic and Soro 1992) was used to calculate the hydraulic conductivity of the samples. This method was chosen to make the results comparable with an earlier study from the area (S. Åberg et al. 2017). The formula for calculating the hydraulic conductivity is:

$$K = \frac{\beta g}{v} \frac{n^3}{(1-n)^2} d_{17}^2$$

where (K) (m/s) is the hydraulic conductivity, (β) is a dimensionless parameter, (g) is gravitational acceleration, (v) is the kinematic viscosity of water at 5 °C, (n) is the porosity of the medium, in this case 0.4 for sand or gravel and 0.3 for diamicton, and (d_{17}) is the grain size of the sample at 17% of its PSD curve.

The main sources for error in laser diffractometry are air bubbles in the medium used to transport the sample and poorly dispersed samples. In this study, both phenomena would exaggerate the significance of the coarser fraction of analysed samples.

3.5. Bedrock Elevation and Sediment Thickness Models

A GIS-based bedrock digital elevation model (DEM) and a sediment thickness model were generated to understand variations in bedrock depth and thickness of strata at Kuusivaara hill and its surroundings. All the relevant data concerning bedrock depth from this study as well as supplementary information concerning bedrock depth was collected and harmonized. They included data from this study's GPR acquisition and test pits, peat cores, heavy weight percussion drilling campaigns (BOT) by AA Sakatti mining Oy, targeting till geochemistry soil coring data (GTK) compiled for the Kersilö database (A. Åberg. et al. 2017a) and interpretations from an earlier GPR survey (Geofcon). In addition, ten hydro-borehole logs and two groundwater monitoring wells (Anne Rautio 2018, pers.comm) were used as references. These data points are shown in Figure 8.

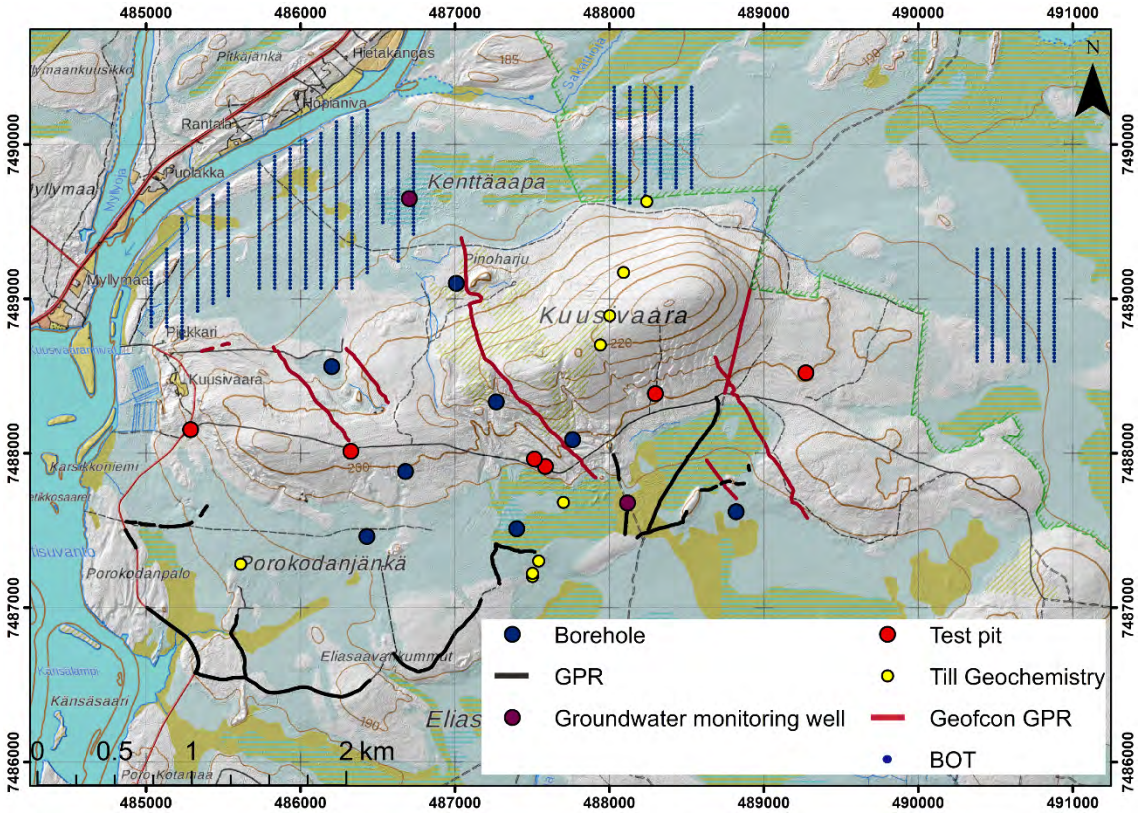

Figure 8. Data used for the Bedrock DEM and sediment thickness models. Base map © National Land Survey of Finland.

The sediment thickness model was initially generated with the Triangulated Irregular Network (TIN) interpolation method. The generated TIN model was converted to a raster and the raster indicating sediment thickness was subtracted from a Light Detection And Ranging Digital Elevation Model (LiDAR DEM) provided by the National Land Survey

of Finland to calculate the altitude variation of the bedrock. All modelling was done with ESRI ArcMap 10.3 software. A TIN model of peat thickness using ESRI ArcMap 10.3 software was generated to better understand peat thickness variation of Porokodanjänkä mire. Peat thickness data from 15 peat cores, 3 hydro-borehole logs and 13 GPR profiles were used as the input data.

4. RESULTS

4.1. Peat Cores

Peat thickness varies between 34 and 535 cm. Thick accumulation of peat is met at the west, east and south of Porokodanjänkä mire. Low peat accumulation is present mainly in the south and centre parts of the area (Figure 4). Basal sediment is most often gyttja and diamicton. The cores, their thicknesses and their basal sediments are summarised in Table 2.

Table 2. Peat thickness at each sampling site and sediment underlying peat.

Peat core	Thickness (cm)	Basal sediment
T1	45	Sand
T2	535	Gyttja/Sand/Diamicton
T3	370	Gyttja/Sand/Diamicton
T4	34	Diamicton
T5	94	Diamicton
T6	345	Gyttja/Sand/Diamicton
T7	300	Gyttja/Sand
T8	130	Gyttja/Sand
T9	530	Silt
T10	175	Gyttja/Sand
T11	< 50	Diamicton
T12	50	Diamicton
T13	340	Gyttja/Sand
T14	105	Gyttja/Diamicton
T15	200	Gyttja/Diamicton

4.2. Ground Penetrating Radar Profiles

GPR acquisition yielded information about the following subsurface characteristics: depth of bedrock surface, bedrock weathering, shape of Porokodanjänkä mire basin, thickness of sorted sediments, thickness of diamictons, and thickness of peat. All examined GPR profiles are displayed as the Appendix 1.

A thin veneer of diamicton covers the lower regions of Kuusivaara hill. It is typically a few metres in thickness at most. Underlying contacts are mostly uncertain. Profiles 30b (Figure 9) and 31a (Appendix 1) suggest that the bedrock is close to the ground surface, but it is disputable. Other clear sediment units are not recognised from GPR interpretation at this section of the studied area. To the east, diamicton thickness increases as seen in profile 38b (Appendix 1). Simultaneously, bedrock contacts become even more difficult to verify. Signal dissipation from several profiles in the area could suggest weathered bedrock above a more solid bedrock surface.

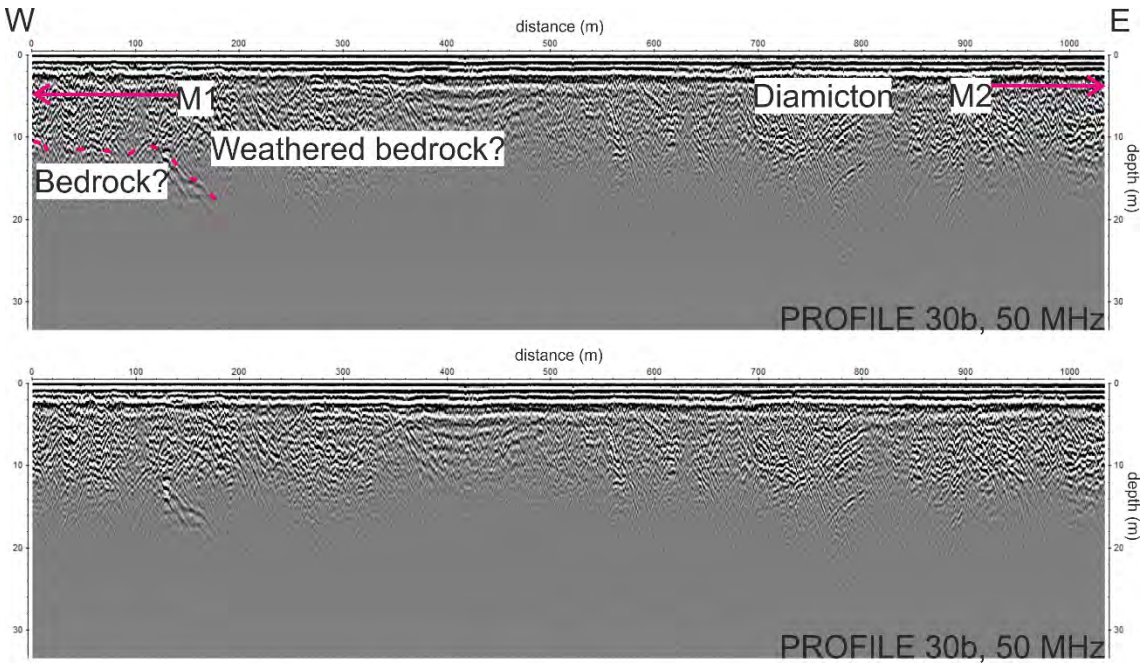

Figure 9. The GPR profile 30b shows a possible solid bedrock contact overlain by weathering products and diamicton. The arrows indicate locations and lower limits of test pits at the ends of the profile. The actual depth of both test pits is approximately two metres. The upper profile is interpreted and the lower profile is not. Location of the profile is shown in Figure 8.

Porokodanjänkä mire can be divided into an east and a west basin, both showing deep accumulation of peat. The east basin has a peat thickness maximum of over 4 metres. The bedrock contact is clearest at this edge of the study area, and can be verified from eight GPR profiles, such as profiles 60b (Appendix 1) and 69b (Figure 10). It is on average deeper than most of the study area, except for the proximity of river Kitinen. Sands and diamictons alternate as dominating inorganic sediment. Weathered material overlaying bedrock can be observed from several GPR profiles towards the centre of the basin. Weathering depths can exceed ten metres. Remnants of an old channel were observed in profile 69b. Possible bedrock fractures are interpreted from the easternmost profiles of 63 and 64 (Appendix 1).

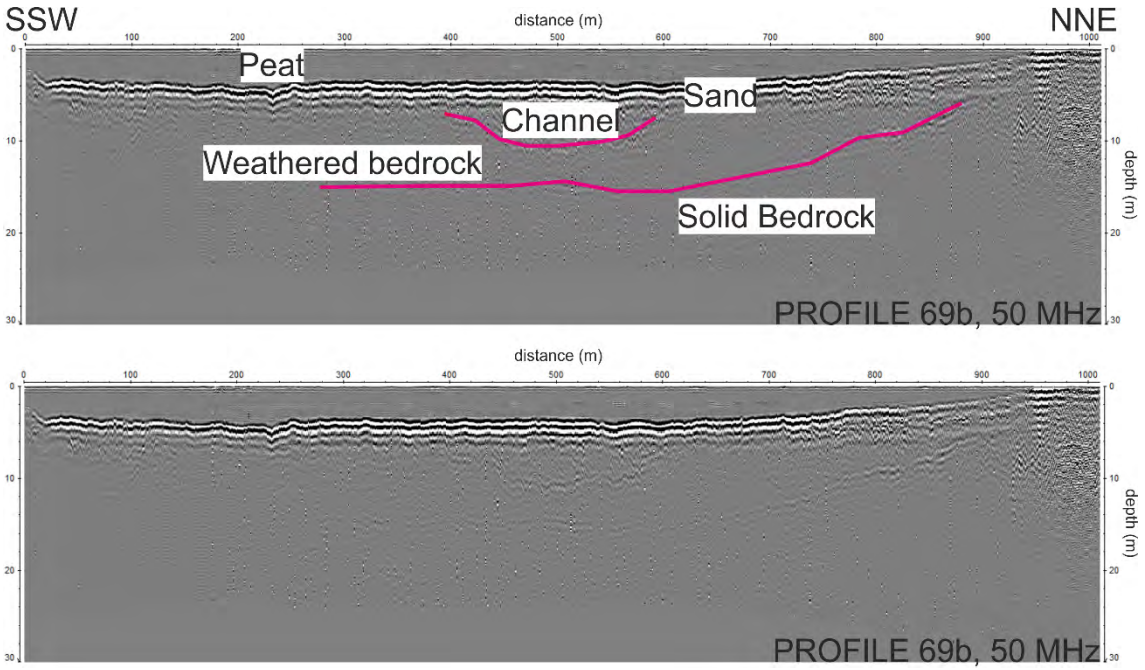

Figure 10. GPR profile 69b displays typical sequence of sediments in the central parts of the east basin of Porokodanjänkä mire. The upper profile is interpreted and the lower profile is not. Location of the profile is shown in Figure 8.

The west basin has a maximum peat thickness of almost 5.5 metres. Bedrock contact can be verified only from profile 43 (Figure 11), where its depth increases towards the west. It is 15 metres below ground surface at its deepest. Weathering of bedrock is unclear from profiles at the west basin. The proportion of diamicton in inorganic sediments is smaller than in the immediate surroundings of Kuusivaara hill. Sands dominate as the topmost

inorganic sediment in most of the GPR profiles from this area, as exemplified in profiles 43a (Figure 11) and 45a (Appendix 1). They are up to two metres in thickness.

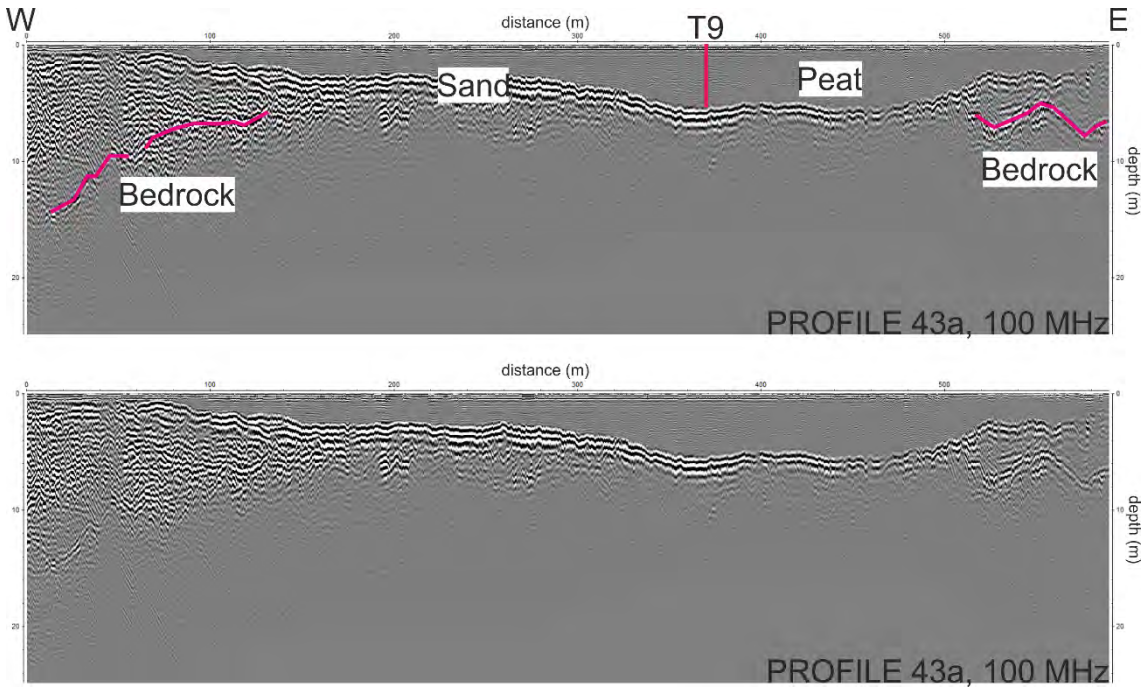

Figure 11. GPR profile 43a.The bedrock depth increases towards river Kitinen in the west. Relatively thin layers of sand underlay the peat. T9 marks location of a peat core used as reference data when calculating true peat depth for the profile. The upper profile is interpreted and the lower profile is not. Location of the profile is shown in Figure 8.

Fluvial deposits of sand or gravel are clearly visible in profiles from the west and southwest parts of the study area. This kind of deposition was interpreted from seven profiles. Bedrock contact was identified from five profiles in the west and southwest (profiles 50, 51 and 53) and from other two (profiles 55 and 56) around Eliasaavankummut to the south. The bedrock contact of profile 51a is shown in Figure 12. Although weathered bedrock cannot be identified, bedrock may be fractured as seen in profile 56a (Figure 13). Profiles 50, 53 and 55 are listed in the Appendix 1.

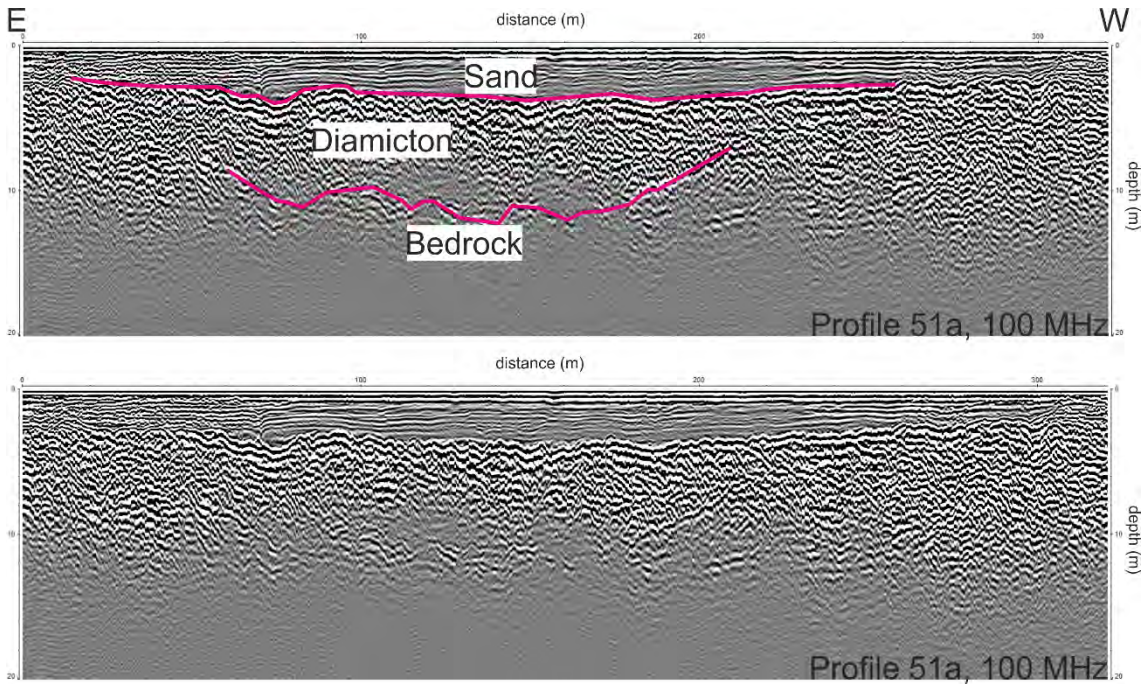

Figure 12. GPR profile 51. Diamicton and horizontal sands overlays bedrock, the contact of which is detectable for almost 150 metres. The upper profile is interpreted and the lower profile is not. Location of the profile is shown in Figure 8.

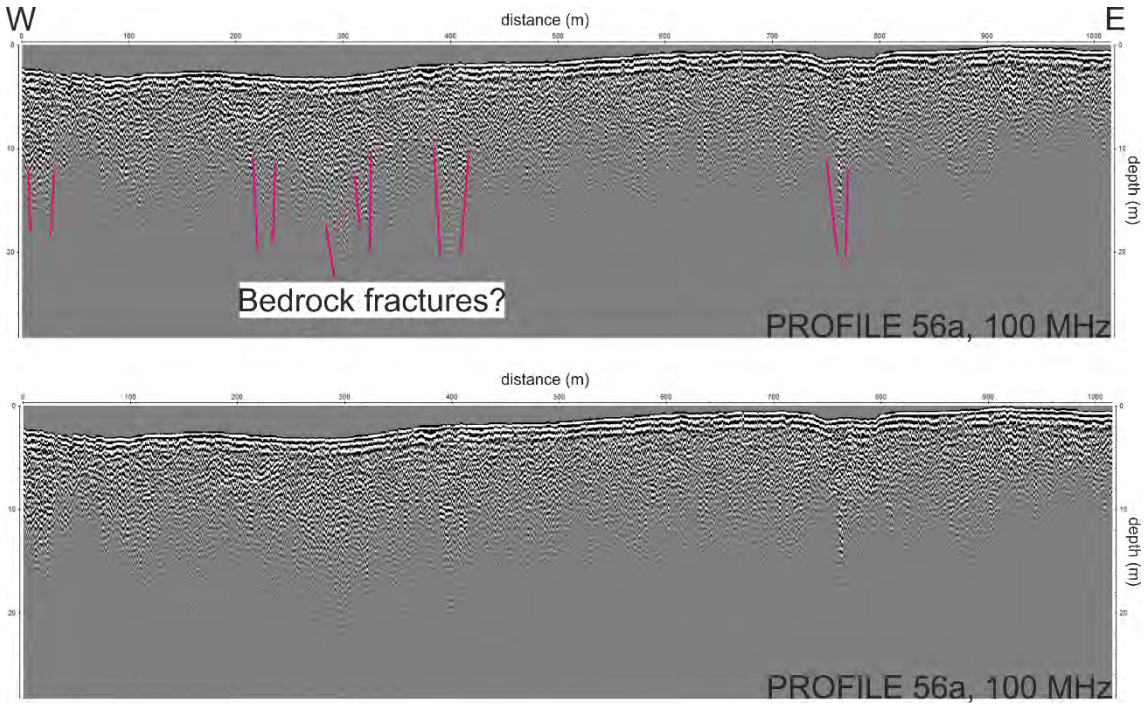

Figure 13. Vertical bedrock fractures could be interpreted from GPR signal suddenly penetrating deep for a very short time and then attenuating. The upper profile is interpreted and the lower profile is not. Location of the profile is shown in Figure 8.

4.3. Sedimentological Observations

The sediments at test pit M1 are 2.7 metres thick (Figure 14). They are underlain by blocky, fractured, weathered bedrock that is difficult to penetrate (Figure 15). Weathered bedrock is overlain by three lithofacies units. The lowermost unit is a diamicton 220 cm thick. At the bottom it is clast-supported and has a gravelly matrix with a reddish tint. It grades upwards into a loose, structureless, grey and sandy diamicton with a crude pebble pavement on top. The second unit is a 5 cm layer of silt. It is overlain by 45 cm of crudely stratified sand.

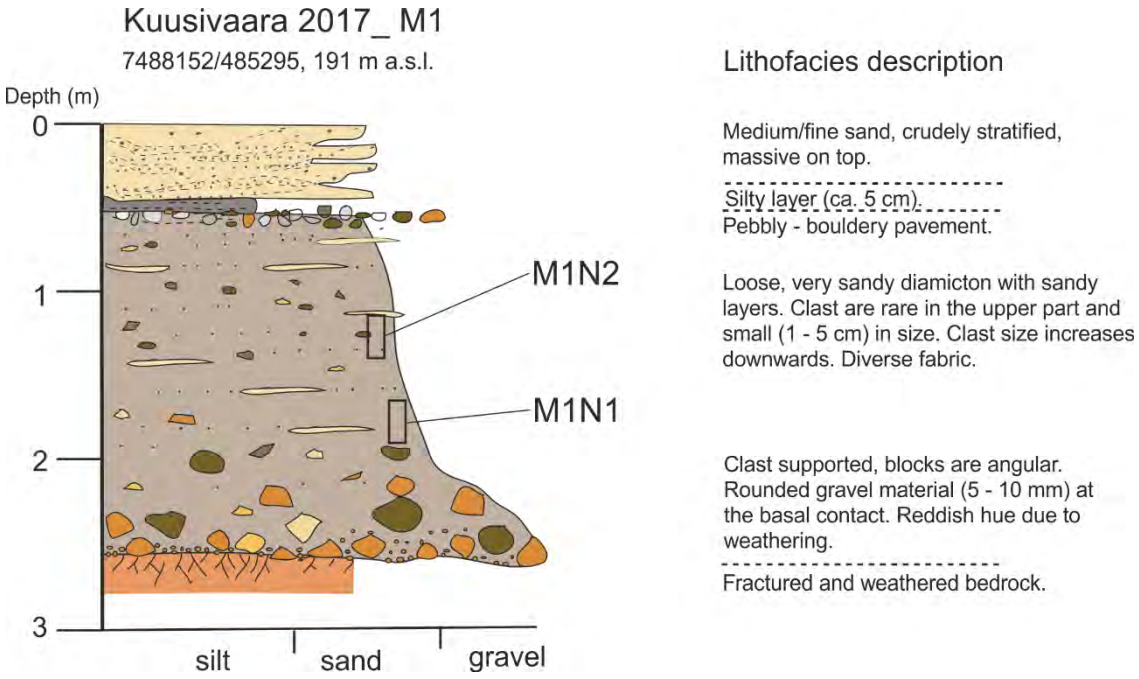

Figure 14. A sediment log of test pit M1. M1N1 and M1N2 refer to sediment samples taken at these depths. Dotted lines in the lithofacies description mark unit boundaries.

Figure 15. A mixture of diamicton and weathered bedrock at the bottom of test pit M1. Photo by Veli-Pekka Salonen.

The Sediments at test pit M2 are 2.1 metres thick (Figure 16). They are underlain by weathered and fractured bedrock not unlike that seen at test pit M1. Black schist is incorporated into the weathered bedrock. The bedrock is overlain by two distinct diamicton units separated by a boulder pavement. The lower diamicton is composed of chemically weathered clasts and a clayish matrix. The clasts show variable degrees of weathering, and fresh clasts are mostly absent. It has a reddish colour. The upper diamicton is very loose, grey, sandy and has horizontal stripes of sand. Clasts are small and rare, up to 5 cm in diameter (Figure 17).

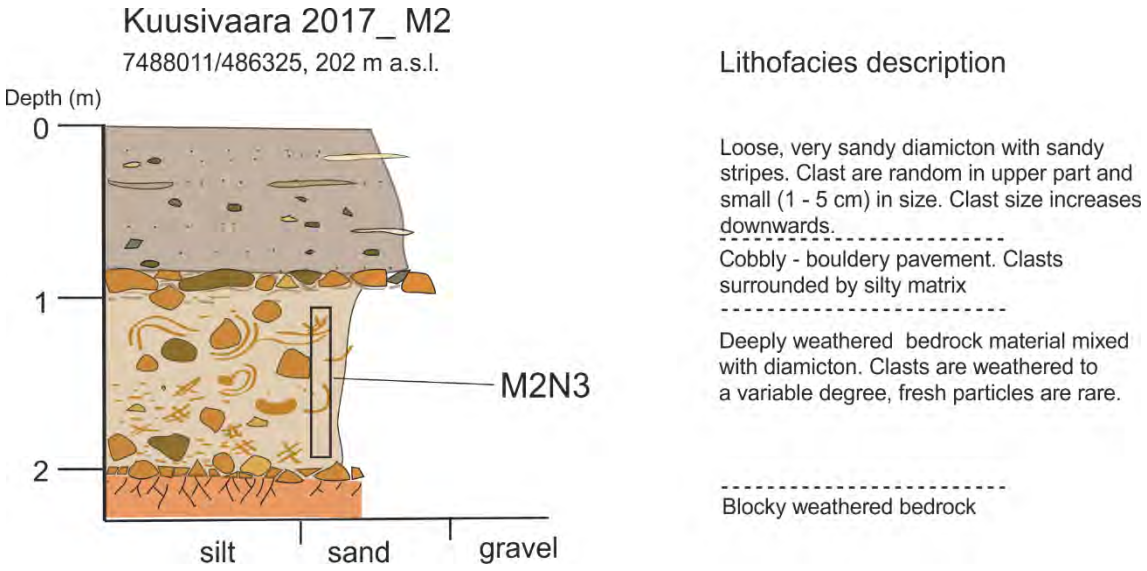

Figure 16. A sediment log of test pit M2. M2N3 refers to sediment sample taken at this depth. Dotted lines in the lithofacies description mark unit boundaries.

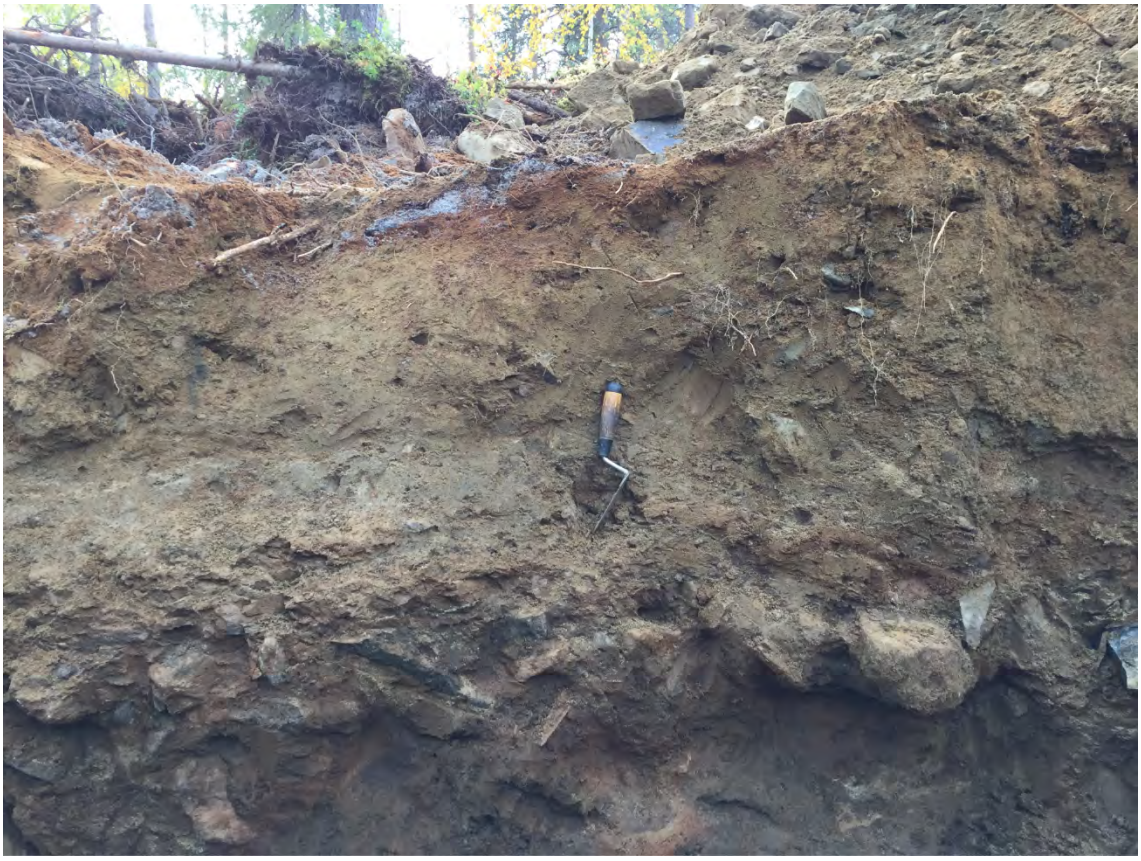

Figure 17. Upper diamicton and boulder pavement at test pit M2. Photo by Veli-Pekka Salonen.

The sediments at test pit M3 are 5.2 metres thick (Figure 18). They are divided into five units. The lowest unit is 40 cm of massive, grey, medium sand. It is saturated with water and its base is not seen. It is overlain by 160 cm of washed gravel with subhorizontal sandy layers (Figure 19). The gravelly unit changes gradationally into 220 cm of clast-supported, bouldery diamicton with prominent inverse grading. Clasts are angular and washed. The unit is crudely stratified. The fourth unit is 30 cm of normally graded, stratified sand. Its lower contact is sharp. The topmost unit is 70 cm of massive sand with scattered larger clasts.

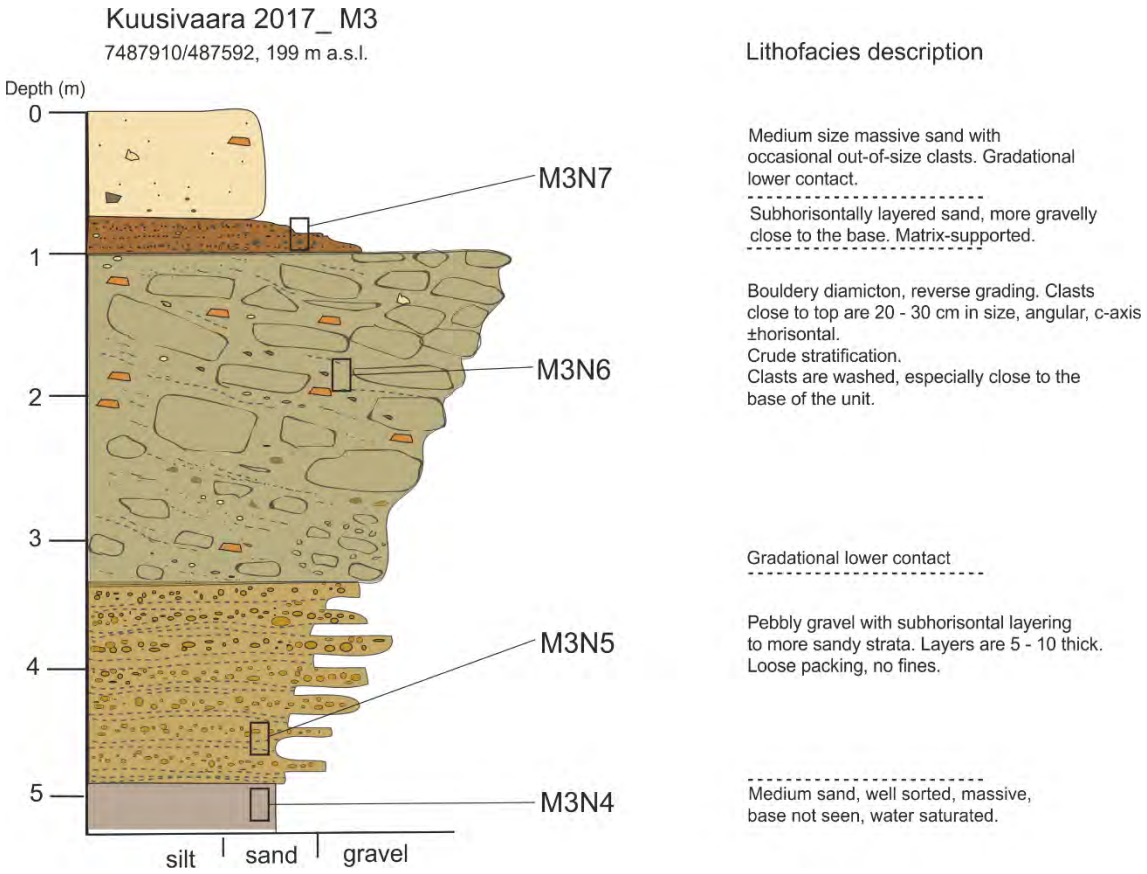

Figure 18. A sediment log of test pit M3. M3N4 to M3N7 refer to sediment samples taken at these depths. Dotted lines in the lithofacies description mark unit boundaries.

Figure 19. Pebbly gravel near the bottom of test pit M3. Photo by Veli-Pekka Salonen.

The test pit M4 consists of 150 cm of fine to medium sand (Figure 20). Water-saturated at the bottom, the base of the unit is not seen. The unit displays alternating horizontal layering and planar cross-bedding. Layers of dark and light coloured minerals alternate throughout the unit. Two ice-wedge remnants are found at the top of the section (Figure 21).

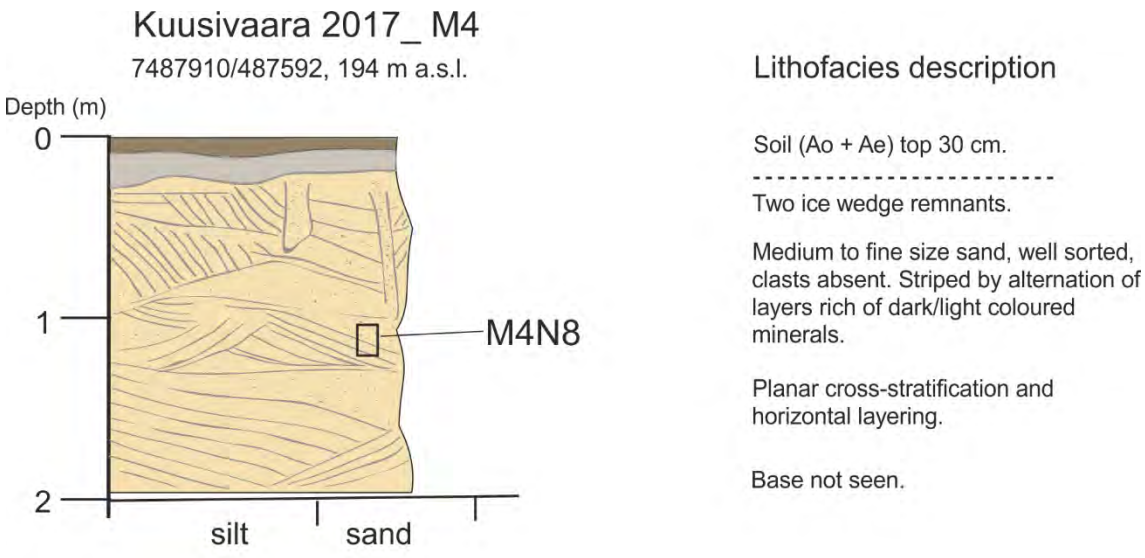

Figure 20. A sediment log of test pit M4. M4N8 refers to sediment sample taken at these depths. Dotted line in the lithofacies description mark unit boundaries and are not to scale.

Figure 21. Test pit M4 is sand from base to top.

The sediments at test pit M5 are 3.4 metres thick (Figure 22). They are divided into three units. The lowermost unit is a bimodal, reddish diamicton 60 cm thick. Its base is not seen. Clasts are abundant, rounded and approximately 5 cm in diameter. The unit is sharply overlain by 10 cm of massive grey sand with an oxidised upper surface. The topmost unit is a loose, stratified to massive, grey, sandy diamicton with solitary angular boulders. Clast content is low and clasts are generally smaller than 5 cm in diameter. The diamicton gradationally changes from stratified to massive from bottom to top.

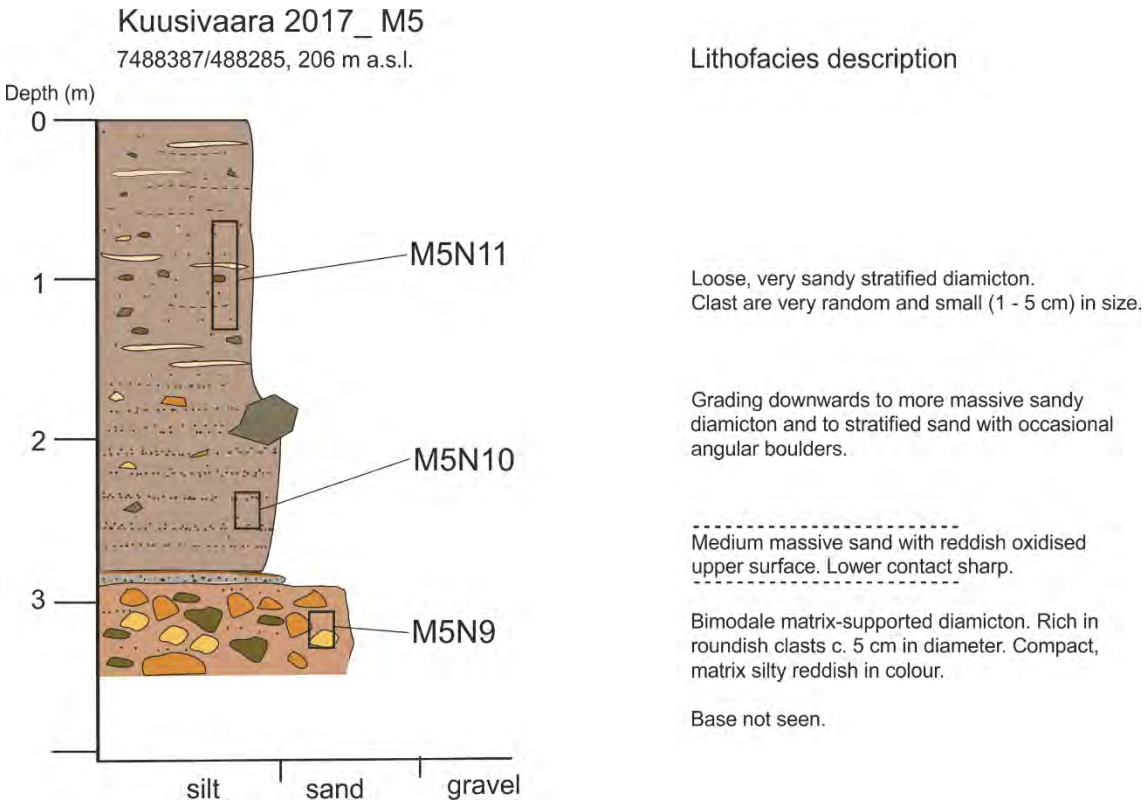

Figure 22. A sediment log of test pit M5. M5N9 toM5N11 refer to sediment samples taken at these depths. Dotted lines in the lithofacies description mark unit boundaries and are not to scale.

The Sediments at test pit M6 are 3 metres thick (Figure 23). They are divided into four units. The lowest unit is a compact, reddish, matrix-supported diamicton rich in clasts. It is 60 cm thick and its base is not seen. A fabric measurement was attempted but could not be completed. It suggests a NNW–SSE clast orientation. The unit is conformably overlain by 20 cm of massive, deformed, medium sand. Remnants of soil horizons are present in the unit (Figure 24). It was OSL-dated at 70 ± 14 ka old. It is sharply overlain by 190 cm

of loose, grey, very sandy diamicton with a very low clast content. Sandy stripes are present in the unit. The topmost unit is 30 cm of Bryales-dominated peat.

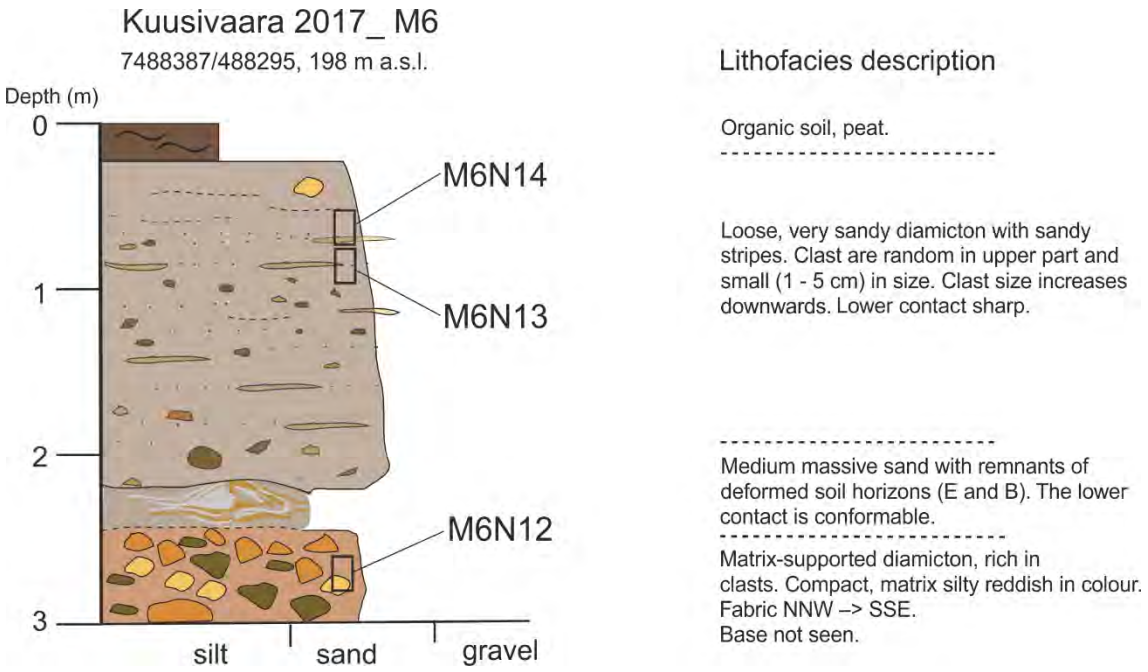

Figure 23. A sediment log of test pit M6. M6N12 to M6N14 refer to sediment samples taken at these depths. Dotted lines in the lithofacies description mark unit boundaries and are not to scale.

Figure 24. Palaeosoil between the till units at test pit M6. Photo by Veli-Pekka Salonen.

4.4. Particle Size Analysis

Out of 14 samples 10, represented unsorted clastic sediments, diamictons. Sample M3N5 and M3N6 were gravels and samples M3N4, M3N7 and M4N8 were sands. Hydraulic conductivity (K-value) of samples varied between $1.1*10^{-7}$ and $1*10^{-3}$ ms^{-1}. Diamicton samples showed K-values ranging from $1.1*10^{-7}$ to $7.9*10^{-6}$ ms^{-1} with an exception of the sample M3N6, having a K-value of $5.4*10^{-4}$ ms^{-1}. The gravel and sand samples had K-values of $1*10^{-3}$ and $7.9*10^{-5}$ ms^{-1}, respectively. All the calculated K-values are listed in Table 3. A full table with uniformity coefficients, kurtosis, sorting indices and skewness are presented as the Appendix 2. PSD curves are listed as the Appendix 3.

Table 3. Test pits, related samples, their classification and hydraulic conductivity. Test pit locations are shown in Figure 8.

Test pit	Sample ID	Depth (cm)	D_{50}	K-value (ms^{-1})	Soil type
1	M1N1	180–200	0.15	$8.1*10^{-7}$	Sandy diamicton
	M1N2	120–140	0.28	$2.6*10^{-6}$	Sandy diamicton
2	M2N3	110–190	0.04	$3.7*10^{-7}$	Silty diamicton
3	M3N4	490–510	0.21	$7.9*10^{-6}$	Medium sand
	M3N5	450–475	5.48	$1.0*10^{-3}$	Gravel
	M3N6	180–200	6.24	$5.4*10^{-4}$	Gravel
	M3N7	70–90	0.25	$3.6*10^{-6}$	Medium sand
4	M4N8	105–120	0.23	$7.9*10^{-5}$	Fine sand
5	M5N9	310–330	0.19	$5.5*10^{-7}$	Sandy diamicton
	M5N10	220–260	0.21	$3.7*10^{-6}$	Sandy diamicton
	M5N11	70–130	0.19	$6.5*10^{-7}$	Sandy diamicton
6	M6N12	260–280	0.21	$4.7*10^{-7}$	Sandy diamicton
	M6N13	80–100	0.17	$3.2*10^{-7}$	Sandy diamicton
	M6N14	60–80	0.09	$1.1*10^{-7}$	Sandy diamicton

4.5. Bedrock Elevation and Sediment Thickness Models

4.5.1. Bedrock Elevation Model

Bedrock elevation ranges between 162 m a.s.l. near river Kitinen in the southwest and 231 m a.s.l. on top of Kuusivaara hill. At and around Kuusivaara hill as well as most of Porokodanjänkä mire, bedrock roughly follows the surface topography. In the proximity of Kitinen river, bedrock elevation is frequently at 170–175 metres or less. Local bedrock depressions are likewise present under Porokodanjänkä mire and Kenttäaapa mire. No major faults or fracture zones can be interpreted from the model. The model is presented in Figure 25.

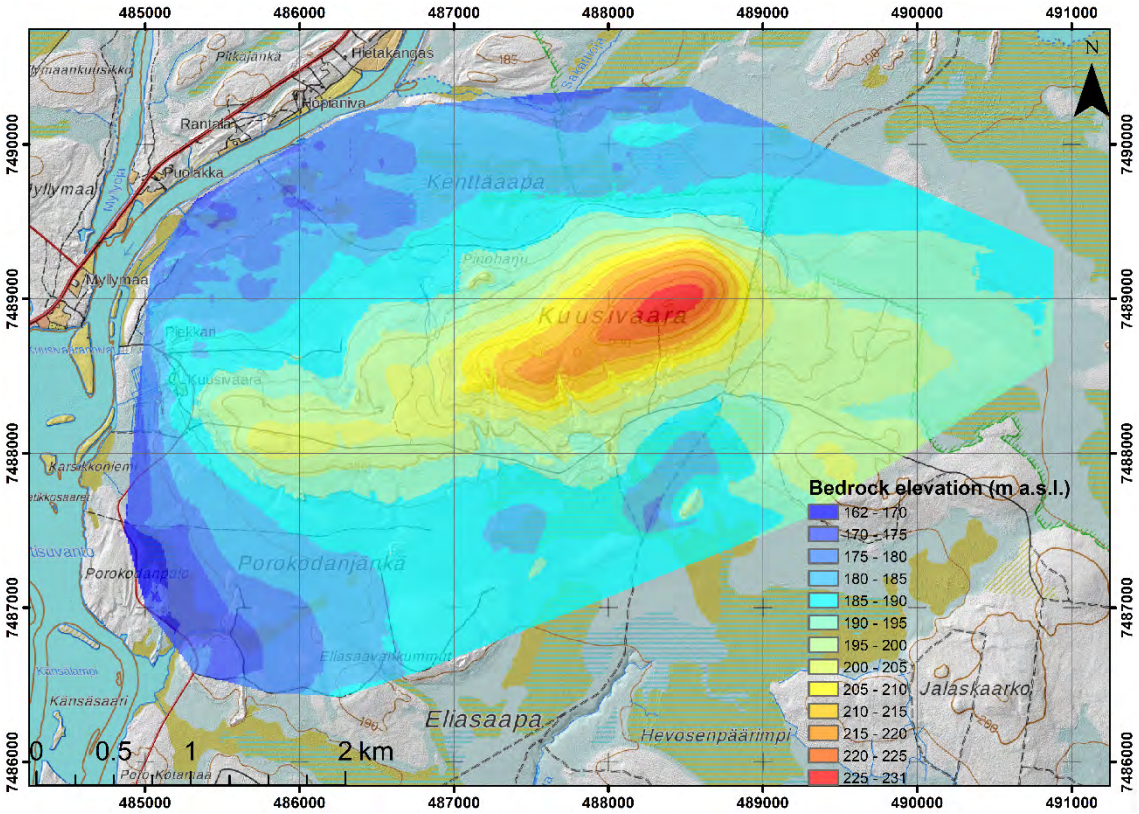

Figure 25. Bedrock DEM of Kuusivaara and its surroundings.

4.5.2. Sediment Thickness Model

The Sediment thickness model is presented in Figure 26. Sediment thickness represents the minimum depth of solid bedrock contact from the ground surface within the modelled area. In the model, sediment thickness varies between 0 and 21 metres with an average of 5.5 metres. Bedrock is at its deepest in Kitinen river valley in the west, where it in places descends to 20 metres or deeper from the ground surface. Other areas with deep bedrock contact are found beneath the eastern parts of Porokodanjänkä mire as well as Kenttäaapa mire. At Porokodanjänkä, bedrock is found below 16 metres at its deepest. The bedrock at Kenttäaapa is frequently located at 10 metres' depth or more. Areas covered by peat most commonly exhibit sediment thickness between 6 and 10 metres. Kuusivaara hill and its immediate surroundings exhibit thin cover of sediment up to 6 metres and frequently less than 2 metres in thickness.

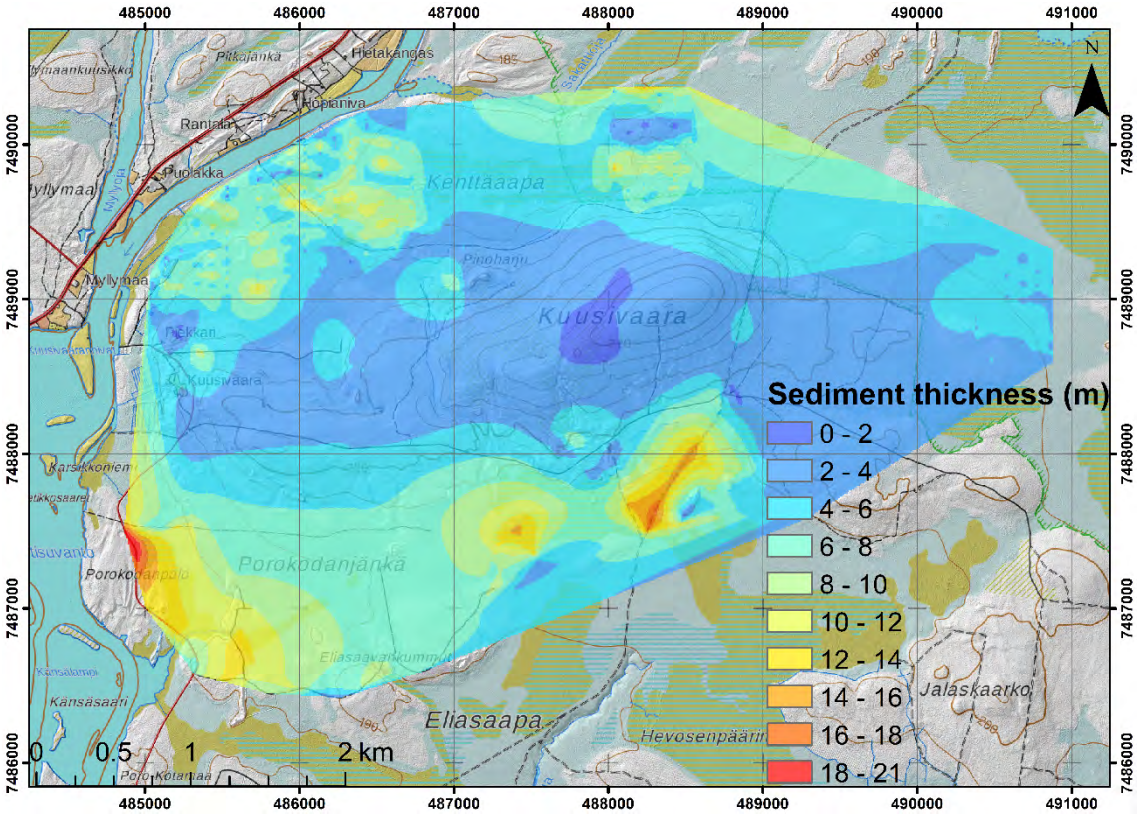

Figure 26. Sediment thickness model of Kuusivaara and its surroundings.

4.5.3. Peat Thickness Model

The peat thickness model is shown in Figure 27. There were a few areas with thick peat accumulations, such as the northern corner of Eliasaapa, and both easternmost and westernmost edges of Porokodanjänkä. In these areas peat was found to be more than four metres thick. For the most, however, peat cover was much thinner, around one to two, or even less than one metre thick. Mean peat thickness is 1.3 metres.

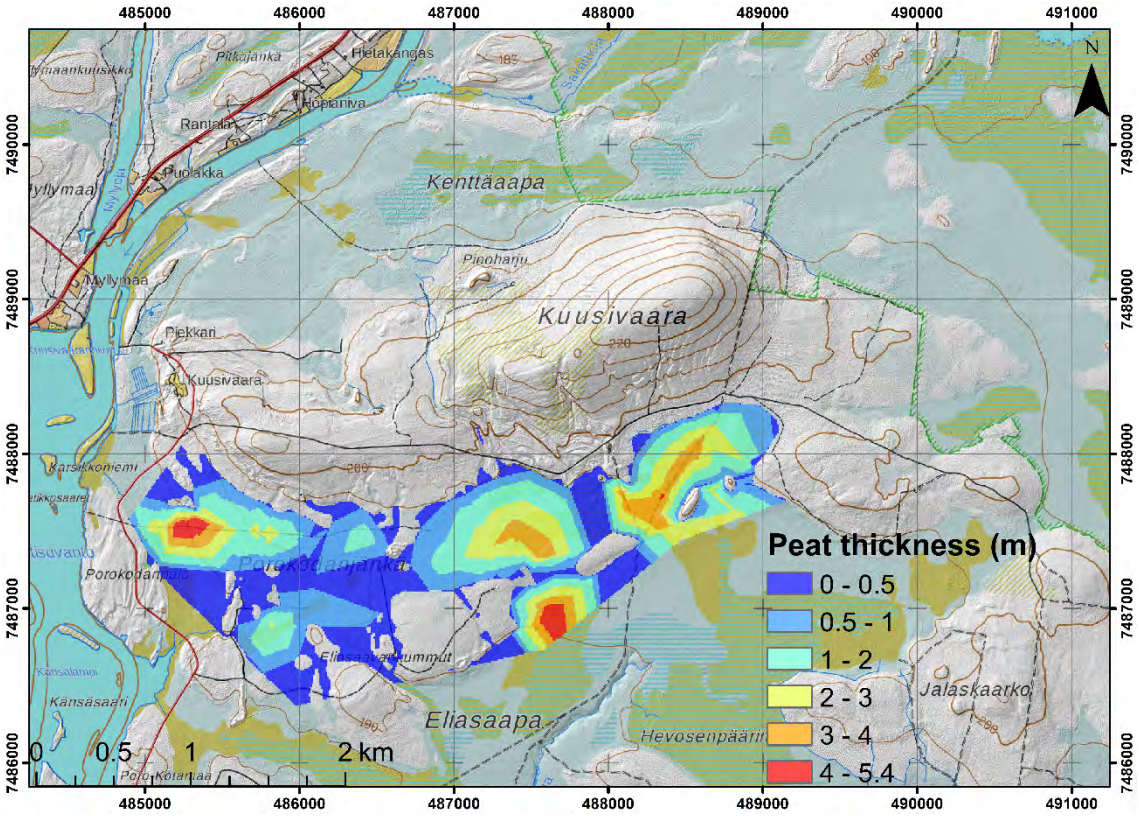

Figure 27. Peat thickness model of Porokodanjänkä mire.

5. DISCUSSION

5.1. Landscape Evolution of Kuusivaara Hill and Its Surroundings

The collation and interpretation of all the gathered and processed data supported with the peat thickness model, bedrock DEM and sediment thickness model helps to identify typical lithofacies combinations for different parts of the study area. In its simplest form, local strata are composed of weathered bedrock overlain by two units of till, thinly covered by topsoil. In places, a sandy interlayer separates the lower and upper till. Thin covers or small accumulations of wind-blown sands overlay the upper till throughout the study area. Local sand and gravel deposits characterise the westernmost parts of the area. Gravity flow deposits are observed on the southern slope of Kuusivaara hill. Extensive peat deposition blankets the lowlands in the north and south of the study area. A schematic overview of sediments along Kuusivaara road is presented in Figure 28.

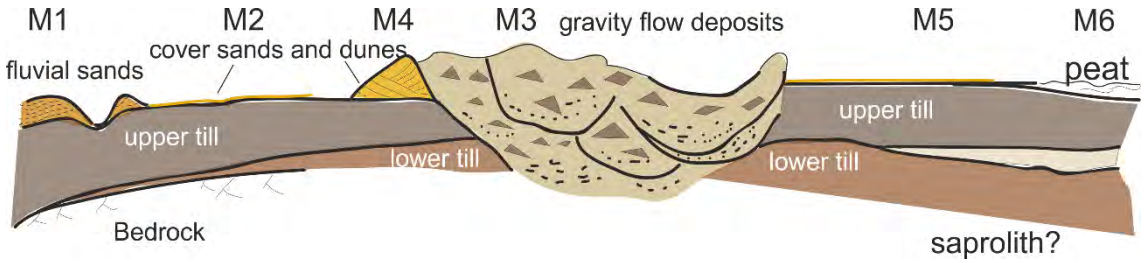

Figure 28. A Schematic drawing of sediments and test pit locations along Kuusivaara road. This illustration is not to scale.

The lower diamicton overlaying bedrock is reddish brown in colour, has high content of fines and seems to represent a mixture of saprolith, older sediments and glacially produced fresh debris (Figure 29). In test pit M6, the unit has a fabric indicating mean clast orientation at 310°, but the clastic orientation analysis could not be completed. The lower diamicton is interpreted to represent a glacial till, deposited by a glacier flowing from NE. Genetically the sediment can be classified as deformation or lodgment till. It can be correlated with the Early Weichselian lower till deposited by a glacier flowing here from the northwest, described in Kevitsa (Hirvas et al. 1994) and elsewhere in Sodankylä (Hirvas et al. 1977) as well as widely over most of Lapland (*e.g.* Hirvas 1991, Sarala 2005, Lunkka et al. 2015). It might also correlate with the lowest till observed in Kersilö, Sodankylä (A. Åberg et al. 2017a). Its hydraulic conductivity is very low, with K-values in the order of 10^{-7}–10^{-6} ms^{-1}. Abundant observations of an Early Weichselian till act as evidence for the weak erosional power of subsequent glacier advances.

Figure 29. The lower diamicton at test pit M2. The unit reaches from the bottom of the picture to the handle of the spatula. Notice the boulder pavement above the spatula.

The upper diamicton is loose, has a sandy matrix and low clast frequency. Its thickness varies between 80 and 275 cm. It displays abundant horizontal sand lenses, especially in the upper part of the unit (Figure 30). Fabric is poorly developed. The diamicton can be interpreted to represent glacial till, deposited by subglacial melt-out. Based on its position and properties, it correlates with the Late Weichselian upper till observed in Kevitsa (Hirvas et al. 1994) and with the melt-out till described in Kärväsniemi (A. Åberg et al. 2017a). Like the lower till bed, this unit has been described in most of Lapland (*e.g.* Peuraniemi 1989, Hirvas 1991, Sutinen 1992). The hydraulic conductivity of the upper till is very low, with K-values in the order of 10^{-7}–10^{-6} ms^{-1}.

A layer of sand between the two till units was described at test pits M5 and M6. Early to Middle Weichselian (70 ± 14 ka BP, MIS 5a to MIS 4) age was obtained for it by OSL dating. An analogous succession of two tills with a sandy interlayer has been described from Kärväsniemi, Sodankylä (A. Åberg et al. 2017b), indicating similar age (67–79 ka BP) of deposition during an ice-free event. Interstadial deposits from MIS 5a to MIS 4

have likewise been dated elsewhere in Lapland, for example at Sokli, Savukoski (Helmens et al. 2007) and Rautuvaara, Kolari (Lunkka et al. 2015).

Figure 30. Upper diamicton at test pit M5.

Till stratigraphy relies heavily on test pit data. Contact of till and fractured bedrock is difficult to ascertain from GPR profiles as illustrated earlier in Figure 9. Profiles that showed no clear bedrock contact or internal structures or lacked sufficient reference data from peat coring or test pits yielded the most unreliable data for interpretation, as illustrated in Figure 31. This profile lacks any reference data, and in no parts of the profile are clear signs of internal structure or bedrock contact present.

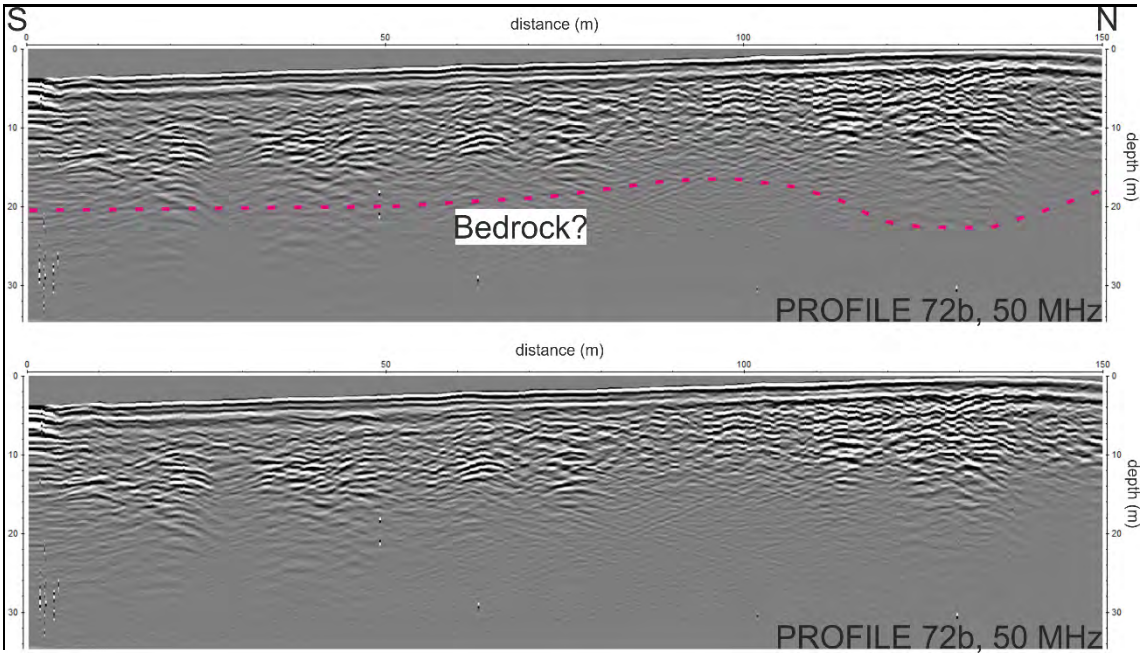

Figure 31. Structures and contacts are difficult to interpret from GPR profile 72. The upper profile is interpreted and the lower profile is not. Location of the profile is shown in Figure 8.

Ancient fluvial action at the flanks of Kitinen is attested by abundant deposition of sand and gravel. Sand and gravel beds spanning several hundred metres from the western and southwestern parts of the study area are described in five GPR profiles of this study, three of which are presented in Figure 32. These units may have been deposited in Kitinen river taking a wider or a different course compared with today. Similar deposition in glacifluvial environments has been interpreted from GPR data by *e.g.* van Overmeeren (1998) and Vandenberghe and van Overmeeren (1999). Channels running towards Kitinen river were observed at location, and are presented in GPR profiles 40 (Appendix 1) and 53 (Figure 33). The Kuusivaara road, along which the aforementioned profiles were acquired, has altered local hydrology and thus these channels may not be presently active.

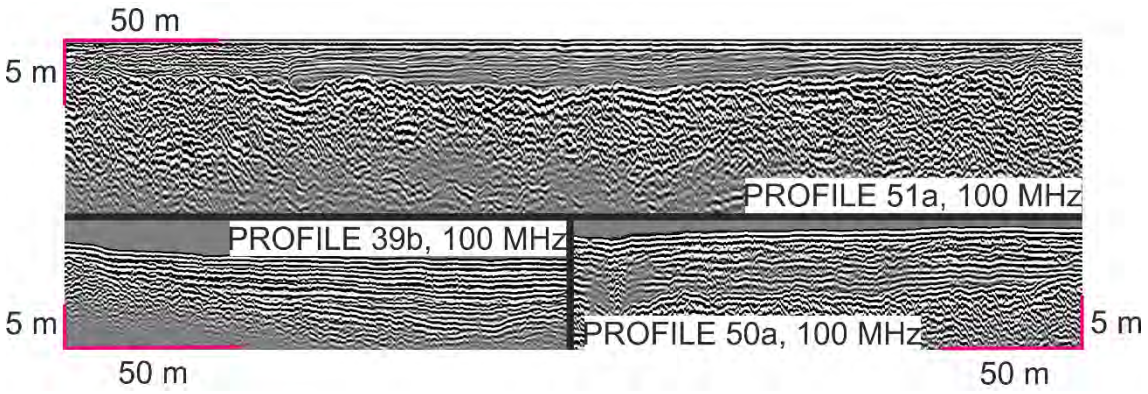

Figure 32. Horizontal deposition is evident from GPR profiles 39, 50 and 51. The vertical scale might be exaggerated. If the units are water saturated, the used velocity for GPR signal is most likely too high, and the thickness of the units are overestimated. The upper profile is interpreted and the lower profile is not. Location of the profile is shown in Figure 8.

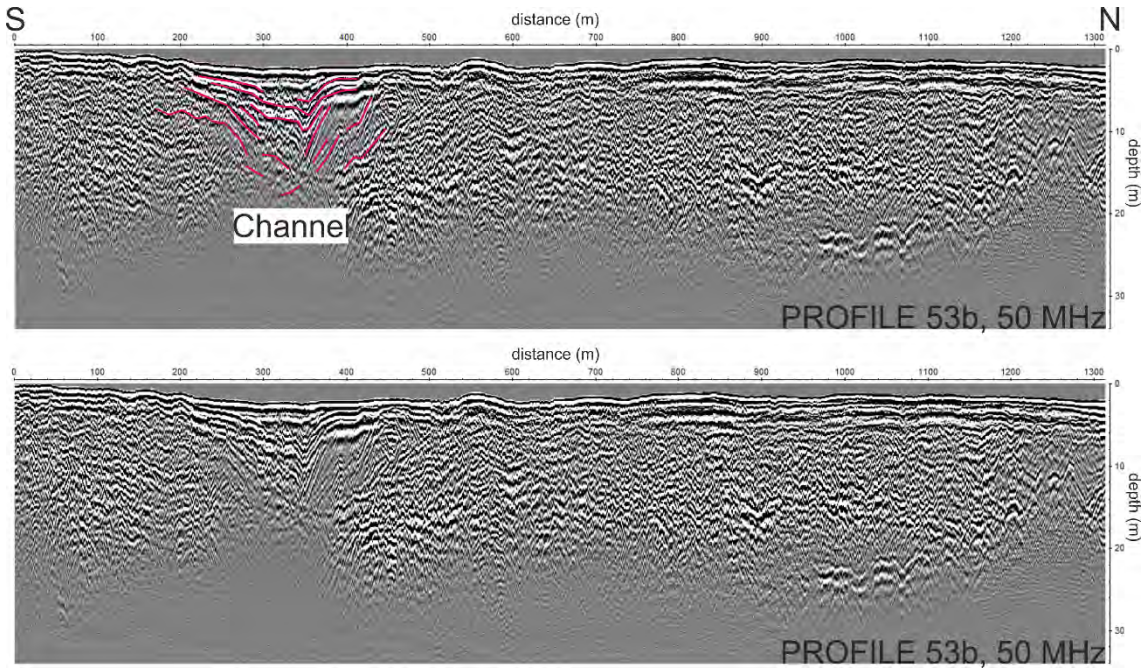

Figure 33. Several channels running towards river Kitinen are interpreted in the west of the study area. The most prominent of them is shown in the image above. The upper profile is interpreted and the lower profile is not. Location of the profile is shown in Figure 8.

Abundant, yet relatively thin cover sands and dunes indicates the beginning of terrestrial sedimentation in harsh windy environments with limited coverage of vegetation (Kasse 2002). A sample from the dune sand of test pit M4 shows low hydraulic conductivity, with a K-value in the order of 10^{-5} ms^{-1}. Aeolian sands have been described in recently deglaciated environments in both GPR (van Overmeeren 1998, Pedersen and Clemmensen 2005) and sedimentology related literature (*e.g.* Kolstrup and Jørgensen

1982, Schwan 1986, Kasse and Bohncke 1992, Kasse 2002). At Porokodanjänkä, the presence of sand is evident from several GPR profiles, such as profile 68a (Figure 34), but they are obscured by peat coverage. Therefore, the environment in which they were deposited is uncertain. They may be cover sands as elsewhere in the study area, or alternatively they may have been deposited in the lacustrine environment of Moskujärvi ice lake or Ancylus Lake. The thickness of these sands as inferred from GPR imagery is a couple of metres. This may be an overestimation. Literature suggests electromagnetic wave velocity for saturated sands is 0.06 ms^{-1} (Davis and Annan 1989, Neal 2004). Velocity used in this study was 0.1ms^{-1}. As depth scale of GPR profiles is directly calculated from the time for the GPR apparatus to detect signal reflection, scaled depths are directly proportional to velocity estimation (Annan 1989). In this case, the two-metre thick cover sands of profile 68 might be estimated as almost twice as thick as they should be. Unsaturated sands typically have velocities in the range of 0.09−0.13 ms^{-1} (Neal 2004). Therefore their thickness in GPR profiles is more precisely controlled. More exact information on groundwater levels would be needed to determine accurate thickness of sand deposits in GPR profiles, except those acquired at Porokodanjänkä mire and therefore with more certainty being fully saturated.

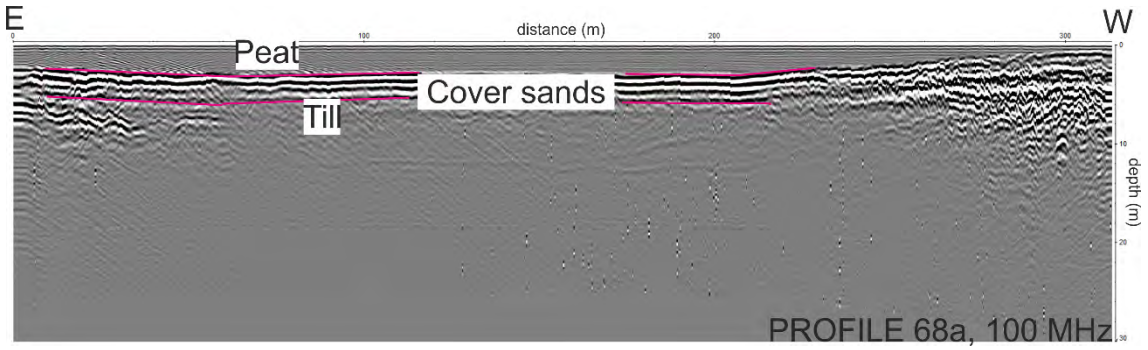

Figure 34. Cover sands resting on till under peat at the east basin of Porokodanjänkä mire. The upper profile is interpreted and the lower profile is not. Location of the profile is shown in Figure 8.

Test pit observations and associated morphological features of the nearby Rytikuru gorge supplemented with LiDAR image analysis indicate flow of sediment on the slopes of Kuusivaara. The affected area spans tens of hectares. The clast-rich diamicton with reverse grading that dominates test pit M3 is interpreted to represent a gravity flow deposit, triggered by deglaciation and unstability of water saturated, poorly compacted

till (Figure 35). These deposits presumably evacuated to the emptying Moskujärvi ice lake, as it was connected to Ancylus Lake. Gravity flows and related deposition of coarse-grained diamictons are a common occurrence in glacial environments (*e.g.* Eyles 1987, Eyles and Kocsis 1988, Benn and Evans 1998). The bouldery diamicton of test pit M3 is the only sample showing good permeability, with a K-value in the order of 10^{-3} ms^{-1}.

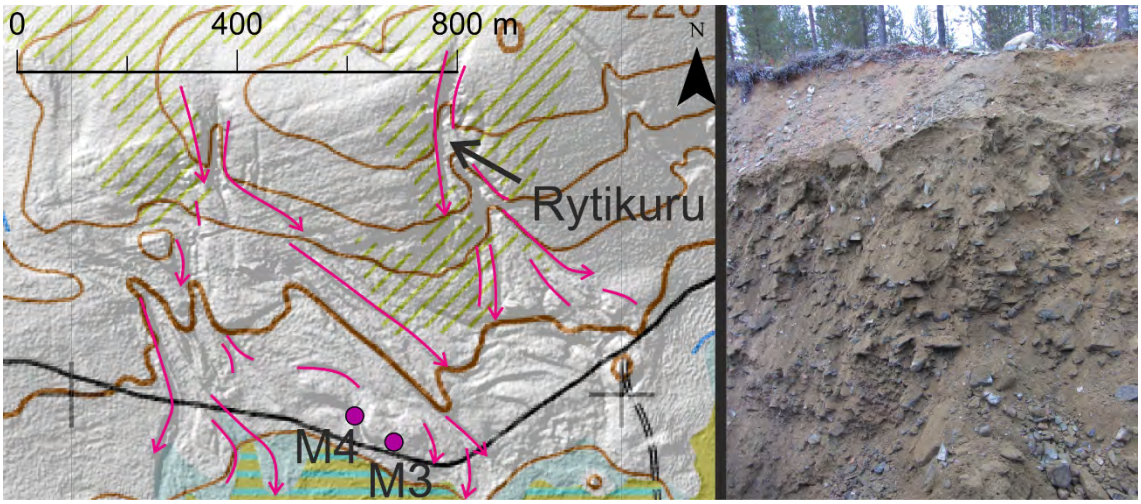

Figure 35. Depressions formed in the aftermath of gravity flows at the southern slope of Kuusivaara (left) and a gravity flow deposit at test pit M3 (right). The black line marks Kuusivaara road. Map © National Land Survey of Finland. Photo by Veli-Pekka Salonen.

As the data coverage was not dense enough to exhaustively cover such a large area as Porokodanjänkä, the interpolation of the peat thickness model is tentative. Even so, peat thickness seems to have certain systematic spatial variation and correlation with bedrock elevation. Thickest peat accumulation is found where bedrock levels descend, such as east and west Porokodanjänkä mire basin. The southern part of the model towards Eliaspaapa mire suggests wide areas of peat accumulation over relatively high bedrock elevation. The bedrock elevation modelled here is possibly flawed. Data coverage was too sparse to accurately model this part of the area.

In nine out of 15 peat cores, a layer of gyttja underlies peat, suggesting freshwater sedimentation before the mire stage. In eight cores the layer was ten centimetres thick or fewer. Only in core T3 a markedly thicker, 45 cm gyttja layer was described. At six coring sites peat was underlain by sand or diamicton. Annual sedimentation rate of gyttja is several millimetres (Gąsiorowski 2008). Thus, peat accumulation at most of

Porokodanjänkä began after a few dozen years as overgrowth of a shallow body of water, or directly after deglaciation on top of clastic sediments. Aapamire complexes occupying lowlands (Lappalainen 1970) started to form directly after deglaciation in Lapland, roughly 10.5 ka BP (Mäkilä et al. 2013). Viiankiaapa mire adjacent to the study area started to develop as waters from Kitinen river flooded the area between 10200 and 9700 years BP (Suonperä 2016).

The Porokodanjänkä mire cannot be considered pristine. An artificial ditch spanning more than one metre has been dug from west to east at the north boundary of Porokodanjänkä mire. Several other ditches have been dug into the west basin of the mire. Mire draining significantly increases surface runoff and compacts the upper peat layer (Mustonen and Seuna 1970) and lowers local water table (Ahti and Päivänen 1997).

5.2. Presence of Weathered Bedrock

Ten till geochemistry samples, eight hydro-borehole logs and on-site observations at two test pits supplemented with several kilometres of GPR interpretation suggest that local bedrock has been exposed to varying degrees of weathering. According to borehole observations, thickness of the weathered zone ranges from 0.8 to seven or more metres. Maximum weathering thickness inferred from GPR data is eight metres. Weathering depths are probably low on the slopes of Kuusivaara hill, where lithology is resistant to weathering. The deepest weathering is found in bedrock depressions of the east basin of Porokodanjänkä mire. Overall, weathering depths in the studied area are low to moderate. At test pits M1 and M2, block-fractured and weathered bedrock was located at a depth of approximately two metres. These locations mark the beginning and end of GPR profile 30b (Figure 36). Some form of weathering or fracturing is visible until approximately 10 metres.

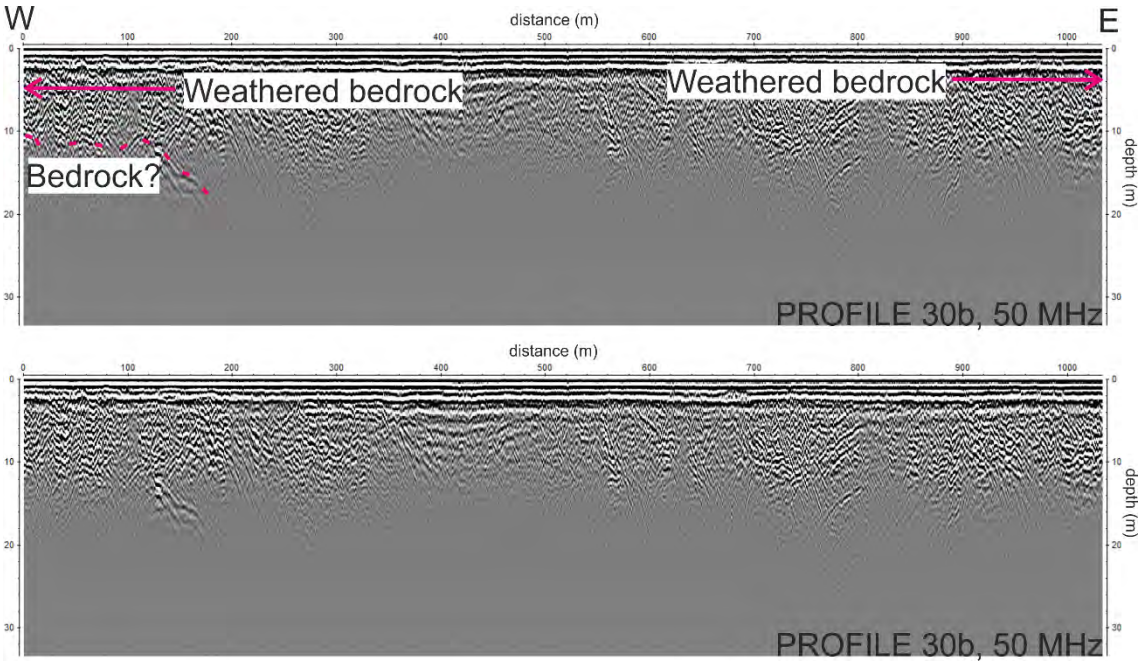

Figure 36. The upper limit of weathered bedrock at test pits M1 and M2 are shown with the arrows. Signal response beneath bedrock is detected until at least 10 metres' depth. The upper profile is interpreted and the lower profile is not. Location of the profile is shown in Figure 8.

Presence of weathered bedrock under Porokodanjänkä mire is evident from three borehole logs. In GPR profiles, its presence is interpreted by the sudden dissipation of GPR signal above solid bedrock (Leopold and Völkel 2003). An example of such weathering is shown in Figure 37. Weathered bedrock under peat is reliably observed in five GPR profiles.

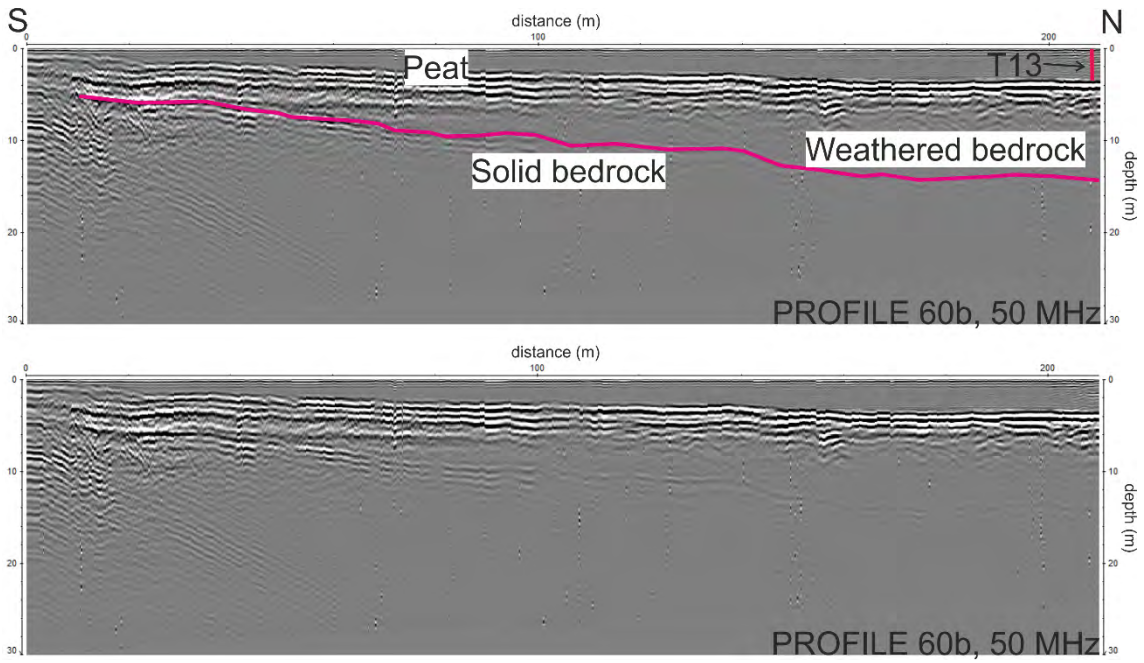

Figure 37. Weathered bedrock, horizontal sands and peat overlay a faint bedrock contact at the east basin of Porokodanjänkä mire.T13 marks the location of peat core 13. The upper profile is interpreted and the lower profile is not. Location of the profile is shown in Figure 8.

Neogene weathering of bedrock is a common occurrence in the ice divide zone (Hirvas 1991) due to limited glacial erosion stemming from frozen bed conditions (Sugden 1978, Kleman et al. 2008). Terminology regarding the chemical weathering phenomena is based on the physical appearance of the weathered product. Saprolith is weathered rock that has preserved the fabric of its parent material. It is further divided into saprolite and saprock. Saprolite is highly weathered saprolith with increasing amount of original minerals replaced by fine-grained pseudomorphs as weathering intensifies. Gruss is sandy saprolite with a low fines content whereas clay has a high fines content and a low sand content. Saprock is weathered and fractured bedrock, where individual blocks remain undisturbed in their place with signs of weathering only on their surfaces (Hall et al. 2015). Based on GPR interpretation, borehole data and test pit observations, saprock as well as saprolite of both kinds are present in the study area.

In Pahtavaara, west of Sodankylä, weathering in carbonates and calcium-silicate gneisses exceed 20 m whereas mafic volcanic rocks are weathered up to 10 m deep. Quartzites from Pahtavaara show weathering up to 5 m or less (Hall et al. 2015). Weathered bedrock with an average depth between 10 and 20 metres (Hall et al. 2015) is present in many places in the ice divide (Hirvas 1991, Hall et al. 2015). Localised zones of weathered

bedrock up to dozens of metres deep have been described from nearby Siurunmaa (Rask & Lintinen 2001), Kevitsa (Malehmir et al. 2012) and Sakatti (Hall et al. 2015).

The variation in saprolith thickness observed in this study is in line with other related studies (Islam et al. 2002, Hall et al. 2015). Susceptibility to weathering is correlated with local geology, topography, and fracture zones (Hall et al. 2015). Typically, resistant rocks such as gabbros and quartzites are weathered to <5 metres deep and form local topographic highs. Less resistant rocks often weather to thicknesses of 10–20 metres. Only the very weakest rock types, such as ultrabasics and micaceous schists in fracture zones display weathering profiles tens of metres or more in thickness (Hall et al. 2015. Deeply weathered bedrock is typically found beneath thick deposits of peat and till (Rask & Lintinen 2001, Hall et al. 2015). Despite the high variation in weathering depths in Lapland, saprolith is most often a few metres thick (Islam et al. 2002).

Weathering horizons beneath solid bedrock is not an uncommon occurrence in Lapland (Hall et al. 2015). This, accompanied with faint bedrock contact observations in GPR profiles unsubstantiated with borehole data, and signal dissipation immediately below, makes it possible that weathering is present deeper beneath Porokodanjänkä mire than described here. Without further borehole data or other robust evidence, this notion cannot be proven one way or the other.

Saprolite or saprock was not reliably identified from GPR profiles at the west-southwest parts of the study area. Nor were there test pit observations or borehole data from this area. Likewise, solid bedrock observations are limited. Two explanations for the lack of reliable bedrock and saprolith record are addressed here. As stated before, valley of river Kitinen has been exposed to continuous erosion (A. Åberg et al. 2017a). It is entirely possible that most weathering products, especially the loose gruss over fractured bedrock has been washed away. Alternatively, saprolith and solid bedrock may be located too deep for the GPR signal to reach, or widespread saprolith does not exist in these parts of the study area in the first place. In GPR profile 53, sediments and a short bedrock contact is visible at below 20 metres. Barring solitary fractures observed at close to 30 metres below ground surface, in no profile deeper structures or contacts were observed. Maximum penetration depth for the 50 MHz antenna signal in the subsurface sediments of the study area is most likely at around 20 metres. The deep bedrock contact and its fading can be observed in Figure 38.

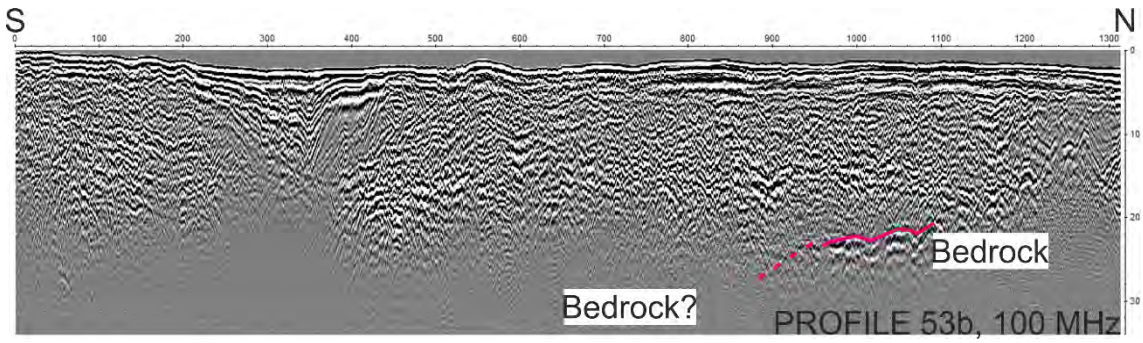

Figure 38. Maximum signal penetration depth at GPR profile 53 near river Kitinen is no more than 20 metres. The upper profile is interpreted and the lower profile is not. Location of the profile is shown in Figure 8.

GPR penetration depth depends largely on the antenna frequency and local subsurface sediments. Under ideal conditions, the 50 MHz antenna can reach depths of nearly 50 m (Smith and Jol 1995) over fluvial sediments. In another experiment over fluvial sediments, the 50 MHz antenna penetration depth was 24 metres at most. Tills are known to be a medium that increases GPR signal attenuation (Davis and Annan 1989). Considering, it is possible that the GPR signal does not penetrate through the weathered zone above solid bedrock. In light of this, it is not possible to make assumptions on the total thickness of weathering and the upper limit of solid, crystalline bedrock.

5.3. Concerns and Potential Related to the Siting of Mining Infrastructure

When considering the suitability for siting mining infrastructure in the area studied here, a number of factors are important to consider. They include bedrock weathering and fracturing, water issues, bearing capacity and building properties of overburden, conservation areas, impacts to reindeer herding and the view from nearby settlements.

Saprolite and saprock of unknown depth are widely present under Porokodanjänkä mire. Bedrock fractures and weathering may extend deeper than observed with the means of the study and may act as routes for limited groundwater movement (Sarala 2015). Hydraulic conductivity of saprolith is generally low. Schoeneberger and Amoozegar (1989) calculated K-values for soil-saprolite sequences in the order of 10^{-6}–10^{-8} ms^{-1}, whereas George (1992) presents values in the range of between10^{-6} ms^{-1} for gruss-type weathering of granite. Weathering and fracturing may require special attention when designing foundations for mining infrastructure. Deeply weathered gruss is prone to

disintegration when exposed to the elements, and may increase fines content of sediments when present. This phenomenon was experienced first-hand as seemingly solid rock fragments of sediment sample M2N3 disintegrated in water during wet sieving. The bearing capacity of deeply weathered rock in foundations is comparable with sand rather than solid bedrock (Yasufuku and Hyde 1995).

The majority of the overburden in the area is glacial till. It forms morainic landscape around Kuusivaara hill and, according to the sediment thickness model, it averages at 2 to 6 metres in thickness. It can be divided into a compact lower till with a high proportion of fines, and a looser, sandy upper till. The high fines content of the lower till likely stems from saprolitic clay minerals that have been incorporated within from weathered bedrock. These till reserves offer suitable construction material for roads, embankments, lining structures and other infrastructure. Tills have recently been used in the construction of embankments of a tailings pond at the nearby Kevitsa mine (Kvist 2018). Both the lower and upper till from Kuusivaara have very low K-values. Attention must be paid to the tendency of tills with low permeability in regard to draining and freezing. Bearing capacity of poorly drained tills is significantly reduced. Freezing porewaters within the till matrix cause it to expand. Sandy and silty tills are therefore not suitable for particularly demanding construction (Salmenkaita 1993).

Wind-blown cover sands and dunes have no practical importance as groundwater reservoirs. However, as sandy deposits are frequent below peat, they may act as groundwater conduits beneath the mires in the area. In places, groundwater is also discharging beneath the peat deposits, as springs at the mire are indicating. There are no eskers, glaciofluvial systems or related groundwater resources in the area (Väisänen and Maunu 2004). Local, small scale groundwater discharge is indicated by domestic wells in the west of the study area as well as water seeping into test pits M3 and M4 while being excavated. K-values for samples from test pits M3 and M4 are the highest observed, in part explaining groundwater seepage in the area. This water is most likely recharged at Kuusivaara hill, as indicated by several seasonal springs at Kuusivaara and Porokodanjänkä.

Aapamires of Sodankylä region are commonly patterned by dry, slightly elevated strings and wet flarks between them (Maunu and Virtanen 2005). Surface water flow at mires is perpendicular to string orientation (Lindholm and Heikkilä 2006). The Kuusivaara

watershed indicates that the northern part of the study area is draining towards Viiankiaapa mire complex. This sector is proposed to be free from any building activities. Drainage pattern from the southeast sector of Kuusivaara is directed towards Eliasaapa and ultimately to river Kitinen. Surface drainage from the southwest part of Kuusivaara connects directly to Kitinen. Surface draining directions have been inferred from string-and-flark patterns, and are illustrated in Figure 39.

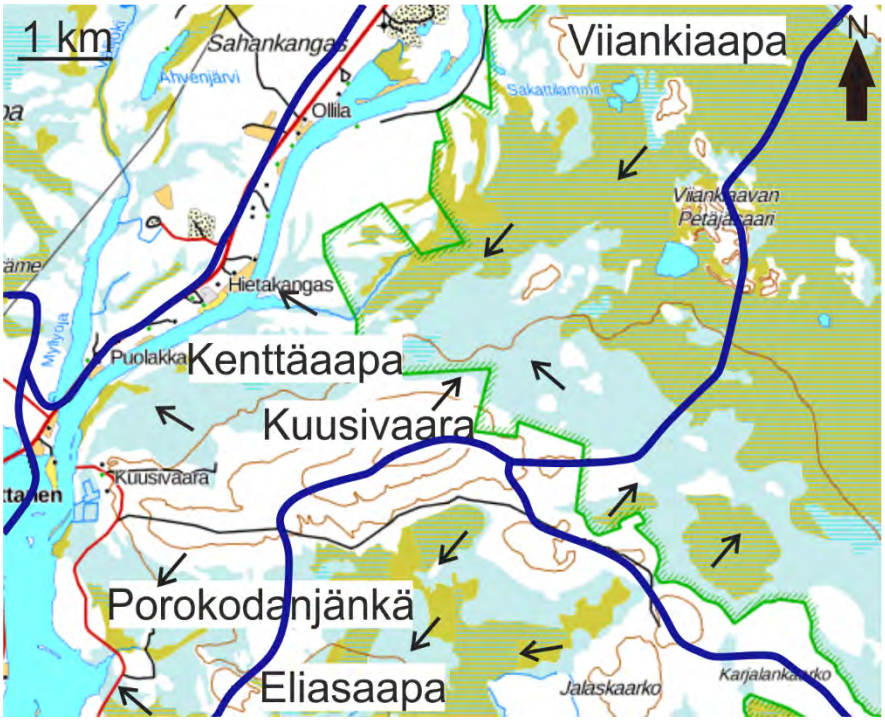

Figure 39. Local watersheds (blue lines) and simplified runoff directions of surface water (black arrows) as inferred from string-and-flark patterns at mires surrounding Kuusivaara hill. Map © National Land Survey of Finland.

Suitable and potential areas for mining infrastructure and waste management can be found from the southern side of Kuusivaara hill. The western basin of Porokodanjänkä is no longer in its natural state. There are a few major man-made ditches, so the hydrology has already been altered. Porokodanjänkä has potential to host a wet tailings pond and associated linings and embankments. Aapamires have been deemed suitable locations for such mining infrastructure at, for example, the nearby Kevitsanaapa at Kevitsa mine (Kvist 2018). The eastern shore of Kitinen basin is affected by historical fluvial activity. It hosts thick and permeable riverbank gravels and sands as observed in the sediment

thickness model and GPR interpretation. This area could be left as a green zone between mining activities and river Kitinen.

7. ACKNOWLEDGEMENTS

I extend my sincerest thanks to my supervisors Seija Kultti, Veli-Pekka Salonen and Emilia Koivisto for their guidance and patience throughout this thesis project. I would also like to thank AA Sakatti Mining Oy for making this thesis possible in the first place. Special thanks go to Annika Åberg for providing GIS-related help whenever I needed it.

8. REFERENCES

Aalto, M., Eriksson, B. and Hirvas, H. 1992. Naakenavaara interglacial – A till-covered peat deposit in western Finnish Lapland. 13 p.

Åberg, A.K., Salonen, V.-P., Korkka-Niemi, K., Rautio, A., Koivisto, E. and Åberg, S.C. 2017. GIS-based 3D sedimentary model for visualizing complex glacial deposition in Kersilö, Finnish Lapland. Boreal Env. Res. 22: 277−298.

Åberg, A.K., Salonen, V.-P., Kaakinen, A., Korkka-Niemi, K., Rautio, A. and Åberg, S.C. 2017. Weichselian history of sedimentation in Kitinen basin, Sodankylä. In: Hölttä, P., Nenonen, K. and Eerola, T. (eds.) 3rd Finnish National Colloquium of Geosciences, Espoo, Finland March 15−16, 2017. Geological Survey of Finland, Guide 63, 7−8.

Åberg, S.C., Åberg, A.K., Korkka-Niemi, K. and Salonen, V.-P. 2017. Hydrostratigraphy and 3D modelling of a bank storage affected aquifer in mineral exploration area in Sodankylä, Northern Finland. In: Wolksedorfer, C., Sartz, L., Sillanpää, M and Häkkinen, A. Mine Water & Circular Economy (Vol I). p. 237−244. Lappeenranta, Finland.

Andersen, B., Mangerud, J., Sørensen, R., Reite, A., Sveian, H., Thoresen, M and Bergström, B. 1995. Younger Dryas ice-marginal deposits in Norway. Wuaternary International 28, 147−169.

Brownscombe, W., Ihlenfeld, C., Coppard, J., Hartshorne, C., Klatt, S., Siikaluoma, J. and Herrington, R. 2015. The Sakatti Cu–Ni–PGE sulfide deposit in northern Finland. In: O'Brien, W.D.M.L (ed.) Mineral deposits of Finland, Elsevier, Amsterdam, 211-252.

Davis, J.L. and Annan, A.P. 1989. Ground-penetrating radar for high-resolution mapping of soil and rock stratigraphy. Geophysical Prospecting 37, 531–551.

Eyles, N. 1987. Late Pleistocene debris-flow deposits in large glacial lakes in British Columbia and Alaska. Sedimentary Geology 53, 33–71.

Eyles, N. and Kocsis, S. 1988. Sedimentology and clast fabric of subaerial debris flow facies in a glacially-influenced alluvial fan. Sedimentary Geologi 59, 15–28.

Gąsiorowski, M. 2008. Deposition rate of lake sediments under different alternative stable states. Geochronometria 32, 29–35.

George, R.J. 1992. Hydraulic properties of groundwater systems in the saprolite and sediments of the wheatbelt, Western Australia. Journal of Hydrology 130, 251–278.

Gustavsson, N., Noras, P. and Tanskanen, H. 1979. Seloste geokemiallisen kartoituksen tutkimusmenetelmistä. Geologinen tutkimuslaitos, Espoo.

Hall, A.M., Sarala, P and Ebert, K. 2015. Late Cenozoic deep weathering pattern on the Fennoscandian shield in northern Finland: A window on ice sheet bed conditions at the onset of Northern Hemisphere glaciation. Geomorphology 246, 472−488.

Hanski, E. and Huhma, H. 2005. Central Lapland greenstone belt. In: Lehtinen, M., Nurmi, P.A. and Rämö, O.T. (eds.) Developments in Precambrian geology 14, 1–736. Elsevier.

Helmens, K.F., Johansson, P., Räsänen, M., Alexanderson, H. & Eskola, K. 2007: Ice-free intervals continuing into Marine Isotope Stage 3 at Sokli in the central area of the Fennoscandian glaciations. Bulletin of the Geological Society of Finland 79, 17–39.

Hirvas H. 1991. Pleistocene stratigraphy of Finnish Lapland. Geological Survey of Finland, Bulletin 354, 123 p.

Hirvas, H., Alfthan, A., Pulkkinen, E., Puranen, R. and Tynni, R. 1977. Raportti malminetsintää palvelevasta maaperätutkimuksesta Pohjois-Suomessa vuosina 1972−1976. Summary: A report on glacial drift investigations for ore prospecting in northern Finland 1972–1976. Geological Survey of Finland, Report of investigation 19, 58 p.

Hirvas H., Saarnisto M., Hakala P., Huhta P., Johansson P., Pulkkinen E. 1994.

Maaperän kerrosjärjestys ja Geokemia Keivitsassa. Geologian tutkimuskeskus, maaperäosasto. Report. 44 s.

Islam, M.R., Peuraniemi, V., Aario, R and Rojstaczer, S. 2002. Geochemistry and mineralogy of saprolite in Finnish Lapland. Applied Geochemistry 17, 885−902.

Johansson, P. 2005. Jääjärvet. In: Johansson, P. and Kujansuu, R. (eds.) Pohjois-Suomen maaperä. Geological Survey of Finland, Espoo, 127−148.

Johansson, P., 2007. Late Weichselian deglaciation in Finnish Lapland. In: Geological Survey of Finland, Special Paper, 46, 47–54.

Johansson, P., Lunkka, J.-P. and Sarala, P. The glaciation of Finland. In: Ehlers J., Gibbard P.L. & Hughes P.D. (eds.), Quaternary Glaciations – Extent and Chronology, A closer look. Developments in Quaternary Science 15, Elsevier, Amsterdam, 105–116.

Kasse, C. 2002. Sandy Aeolian deposits and environments and their relation to climate during the Last Glacial Maximum and Lateglacial in northwest and central Europe. Progress in Physical Geography 24, 507–532.

Kasse, C. and Bohncke, S. 1992. Weichselian Upper Pleniglacial Aeolian and Ice-cored Morphology in the Southern Netherlands (Noord-Brabant , Groote Peel). Permafrost and Periglacial Processes 3, 327–342.

Kauppila, P., Räisänen, M.L. & Myllyoja, S. 2011 (eds.) Best Environmental Practices in Metal Ore Mining. Finnish Environment Institute. 219 p. ISSN 1796–1637.

Kleman, J. and Glasser, N.F. 2007. The subglacial thermal organisation (STO) of ice sheets. Quaternary Reviews 26, 585–597.

Kolstrup, E. and Jørgensen, J.B. 1982. Bulletin of the Geological Society of Denmark 30, 71–77.

Kujansuu, R. and Hyyppä, J. 1995. Vuotson kartta-alueen maaperä. Summary: Quaternary deposits in the Vuotso map-sheet area. 1:100000. Sheet 3742. Geological Survey of Finland, Espoo, 110 p.

Kvist, K. 2018. Rikastushiekka-altaan alkupatorakenteiden rakentaminen ja laadunvalvonta. Oulu University of Applied Sciences, 44 p. (thesis).

Lappalainen, E. 1970. Über die spätquartäre Entwicklung der Flussufermoore Mittel-Laplands. Geologian tutkimuslaitos, Espoo, 91 p.

Lehtonen, M., Manninen, T., Rastas, P., Väänänen, J., Roos, S.I. and Pelkonen, R. 1985. Keski-Lapin geologisen kartan selitys. Summary: Explanation to the geological map of Central Finland. Geological Survey of Finland, Report of investigation 71, 59 p.

Lehtonen, M., Airo, M-L., Eilu, P., Hanski, E., Kortelainen, V., Lanne, E., Manninen, T., Rastas, P., Räsänen, P. and Virransalo, P. 1998. Kittilän vihreäkivialueen geologia. Summary: The stratigraphy, petrology and geochemistry of the Kittilä greenstone area, northern Finland. Geological Survey of Finland, Report of Investigation 140, 147 p.

Leopold, M. and Völkel, J. 2003. GPR images of periglacial slope deposits beneath peat bogs in the Central European Highlands, Germany. In: Bristow, C.S. and Jol, H.M. (eds.) Ground Penetrating Radar in Sediments. Geological Society, London, Special Publications 211, 181–189.

Lindholm, T. and Heikkilä, R. 2006. Geobotany of Finnish forests and mires: the Finnish approach. In: Lindholm, T. and Heikkilä, R. (eds.) Finland – land of mires. Finnish Environment Institute, Helsinki, 95–105.

Lunkka. J.-P., Sarala, P. and Gibbard, P.L. 2015. The Rautuvaara section, western Finnish Lapland, revisited – new age constraints indicate a complex Scandinavian Ice Sheet history in northern Fennoscandia during the Weichselian Stage. Boreas 44, 68–80.

Mäkilä, M., Säävuori, H., Kuznetsov, O. and Grundström, A. 2013. Suomen soiden ikä ja kehitys. Abstract: Age and dynamics of peatlands in Finland. Geological Survey of Finland, Report of Peat Investigation 443, 69 p.

Malehmir, A., Juhlin, C., Wijns, C., Urosevic, M., Valasti, P. and Koivisto, E. 2012. 3D reflection seismic imaging for open-pit mine planning and deep exploration in the Kevitsa Ni-Cu-PGE deposit, northern Finland. Geophysics 77, 95–108.

Maunu, M. and Virtanen, K. 2005. Soiden käyttö. In: Johansson, P. and Kujansuu, R. (eds.) Pohjois-Suomen maaperä. Geological Survey of Finland, Espoo, 188–190.

Mustonen, S.E. and Seuna, P. 1971. Metsäojituksen vaikutuksesta suon hydrologiaan. Summary: Influence of Forest Draining on the Hydrology of Peatlands. Publications of the water research institute 2, 66 p.

Neal, A. 2004. Ground-penetrating radar and its use in sedimentology: principles, problems and progress. Earth Science Reviews 66, 261–330.

Overmeeren, R.A., van. 1998. Radar facies of unconsolidated sediments in The Netherlands: A radar stratigraphy interpretation method for hydrogeology. Journal of Applied Geophysics 40, 1–18.

Pedersen, K. and Clemmensen, L.B. 2005. Unveiling past aeolian landscapes: A ground-penetrating radar survey of a Holocene coastal dunefield system, Thy, Denmark. Sedimentary Geology 77, 57–86.

Peuraniemi, V. Till stratigraphy and ice movement directions in the Kittilä area, Finnish Lapland. Boreas 18, 145–157.

Pöyry Finland Oy. 2018. Sakatin monimetalliesiintymän kaivoshanke, 266p.

Rask, M., Lintinen, P., 2001. Kaoliinitutkimukset Sodankylän Siurunmaalla vuosina 1978–1988. Geological Survey of Finland 13 (M19/3713/2001/1/82)

Räisänen, M.L., Komulainen, H., Kauppila, P., Kauppinen, T., Törmä, H., Leppänen, M., Tornivaara, A., Pasanen, A., Kemppainen, E., Raunio, A., Marttunen, M., Mustajoki, J., Kauppi, S., Ekholm, P., Huttula, T., Makkonen, H. & Loukola-Ruskeeniemi, K. 2015. Ympäristövaikutusten arviointimenettely kaivoshankkeissa. In: Jantunen, J. &

Kauppila, T. (eds.), Työ- ja elinkeinoministeriö, TEM oppaat ja muut julkaisut 3/2015, 96 p.

Räisänen, J. 2014. Sodankylän alueen maaperäkartoitus 2013–2014 (Väliraportti). Geological Survey of Finland, Rovaniemi. Archived Report 52, 22 p.

Saarnisto, M. and Saarinen, T. 2001. Deglaciation chronology of the Scandinavian Ice Sheet from the Lake Onega Basin to the Salpausselkä End Moraines. Global and Planetary Change 31. 387–405.

Salmenkaita, S. (ed.) 1993. Moreeni ja sen käyttö. Tielaitoksen selvityksiä 20, Oulu, 59 p.

Sarala, P. 2005. Weichselian stratigraphy, geomorphology and glacial dynamics in southern Finnish Lapland. Bulletin of the Geological Society of Finland 77, 71–104.

Sarala, 2015. Surficial geochemical exploration methods. In: Maier, W.D., Lahtinen, R., and O'Brien, H. (eds.) Mineral deposits of Finland. Elsevier, 711–731.

Schwan, J. 1986. The origin of horizontal alternating bedding in Weichselian aeolian sands in northwestern Europe. Sedimentary Geology 49, 73–108.

Schoeneberger, P. and Amoozegar, A. 1990. Directional saturated hydraulic conductivity and macropore morphology of a soil-saprolite sequence. Geoderma 46, 31–49.

Smith, D.G. and Jol, H.M. 1993. Ground penetrating radar: antenna frequencies and maximum probable depths of penetration in Quaternary sediments. Journal of Geophysics 33, 93–100.

Sugden, D.E. Glacial erosion by the Laurentide ice sheet. Journal of Glaciology 20, 367–391.

Suonperä, E. 2016. Holocene paleohydrology of Viiankiaapa mire, Sodankylä, Finnish Lapland. University of Helsinki, department of geosciences and geography, 91p. (master thesis)

Sutinen, R. 1992. Glacial deposits, their electrical properties and surveying by image interpretation and ground penetrating radar. Geological Survey of Finland, Espoo, 123 p. (academic dissertation)

Törmänen, T., Konnunaho, J.P., Hanski, E., Moilanen, M. and Heikura, P. 2016. The Paleoproterozoic komatiite-hosted PGE mineralization at Lomalampi, Central Lapland Greenstone Belt, northern Finland. Mine Deposits 51, 411–430.

Väisänen, U. and Maunu, M. 2004. Sattasen kartta-alueen maaperä. Maaperäkartta 1:20000 explanation, sheet 371707. Geological Survey of Finland, Rovaniemi.

Vandenberghe, J., and Overmeeren, R.A., van. 1999. Ground penetrating radar images of selected fluvial deposits in the Netherlands. Sedimentary Geology 128, 245–270.

Vukovic, M. and Soro, A. 1992. Determination of hydraulic conductivity of Porous media from grain-size distribution composition. Water Resources Publications, Littleton, Colorado, Usa.

Yasufuku, N. and Hyde, A.F.L. 1995. Pile end-bearing capacity in crushable sands. Géotechnique 45, 663–676.

Yuval, D. and Oldenburg, W. 1996. DC resistivity and IP methods in acid mine drainage problems; results from the Copper Cliff mine tailings impoundment. Journal of Applied Geophysics 34, 187–198.

9. APPENDICES

Appendix 1. All GPR profiles processed in this study. Profile numbers are listed below images.

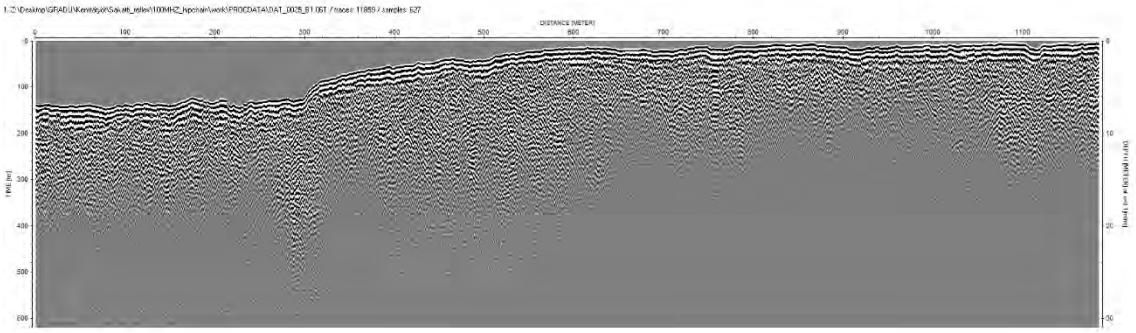

Profile 25b.

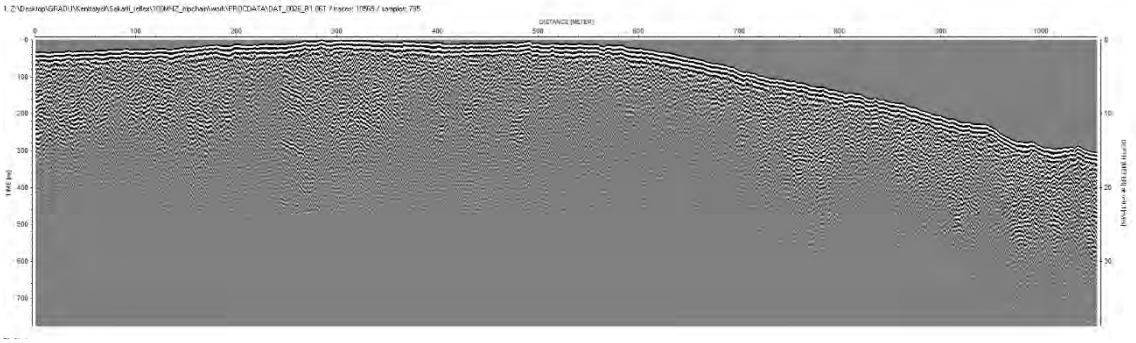

Profile 26b.

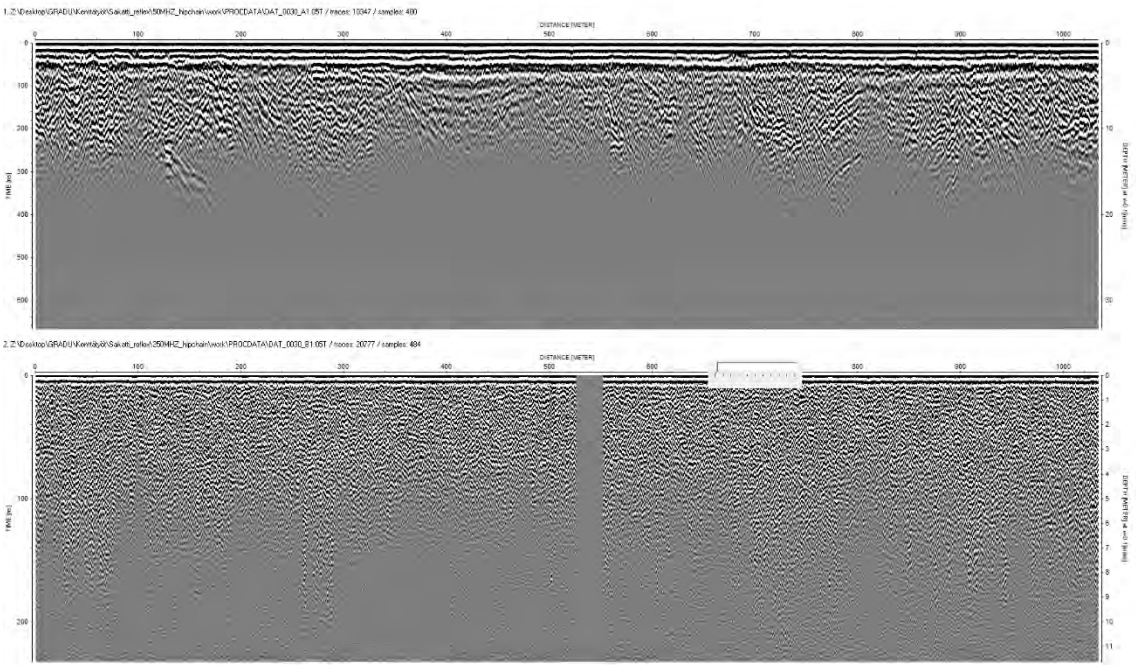

Profiles 30a (top) and 30b (bottom).

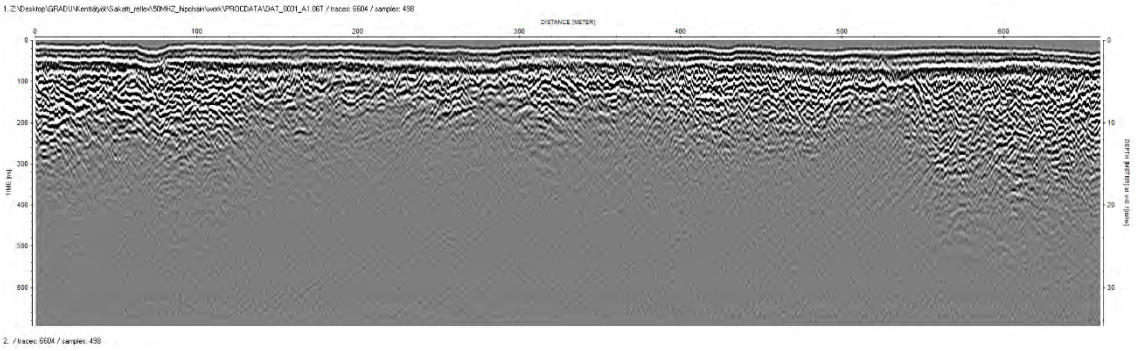

Profile 31a.

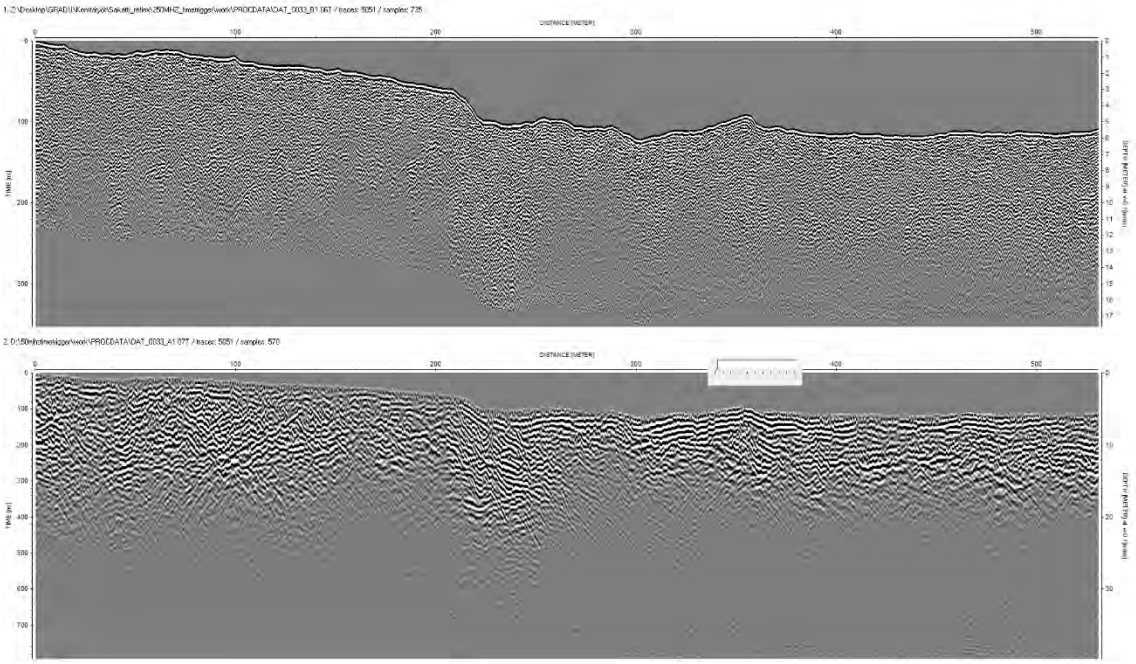

Profile 33b (top) and 33a (bottom).

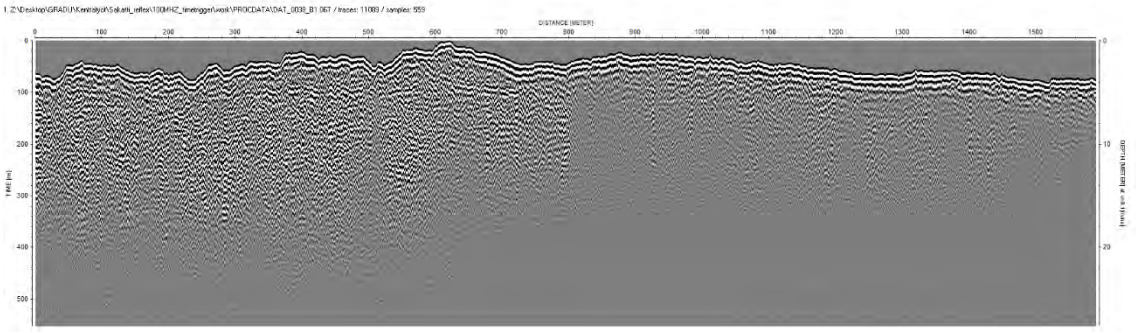

Profile 38b.

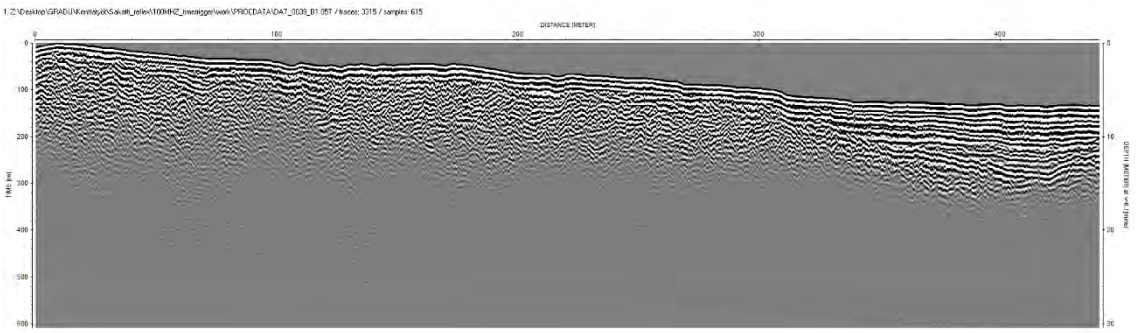

Profile 39b.

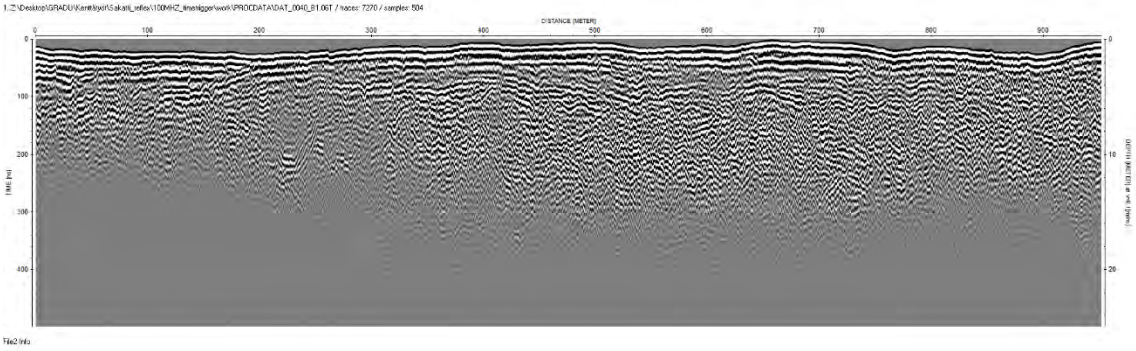

Profile 40b.

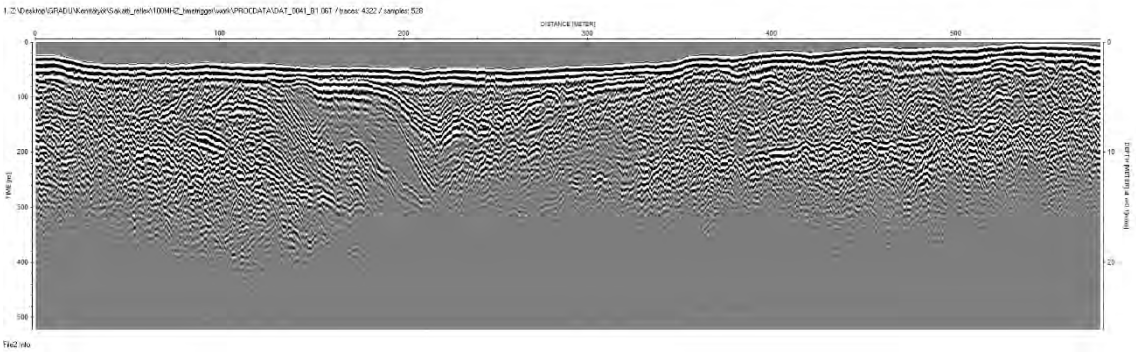

Profile 41b.

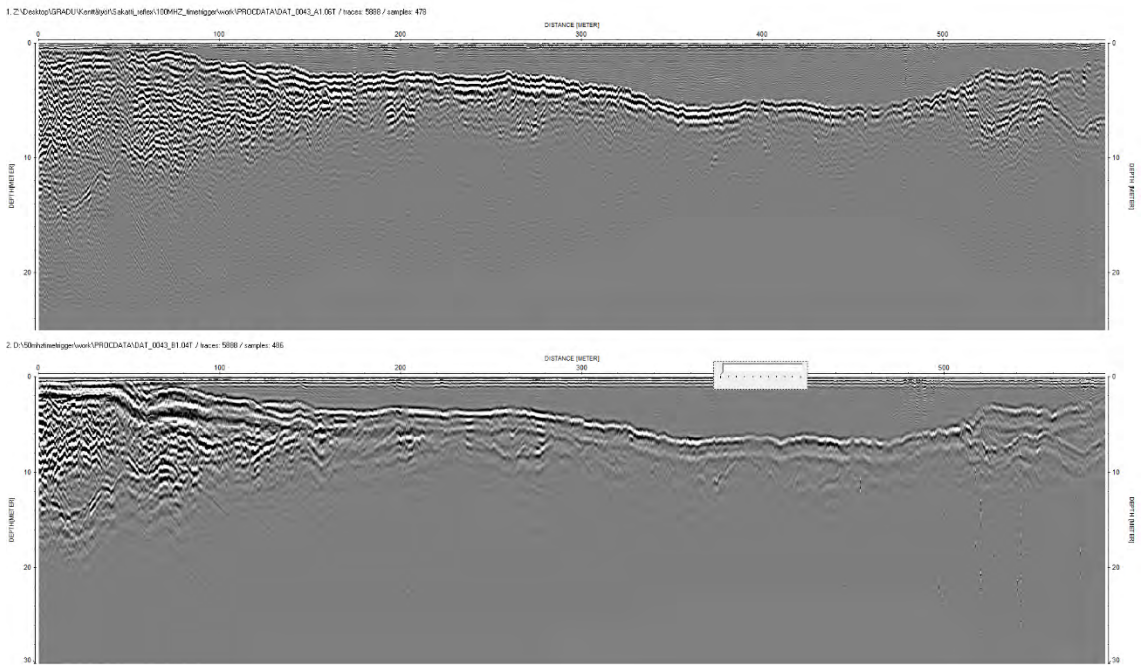

Profile 43a (top) and 43b (bottom).

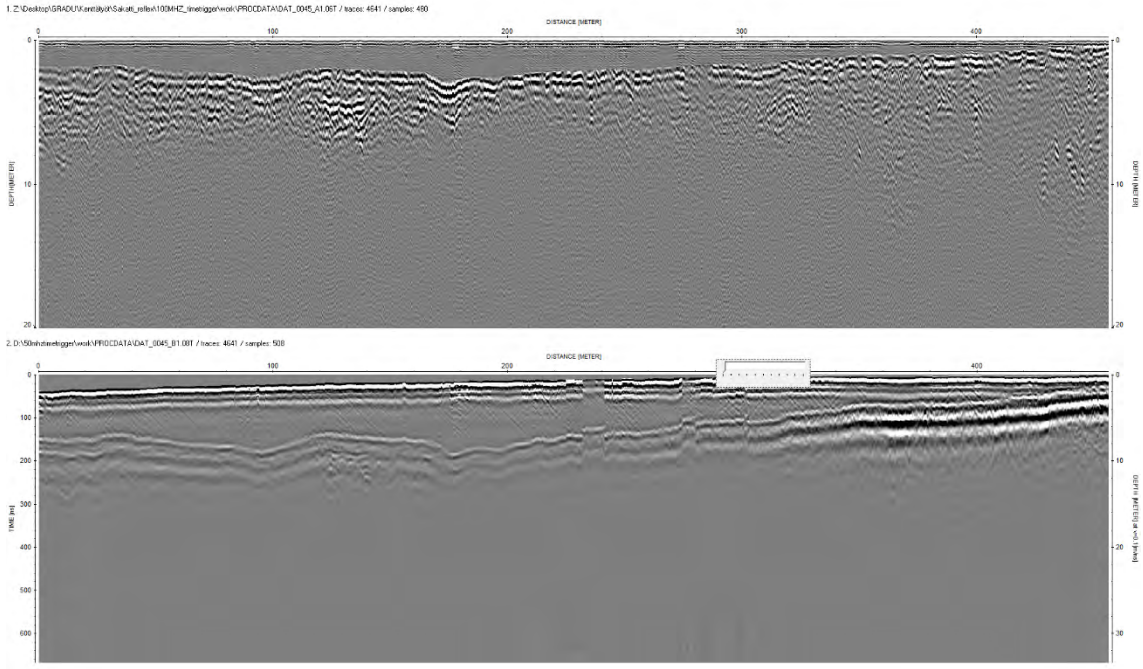

Profile 45a (top) and 45b (bottom).

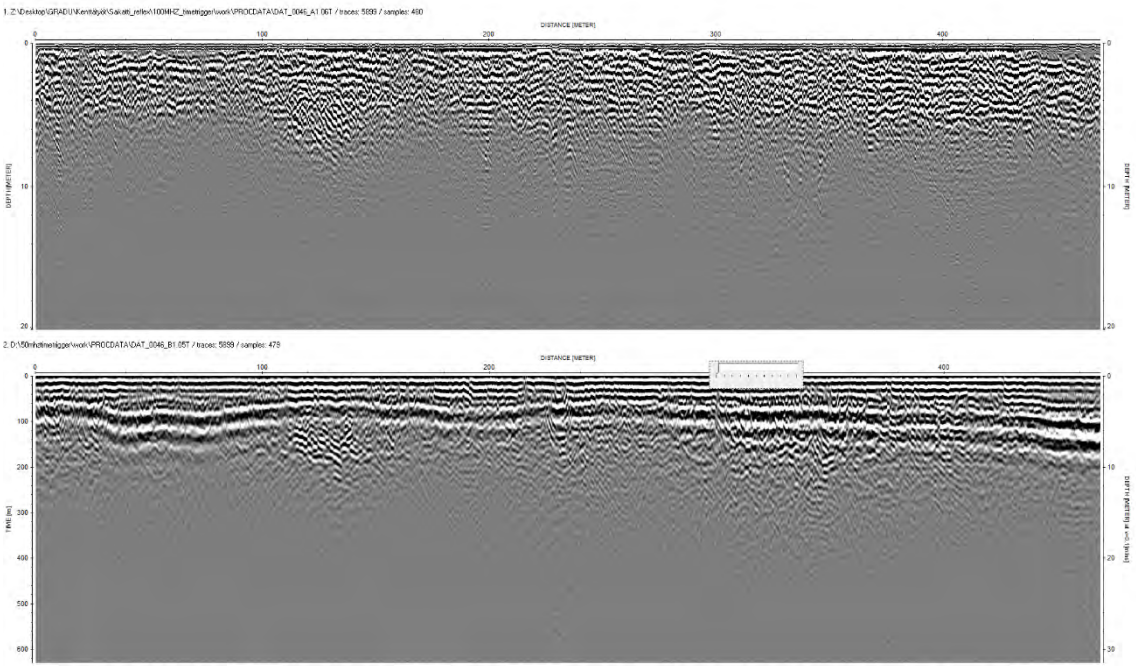

Profile 46a (top) and 46b (bottom).

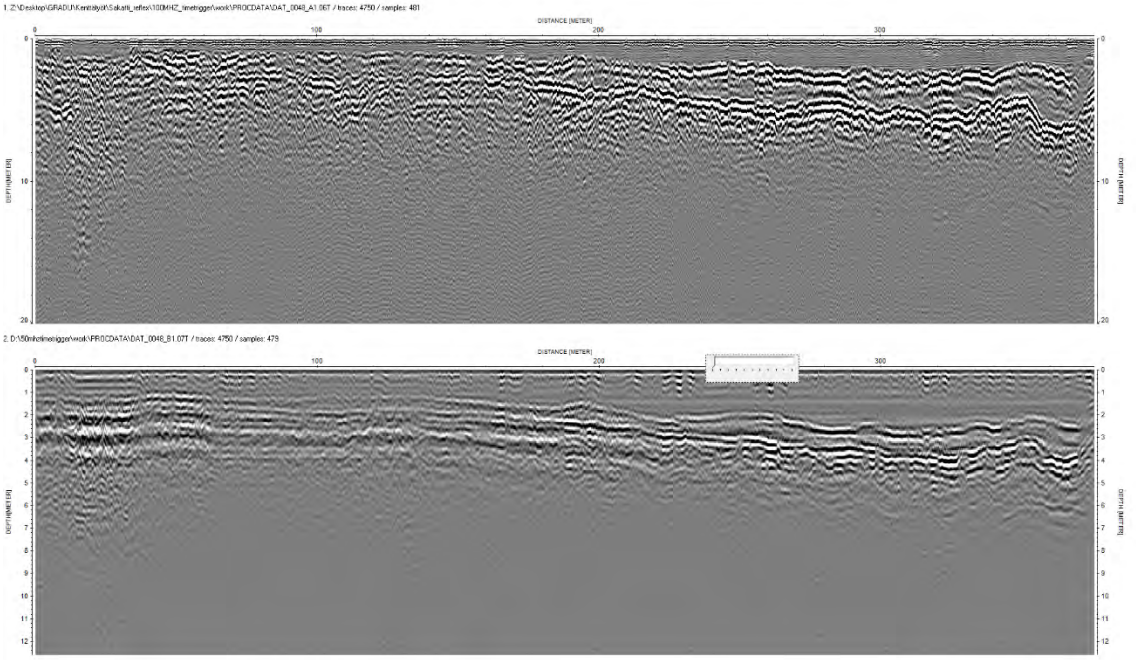

Profile 48a (top) and 48b (bottom).

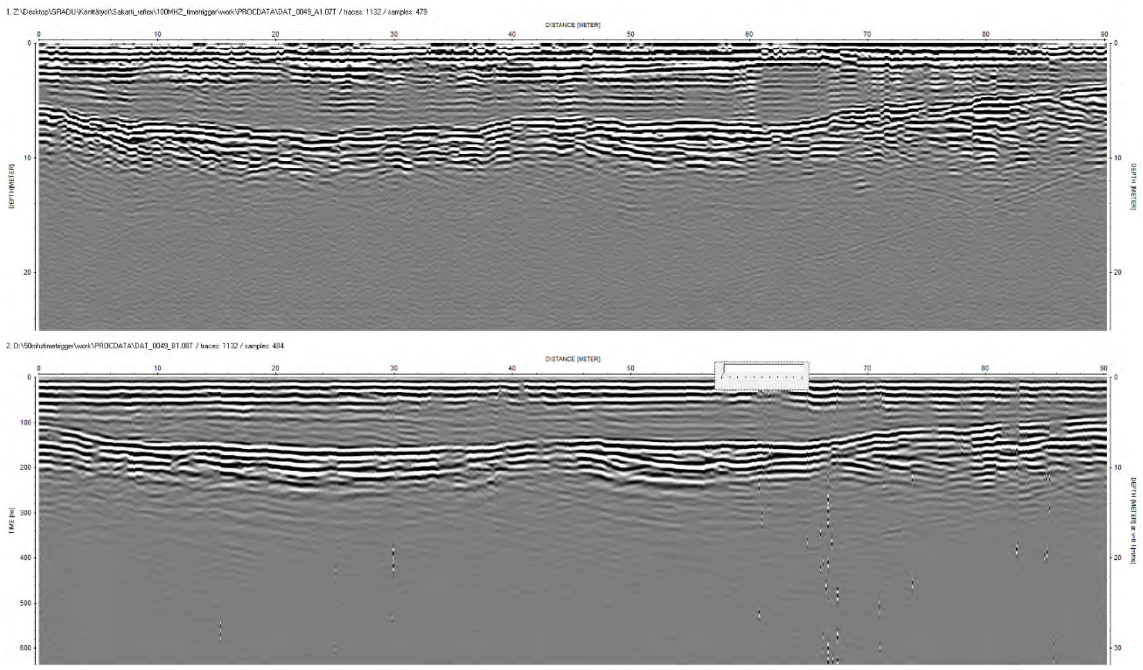

Profile 49a (top) and 49b (bottom).

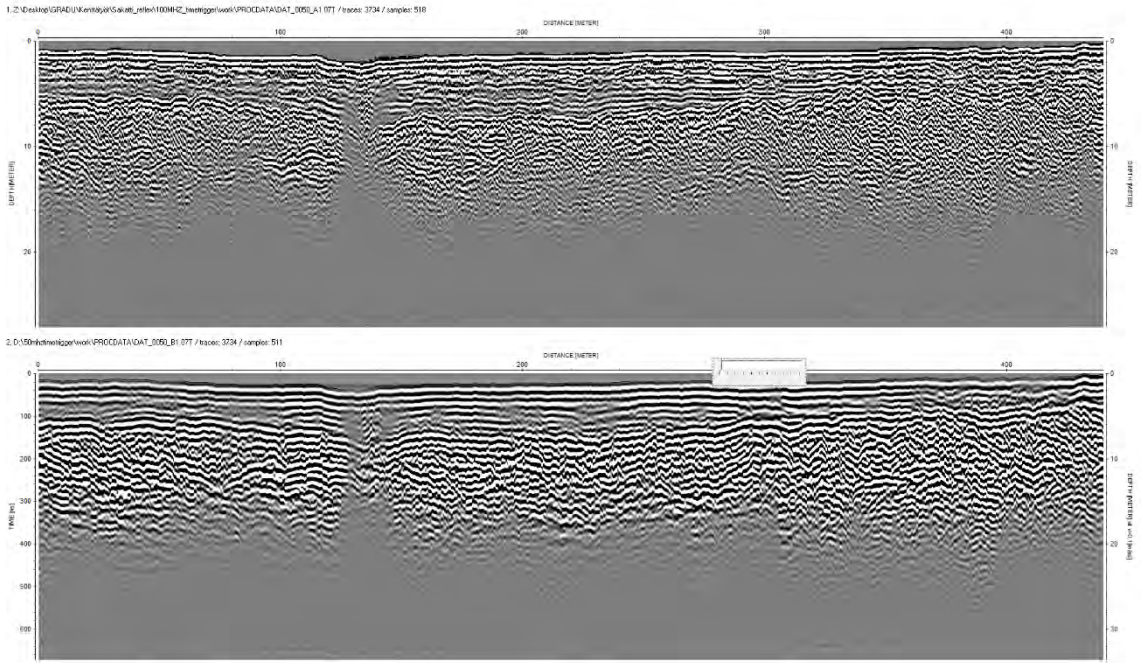

Profile 50a (top) and 50b (bottom).

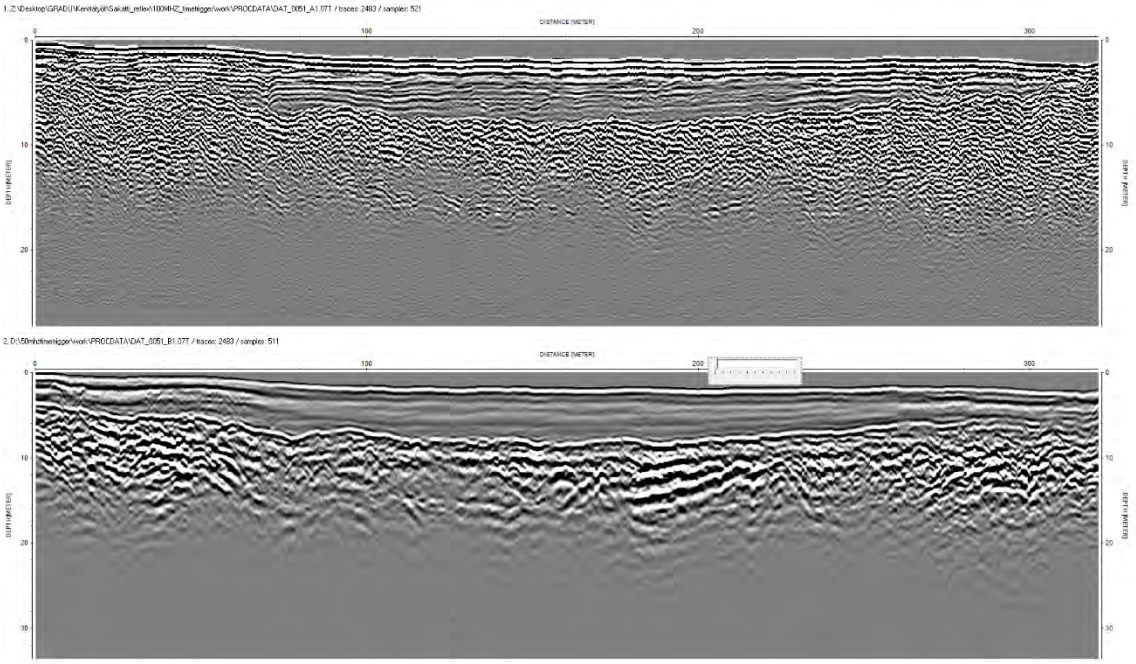

Profile 51a (top) and 51b (bottom).

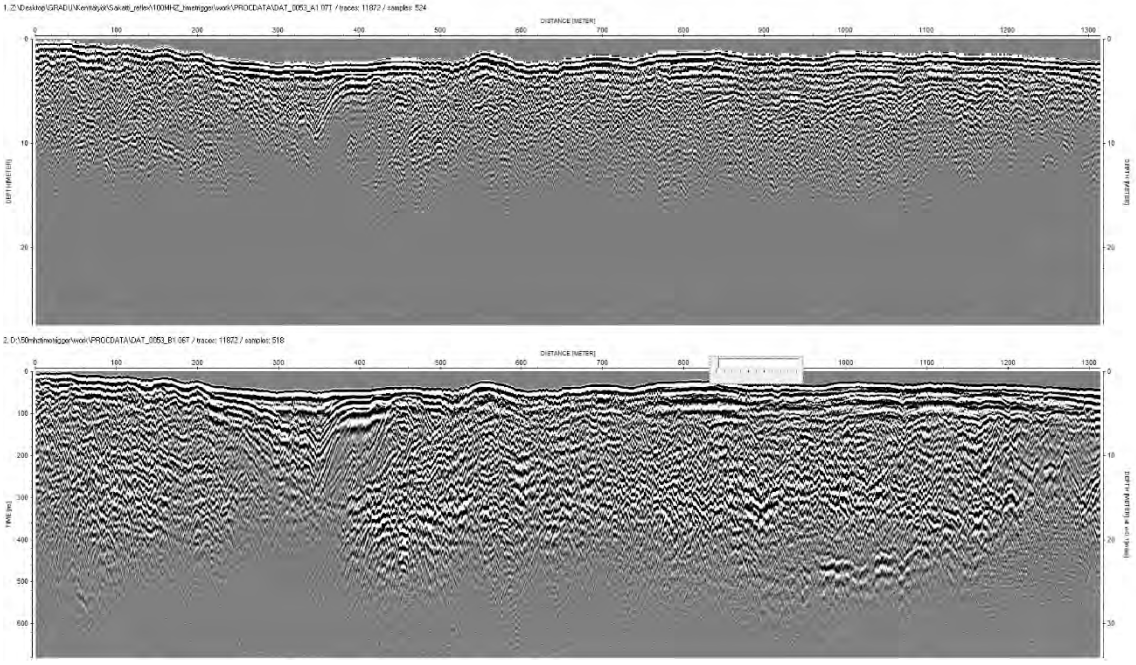

Profile 53a (top) and 53b (bottom).

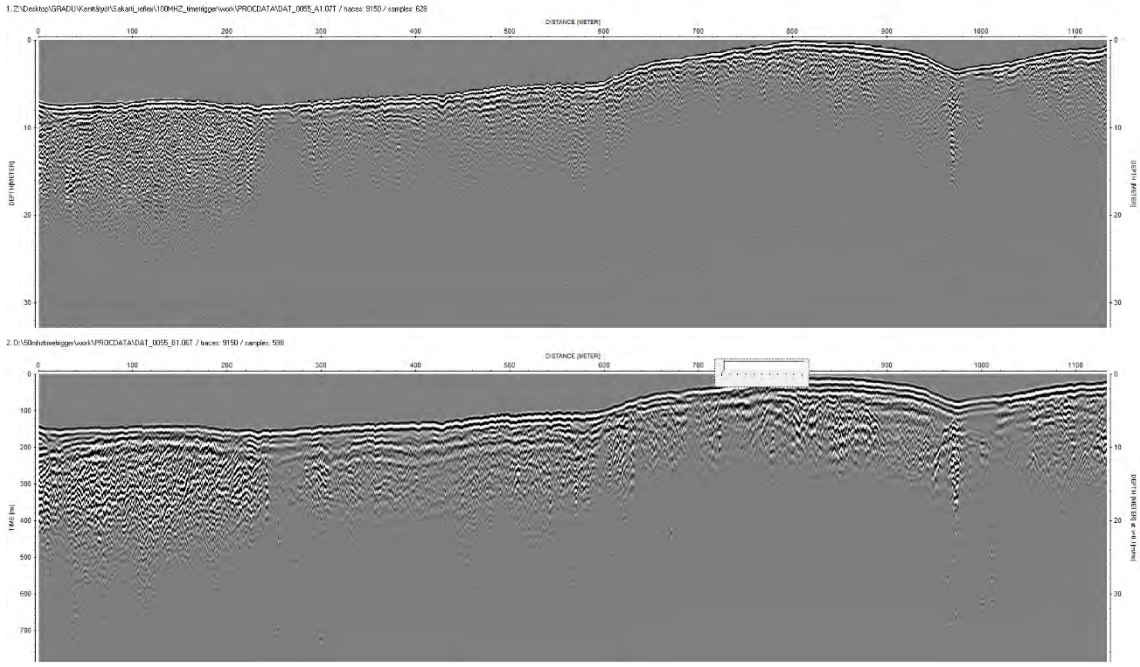

Profile 55a (top) and 55b (bottom).

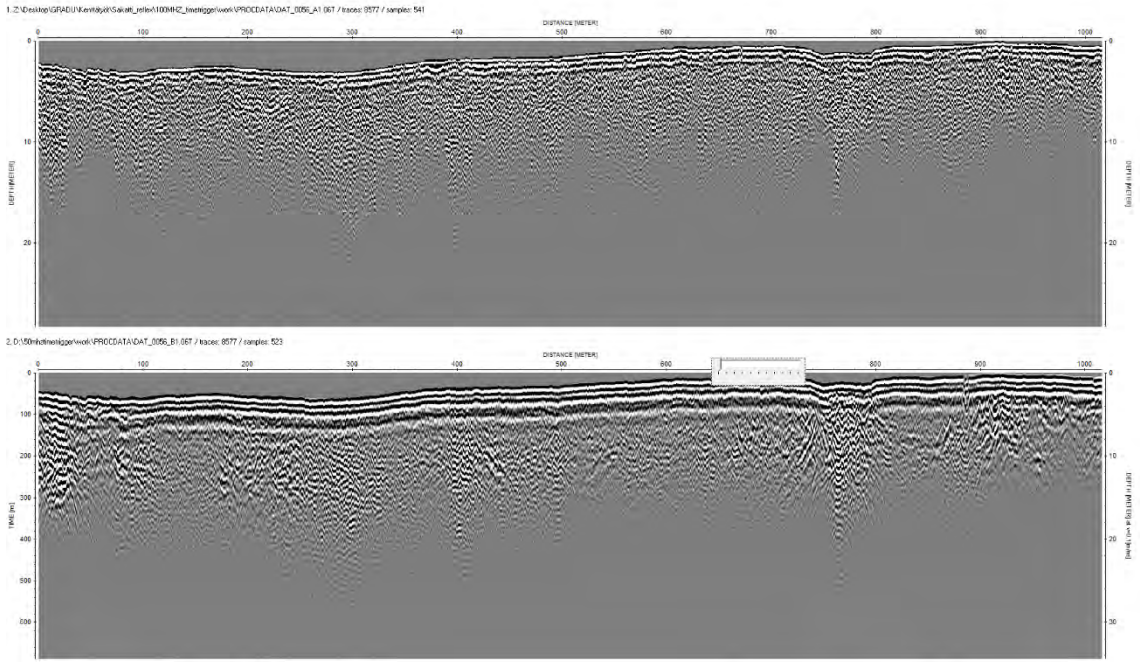

Profile 56a (top) and 56b (bottom).

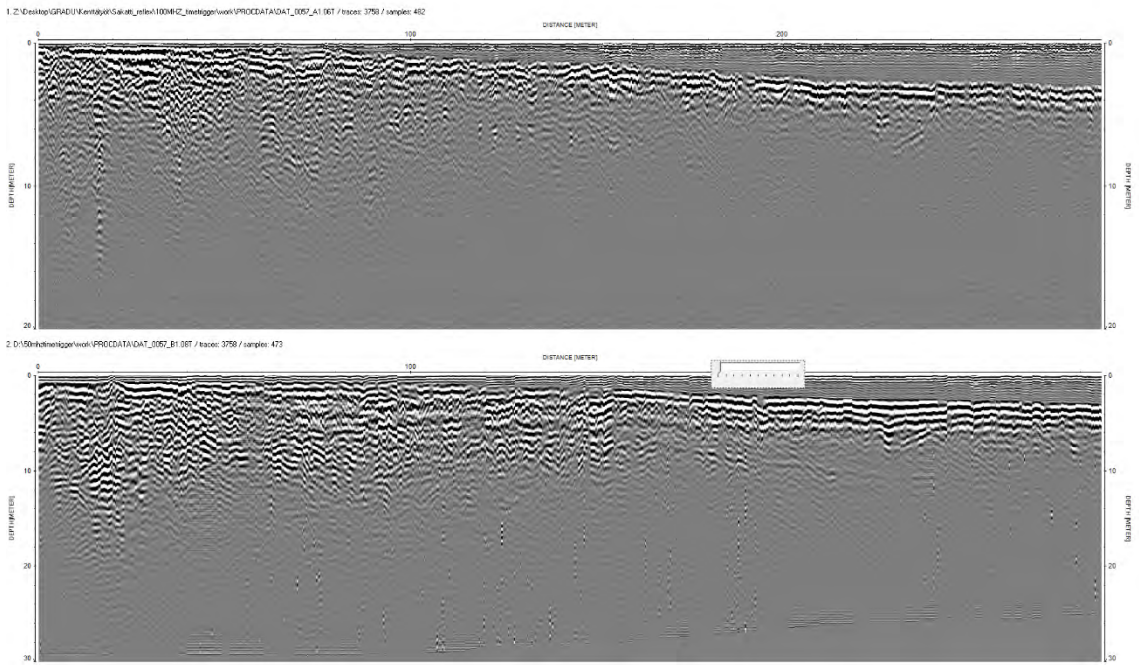

Profile 57a (top) and 57b (bottom).

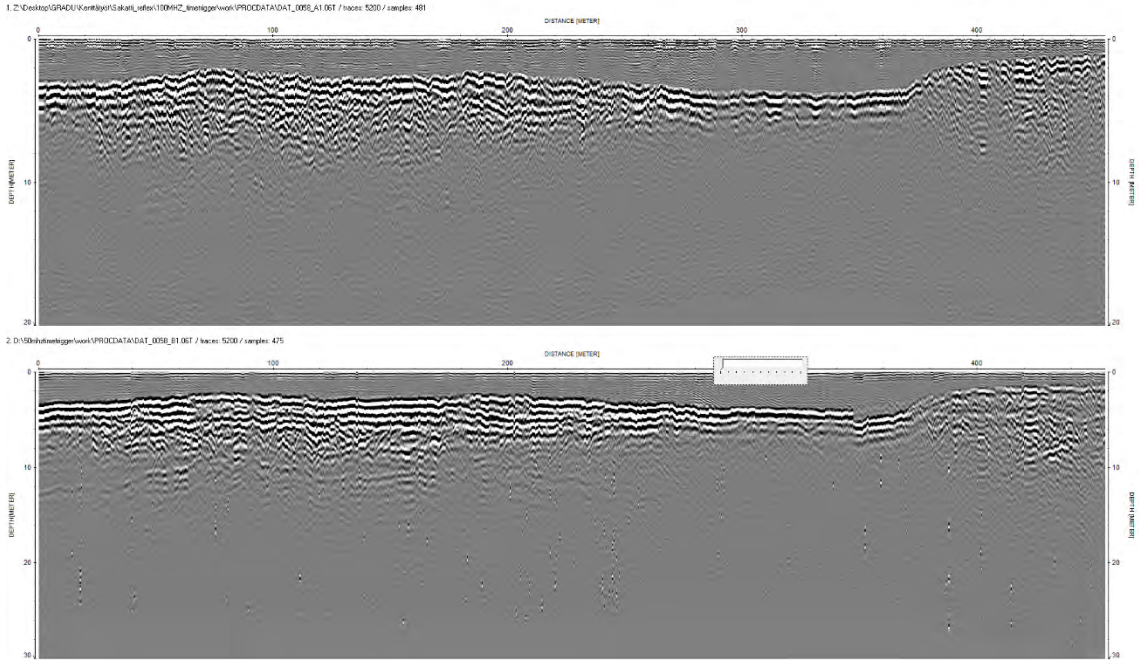

Profile 58a (top) and 58b (bottom).

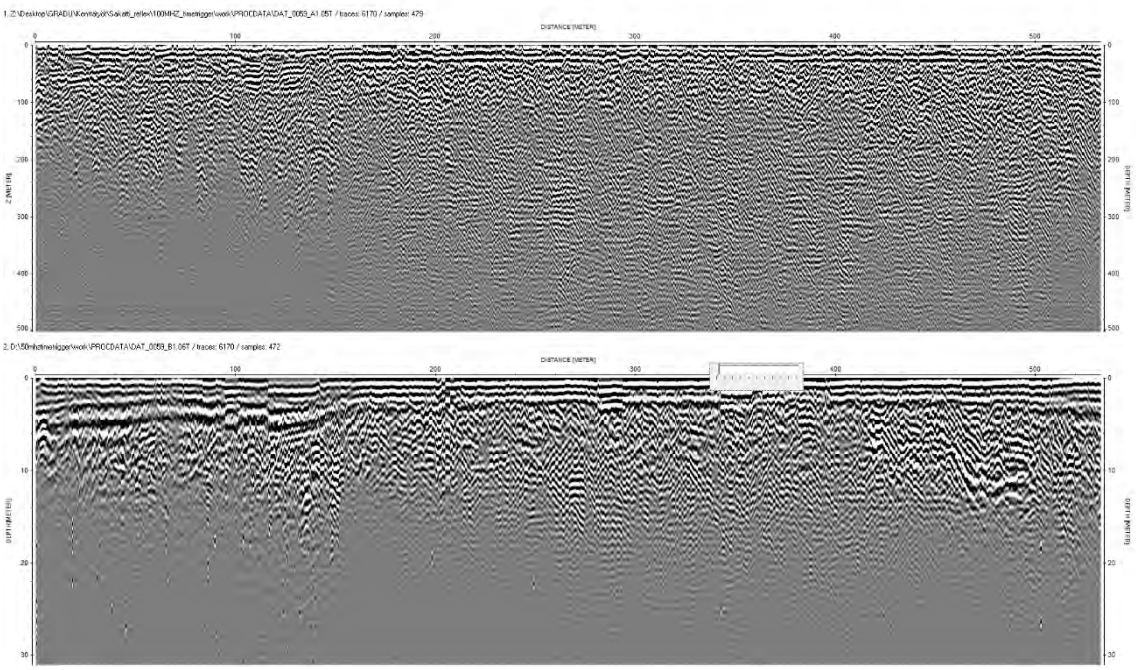

Profile 59a (top) and 59b (bottom).

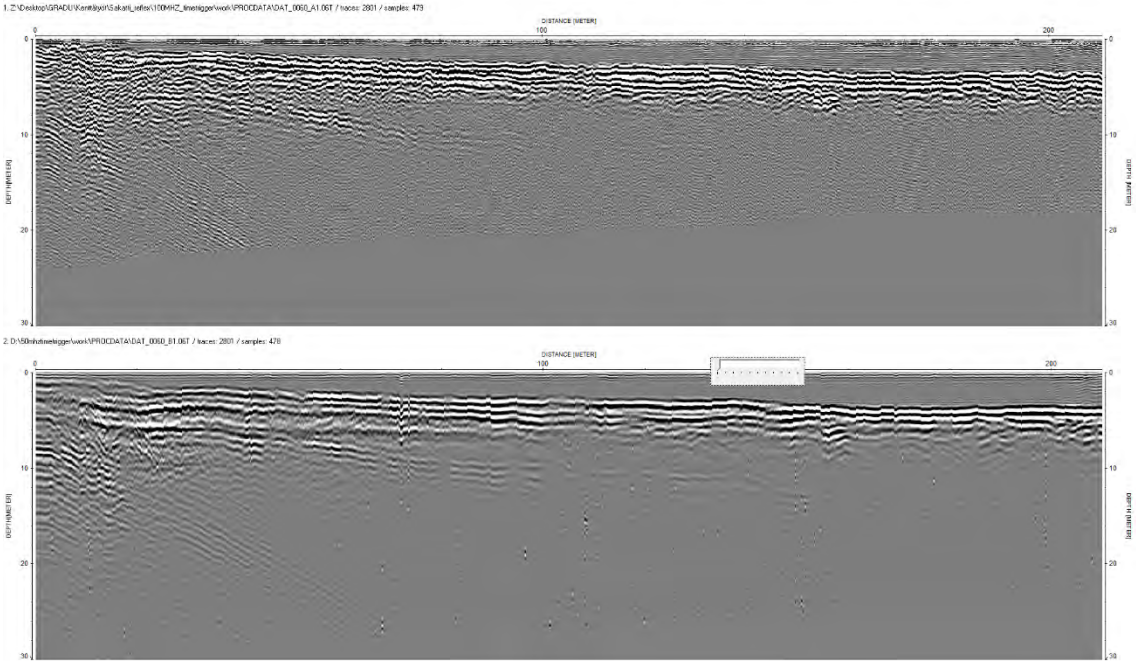

Profile 60a (top) and 60b (bottom).

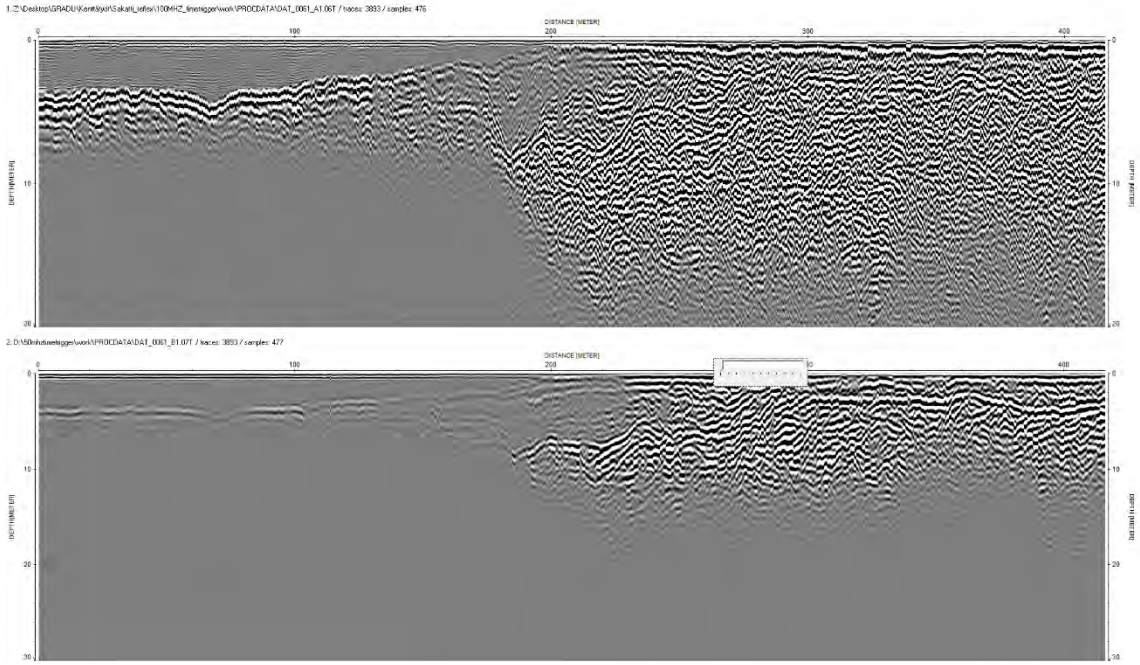

Profile 61a (top) and 61b (bottom).

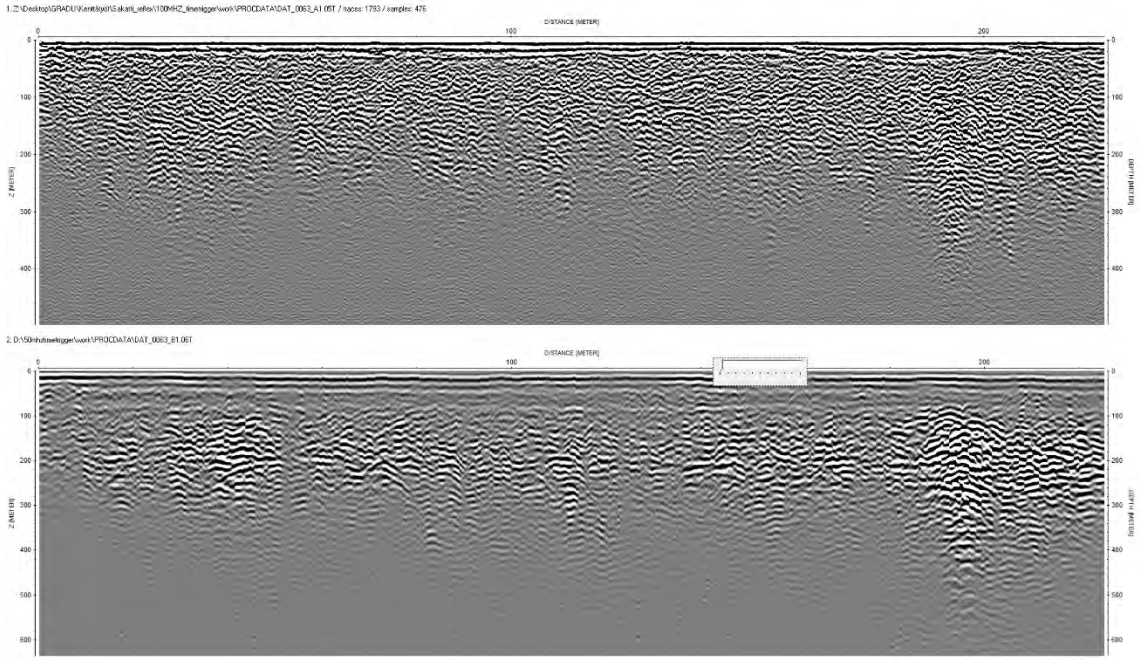

Profile 63a (top) and 63b (bottom).

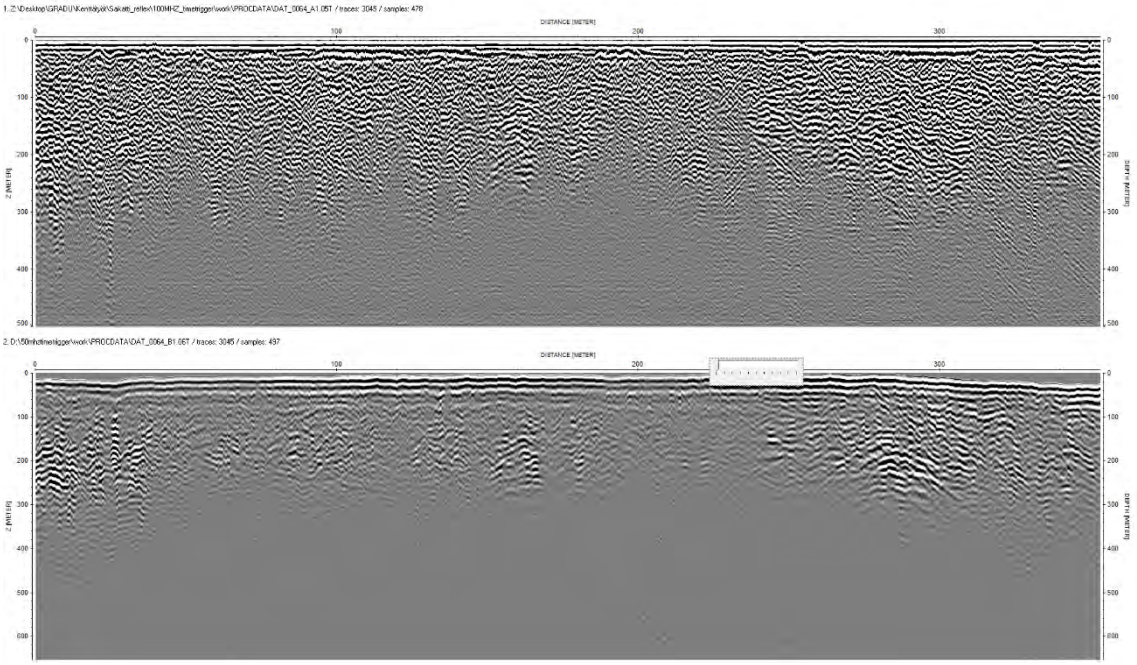

Profile 64a (top) and 64b (bottom).

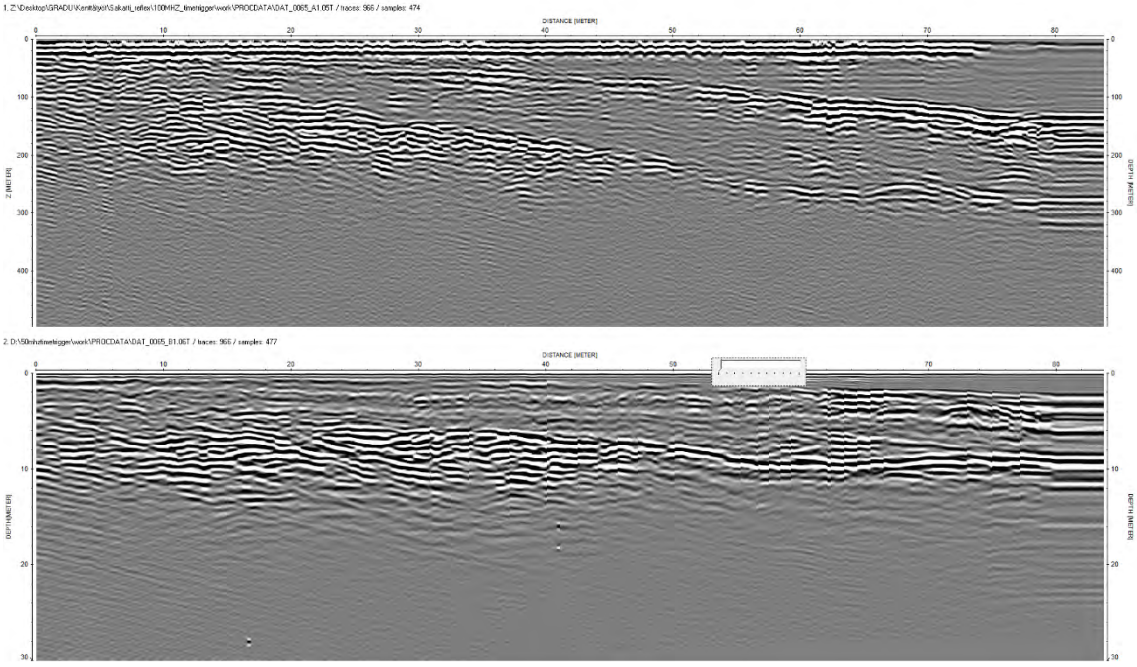

Profile 65a (top) and 65b (bottom).

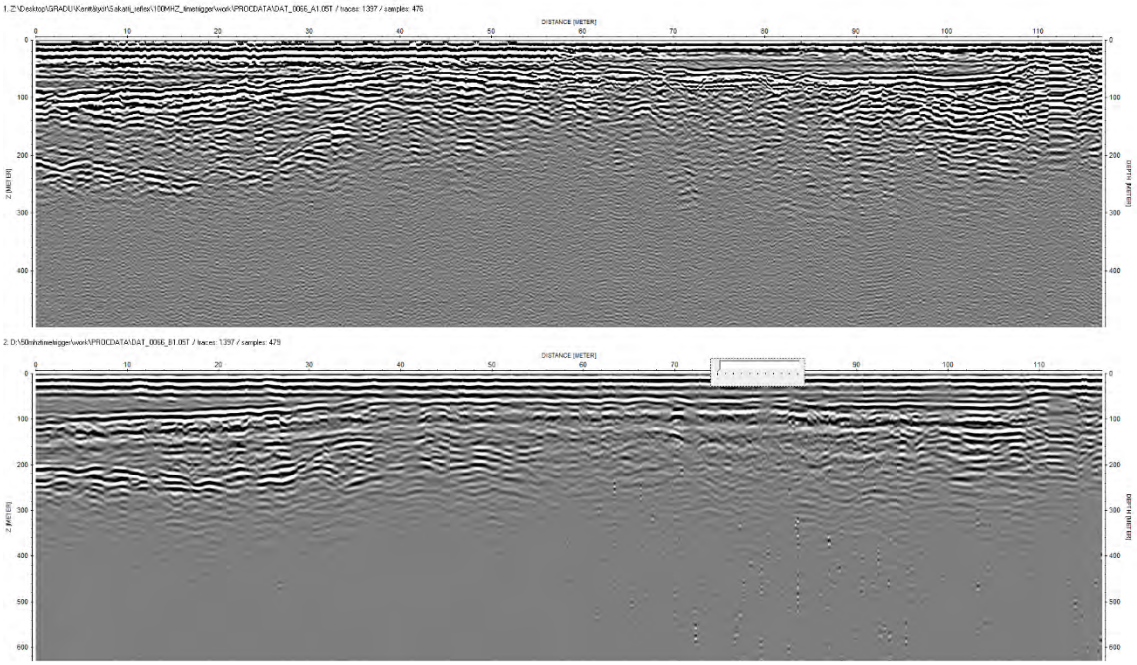

Profile 66a (top) and 66b (bottom).

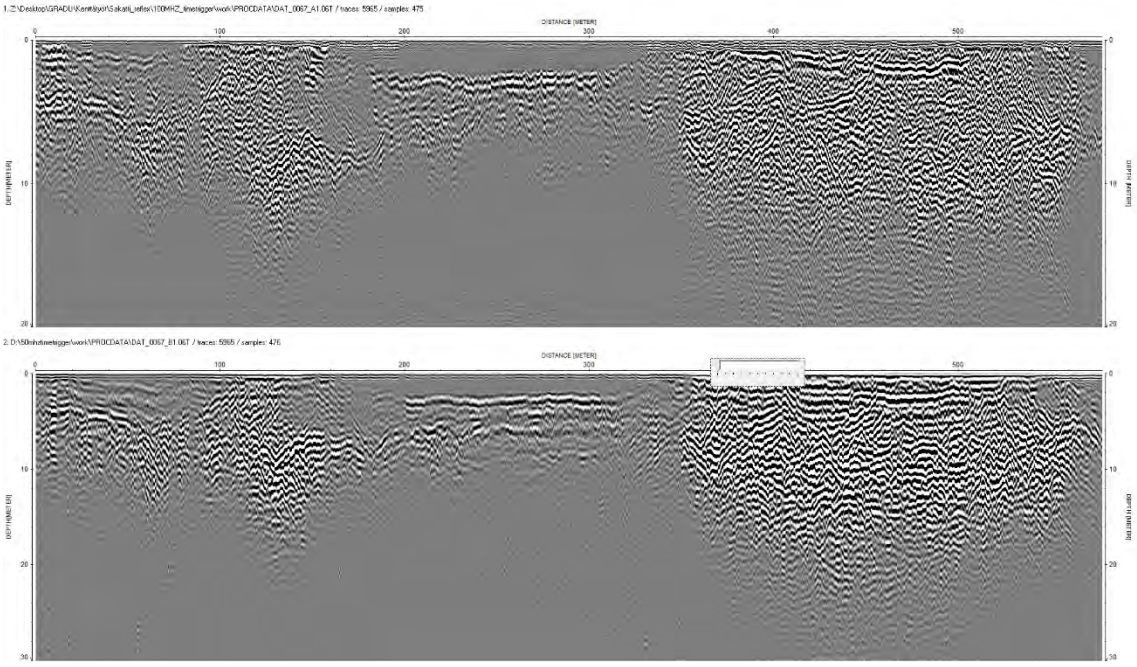

Profile 67a (top) and 67b (bottom).

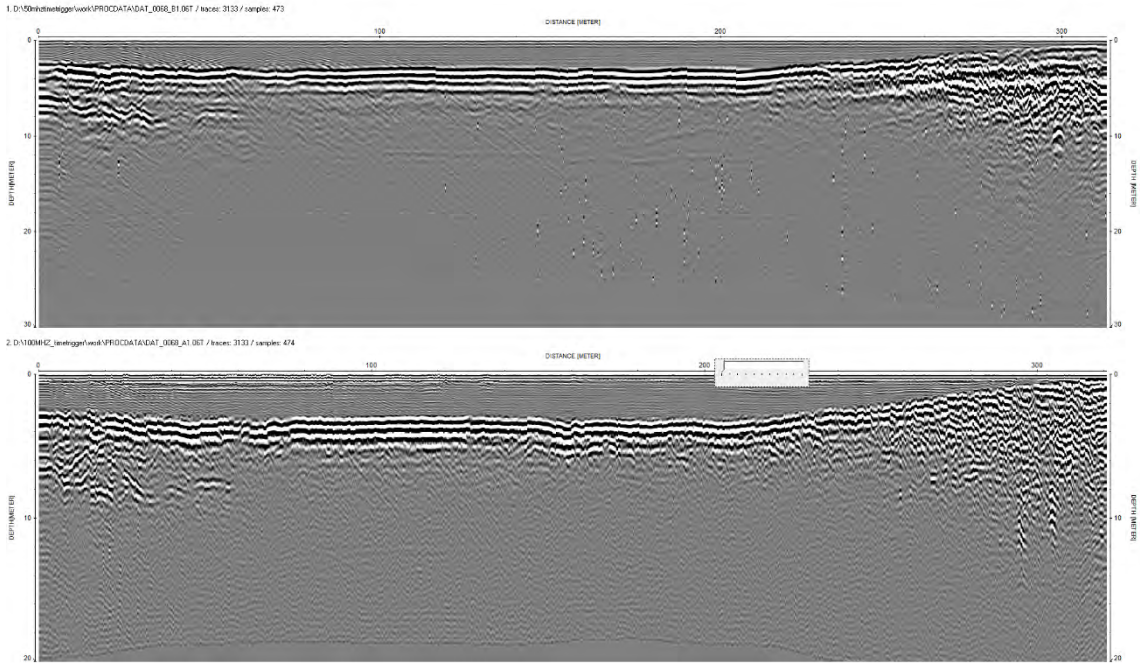

Profile 68a (top) and 68b (bottom).

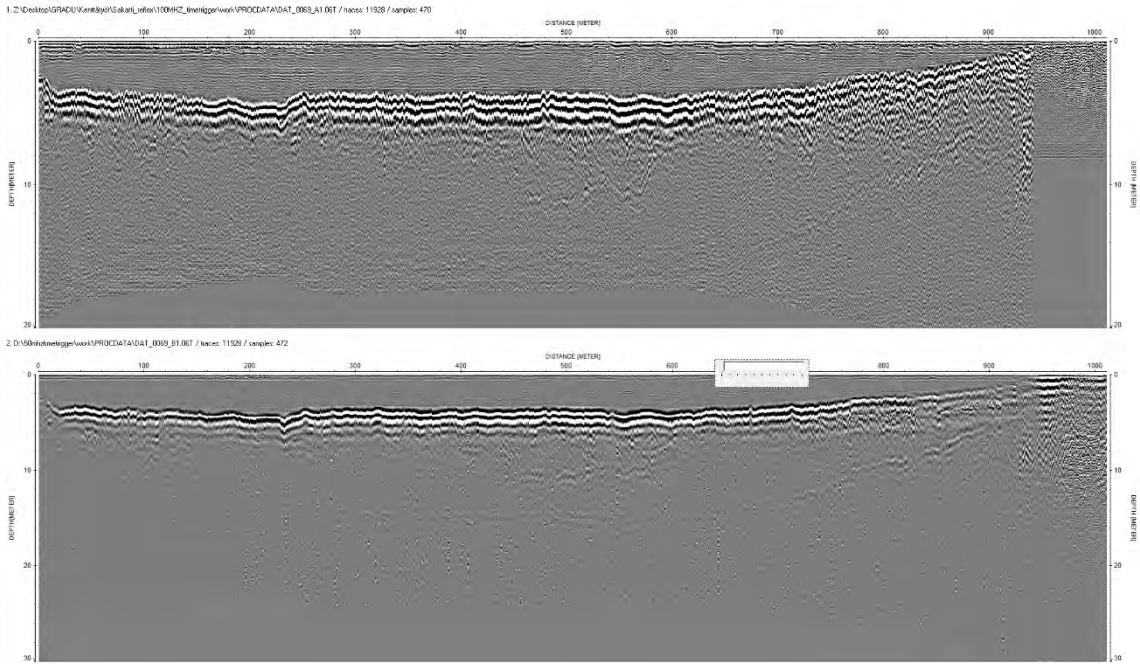

Profile 69a (top) and 69b (bottom).

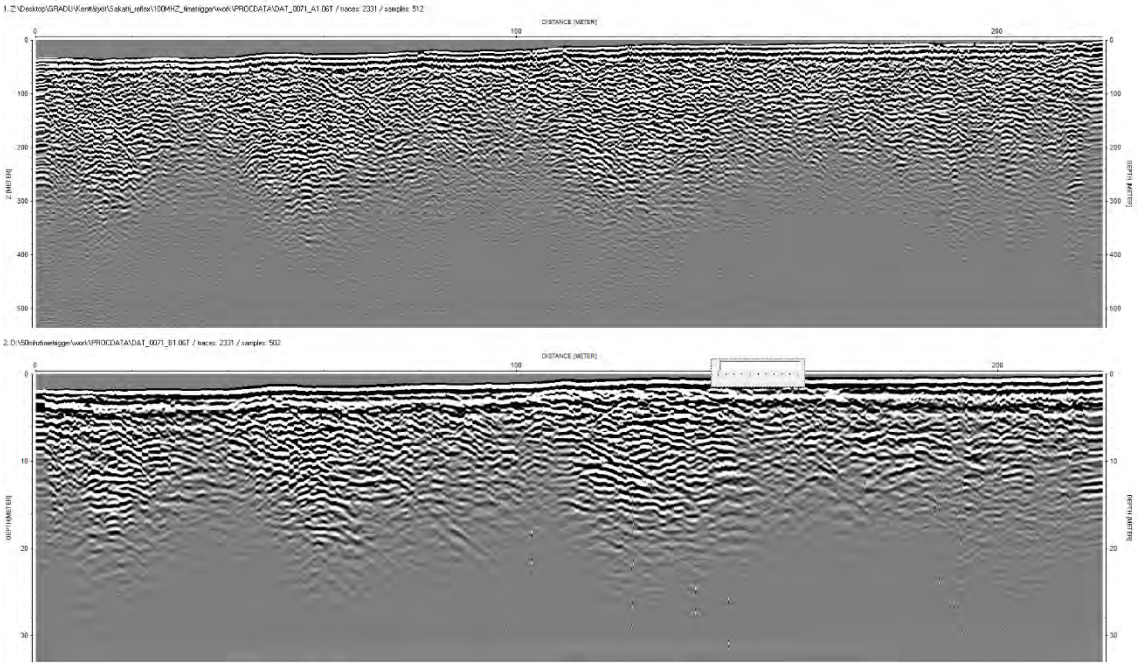

Profile 71a (top) and 71b (bottom).

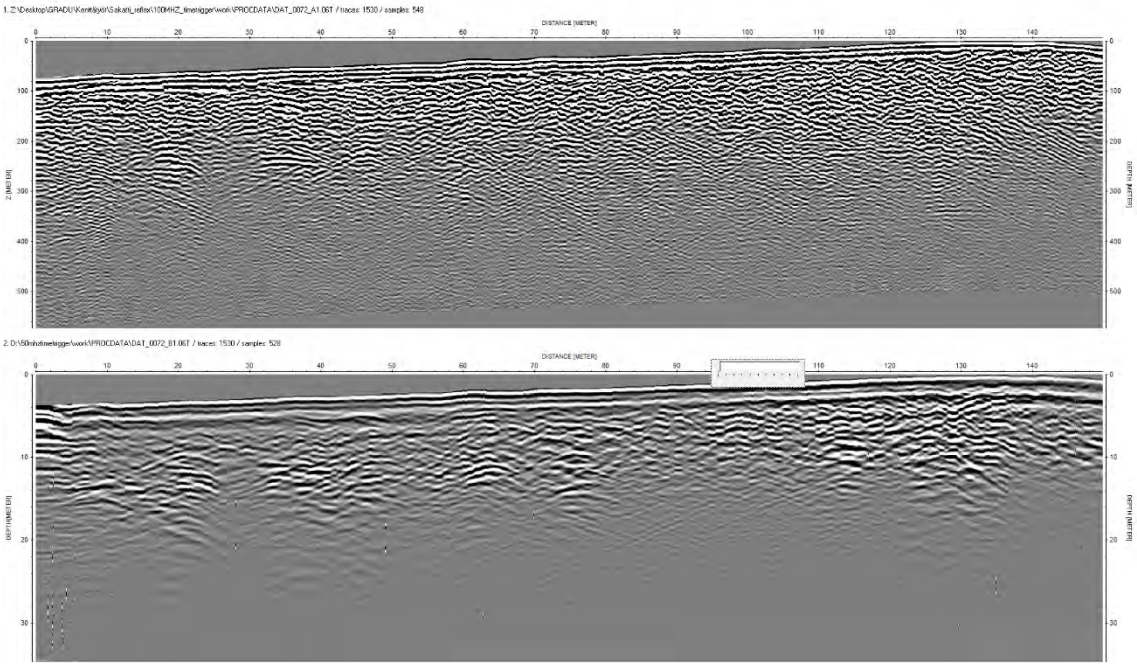

Profile 72a (top) and 72b (bottom).

Appendix 2. Sediment samples and their sedimentological parameters.

Pit	Sample ID	Depth (cm)	Soil type	D_{50}	Uniformity coefficient	Sorting index	Skewness	Kurtosis	K-value (m/s)
1	M1N1	180–200	Diamicton	0.15	21	4.79	1.7	0.05	$8.1*10^{-1}$
	M1N2	120–140	Diamicton	0.28	17	2.36	0.7	0.09	$2.6*10^{-6}$
2	M2N3	110–190	Diamicton	0.04	5	2.61	1.7	0.16	$3.7*10^{-7}$
3	M3N4	490–510	Sand	0.21	8	1.87	1.1	0.12	$7.9*10^{-6}$
	M3N5	450–475	Gravel	5.48	27	3.74	0.3	0.39	$1.0*10^{-3}$
	M3N6	180–200	Gravel	6.24	29	3.69	0.3	0.39	$5.4*10^{-4}$
	M3N7	70–90	Diamicton	0.25	13	2.70	1.1	0.03	$3.6*10^{-6}$
4	M4N8	105–120	Sand	0.23	2	1.51	1.1	0.29	$7.9*10^{-5}$
5	M5N9	310–330	Diamicton	0.19	28	3.10	0.6	0.03	$5.5*10^{-7}$
	M5N10	220–260	Diamicton	0.21	17	1.87	1.1	0.26	$3.7*10^{-6}$
	M5N11	70–130	Diamicton	0.19	23	2.88	0.6	0.11	$6.5*10^{-7}$
6	M6N12	260–280	Diamicton	0.21	39	4.09	0.7	0.04	$4.7*10^{-7}$
	M6N13	80–100	Diamicton	0.17	29	3.41	0.4	0.24	$3.2*10^{-7}$
	M6N14	60–80	Diamicton	0.09	30	4.09	0.5	0.21	$1.1*10^{-7}$

Appendix 3. Particle size distribution curves for all sediment samples. Red part is fine fraction analysed with laser diffractometry. Orange part is coarse fraction analysed with dry sieving.

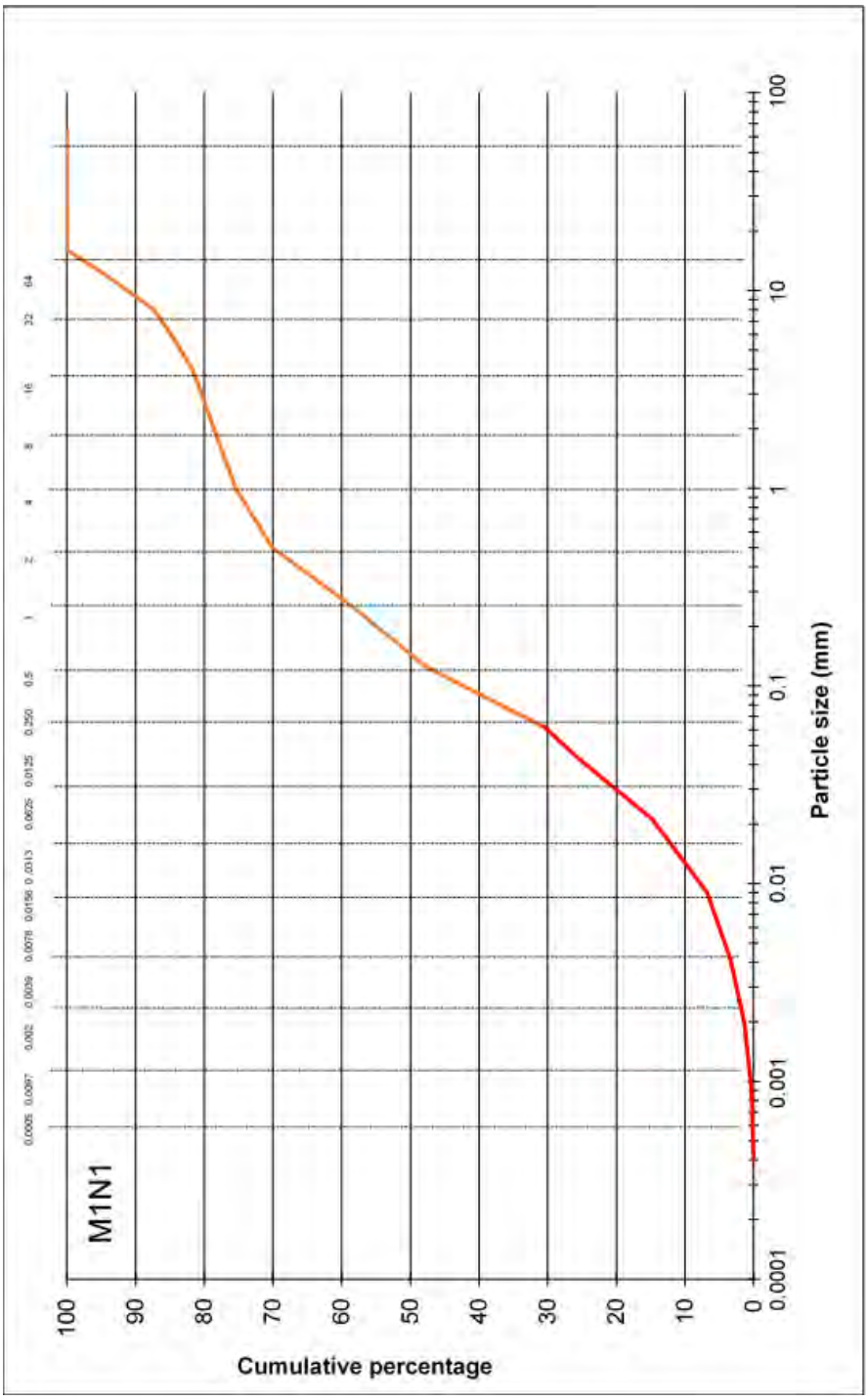

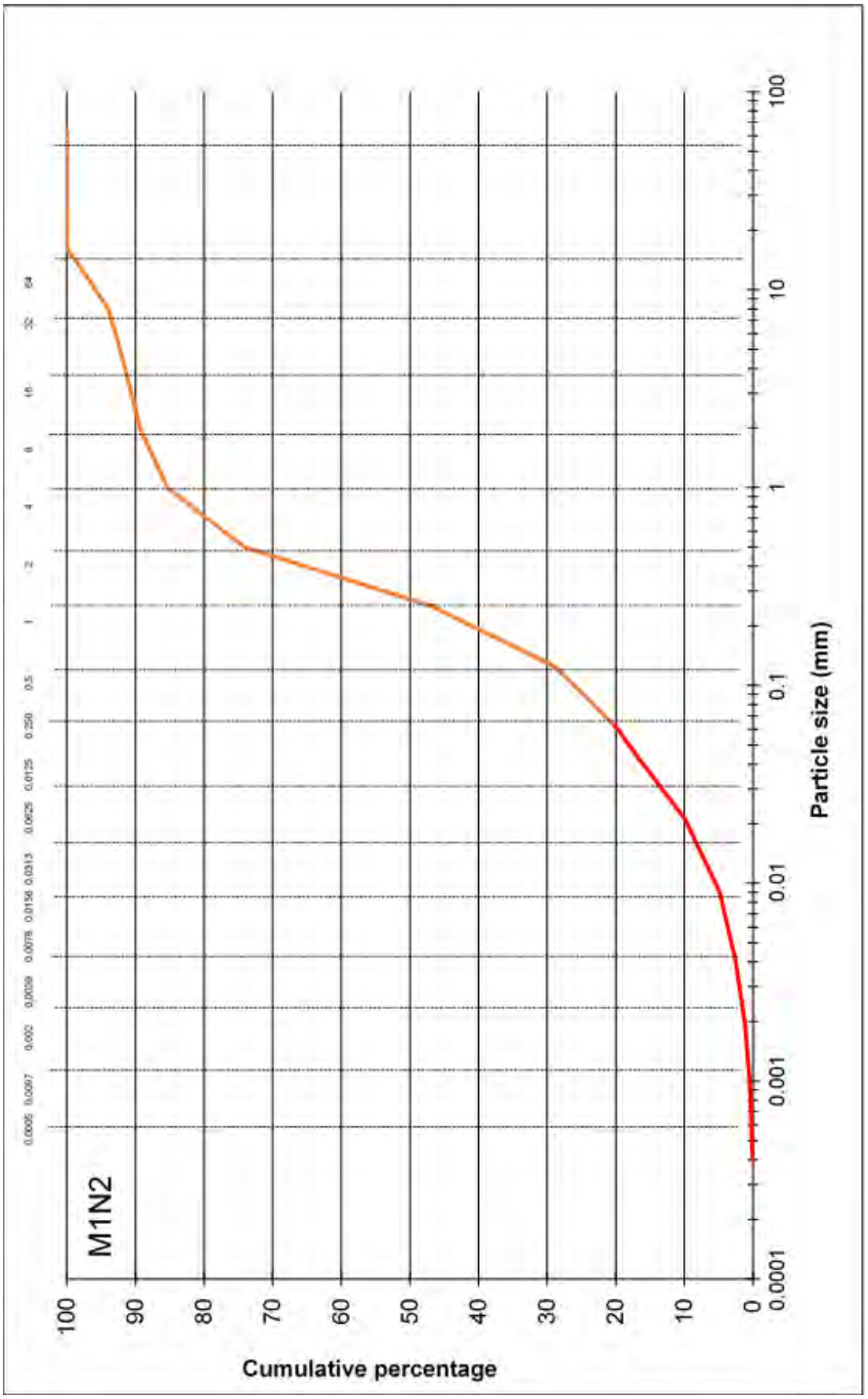
M1N2
Cumulative percentage
Particle size (mm)
100
90
80
70
60
50
40
30
20
10
0
0.0001
0.001
0.01
0.1
1
10
100

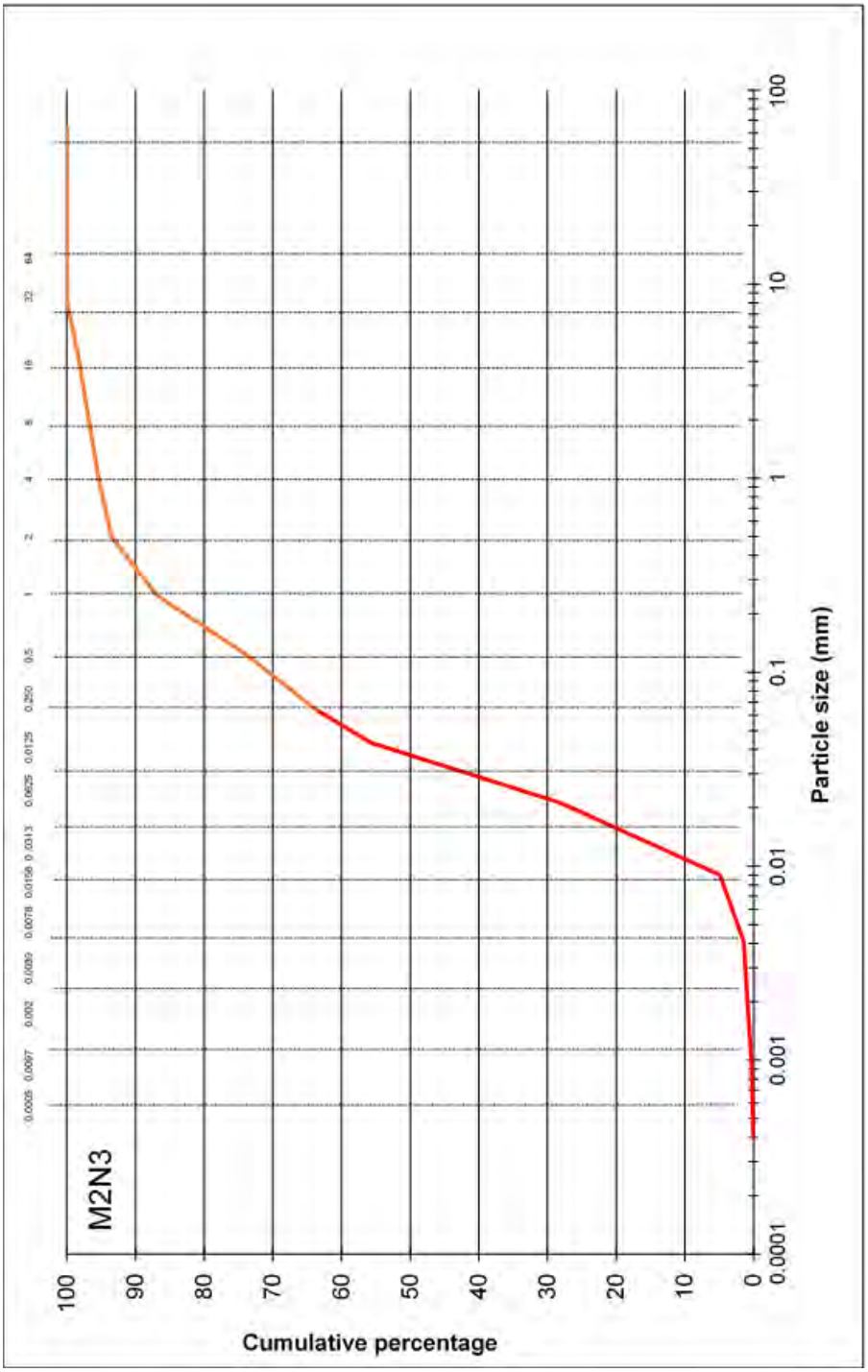
M2N3
Cumulative percentage
Particle size (mm)
100
90
80
70
60
50
40
30
20
10
0
0.0001
0.001
0.01
0.1
1
10
100

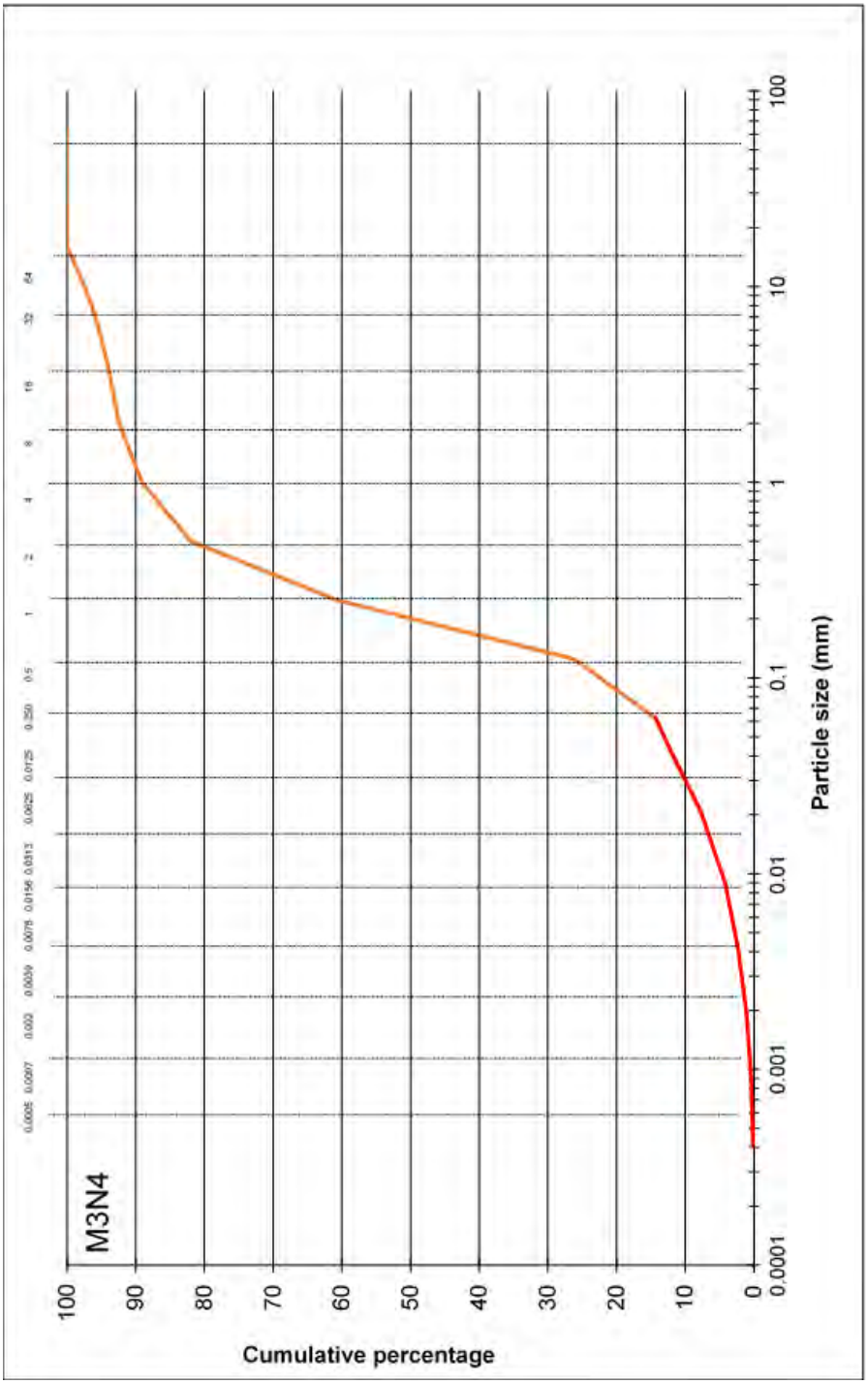
M3N4
Cumulative percentage
Particle size (mm)
100
90
80
70
60
50
40
30
20
10
0
0.0001
0.001
0.01
0.1
1
10
100

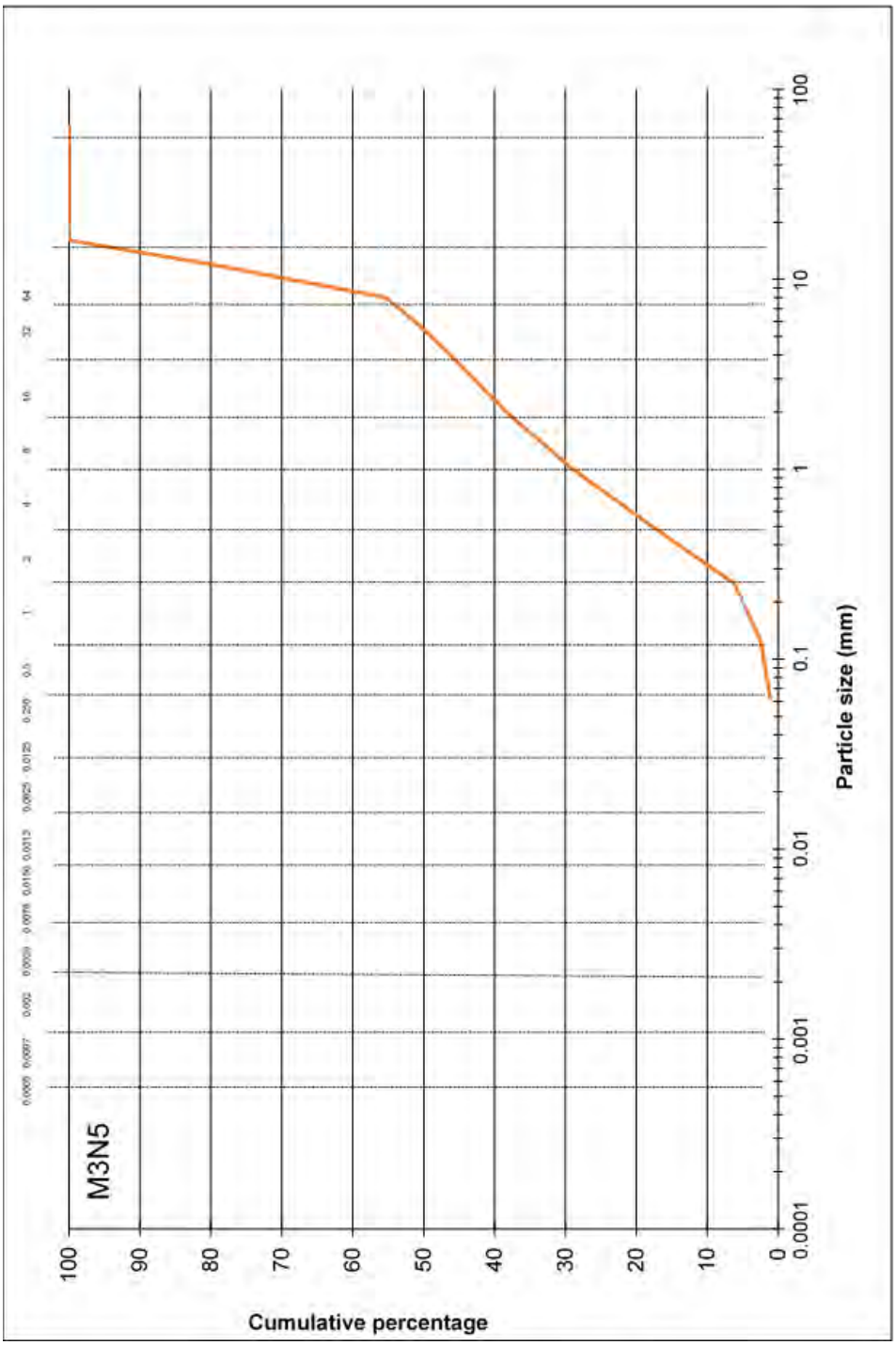
M3N5
Cumulative percentage
100
90
80
70
60
50
40
30
20
10
0
Particle size (mm)
100
10
1
0.1
0.01
0.001
0.0001

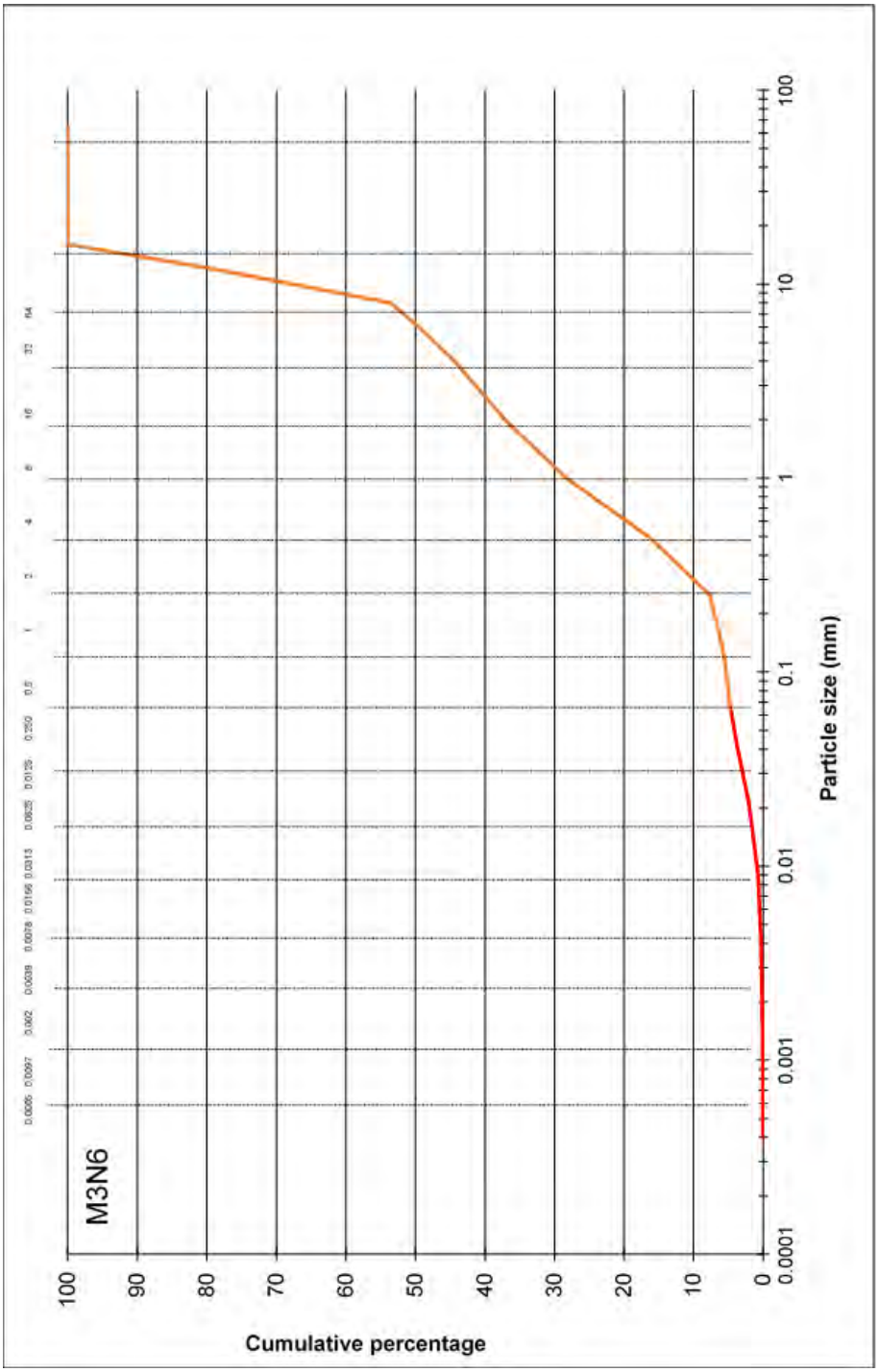
M3N6
Cumulative percentage
100
90
80
70
60
50
40
30
20
10
0
Particle size (mm)
100
10
1
0.1
0.01
0.001
0.0001

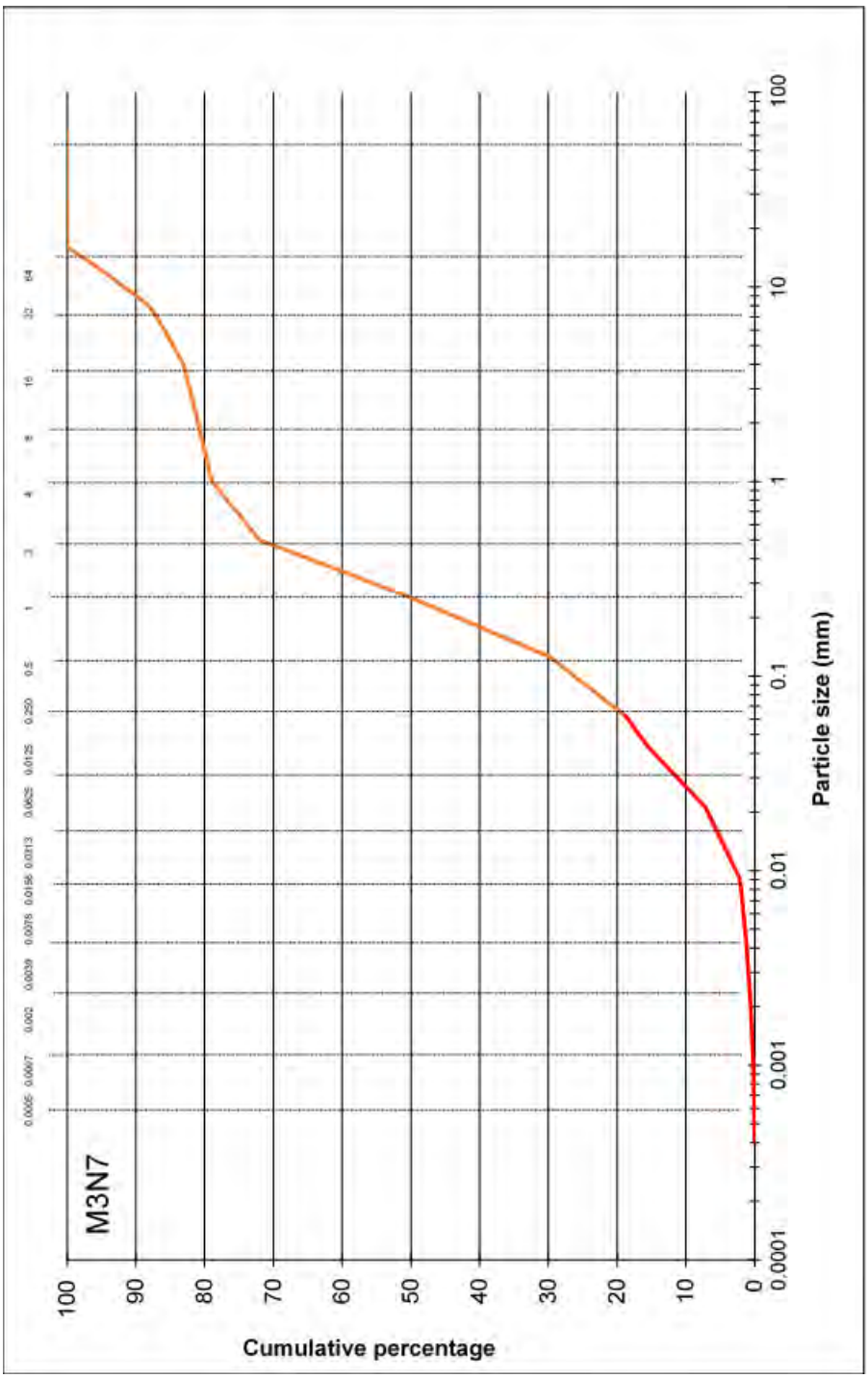
M3N7
Cumulative percentage
Particle size (mm)
100
90
80
70
60
50
40
30
20
10
0
0.0001
0.001
0.01
0.1
1
10
100

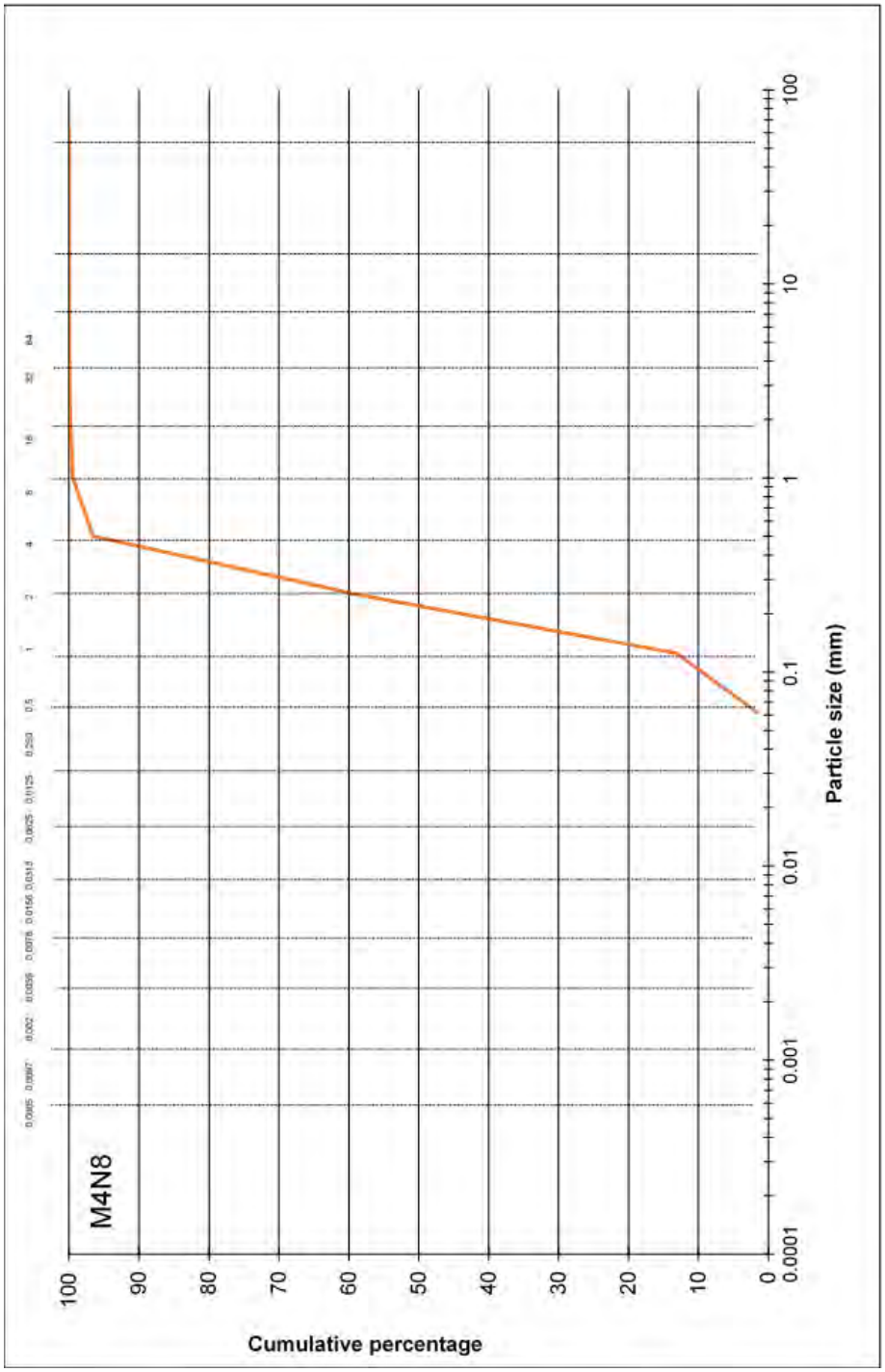
M4N8
Cumulative percentage
Particle size (mm)
100
90
80
70
60
50
40
30
20
10
0
0.0001
0.001
0.01
0.1
1
10
100

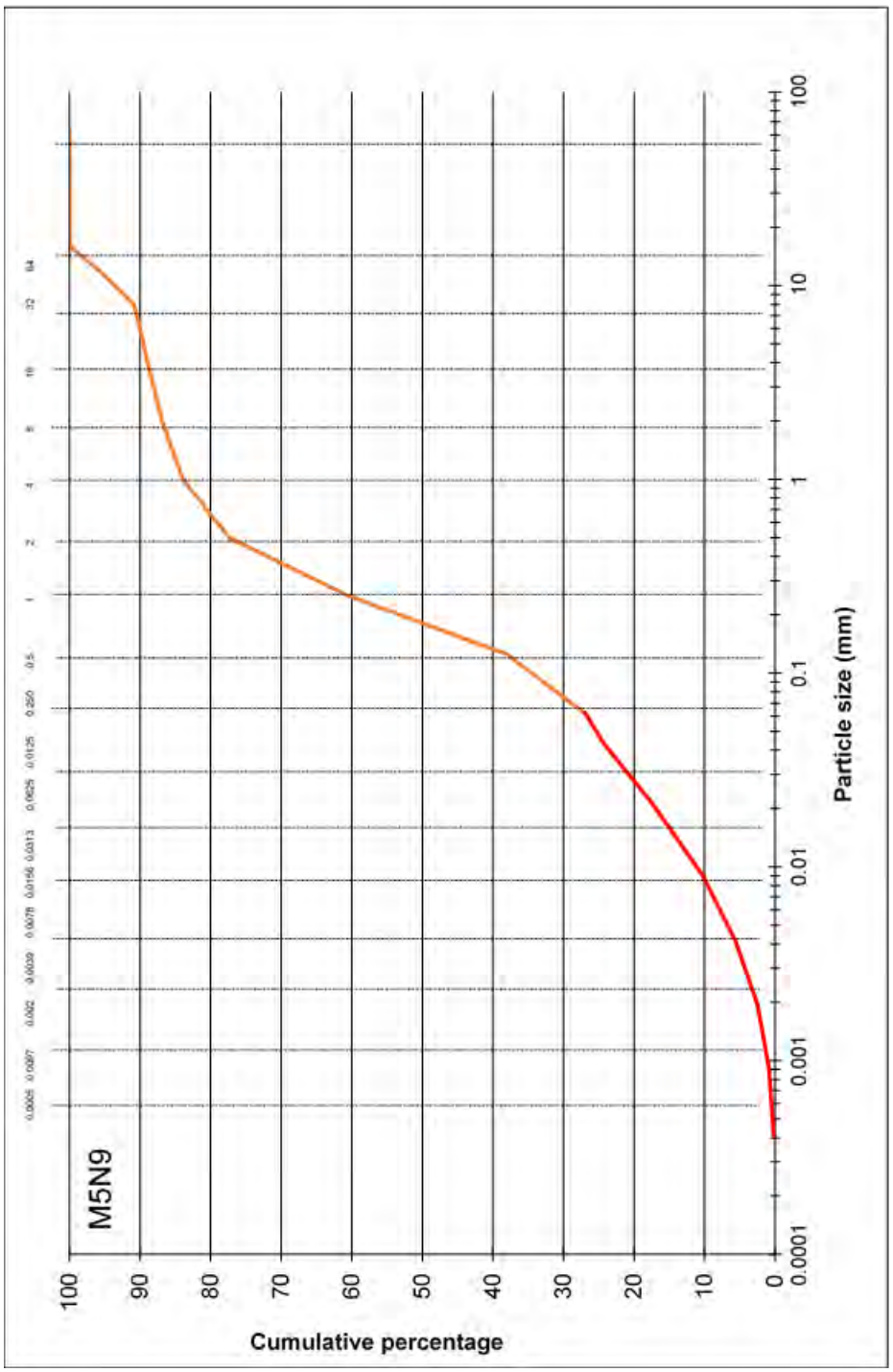
M5N9
Cumulative percentage
Particle size (mm)
100
90
80
70
60
50
40
30
20
10
0
0.0001
0.001
0.01
0.1
1
10
100

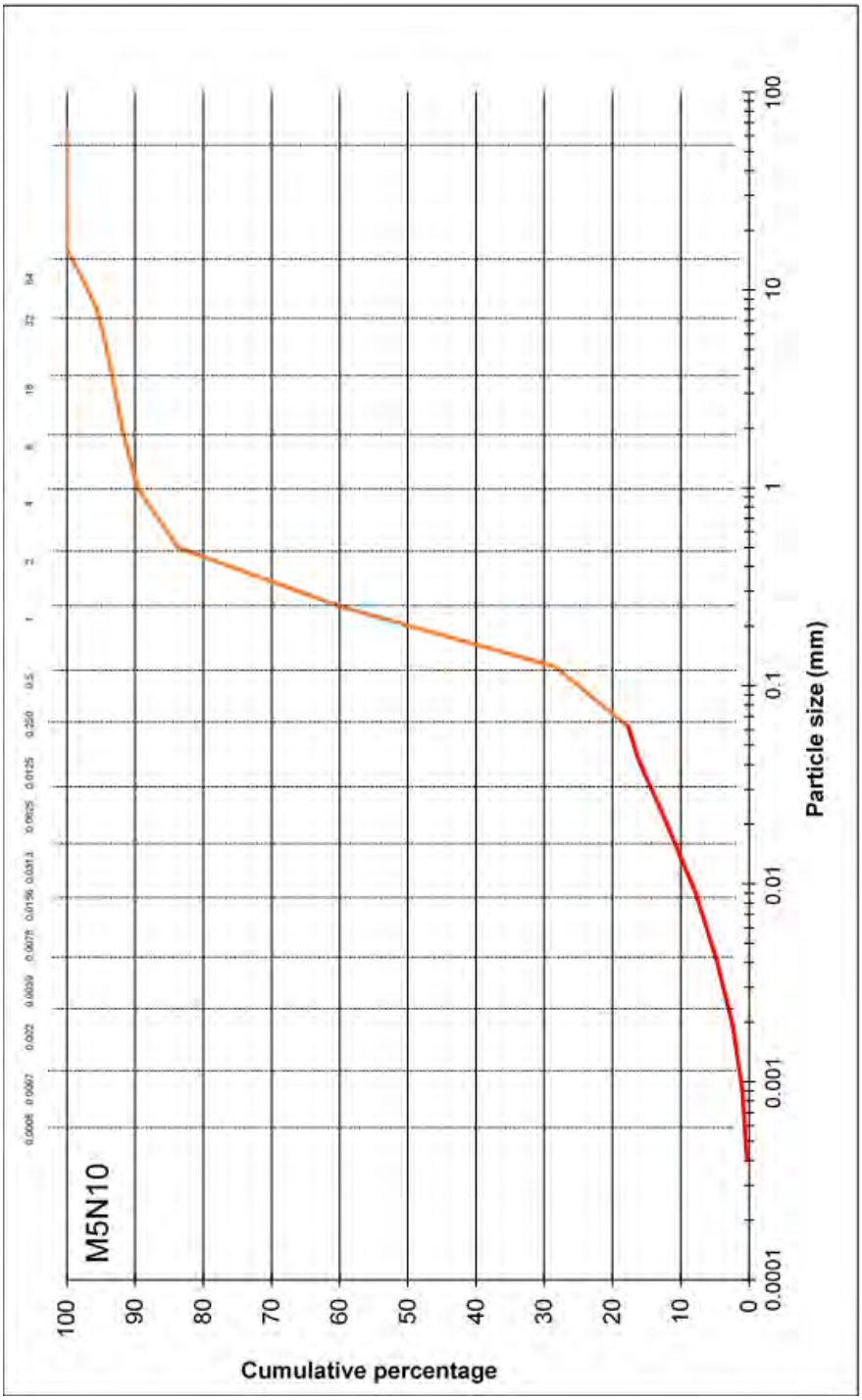
M5N10
Cumulative percentage
Particle size (mm)
100
90
80
70
60
50
40
30
20
10
0
0.0001
0.001
0.01
0.1
1
10
100

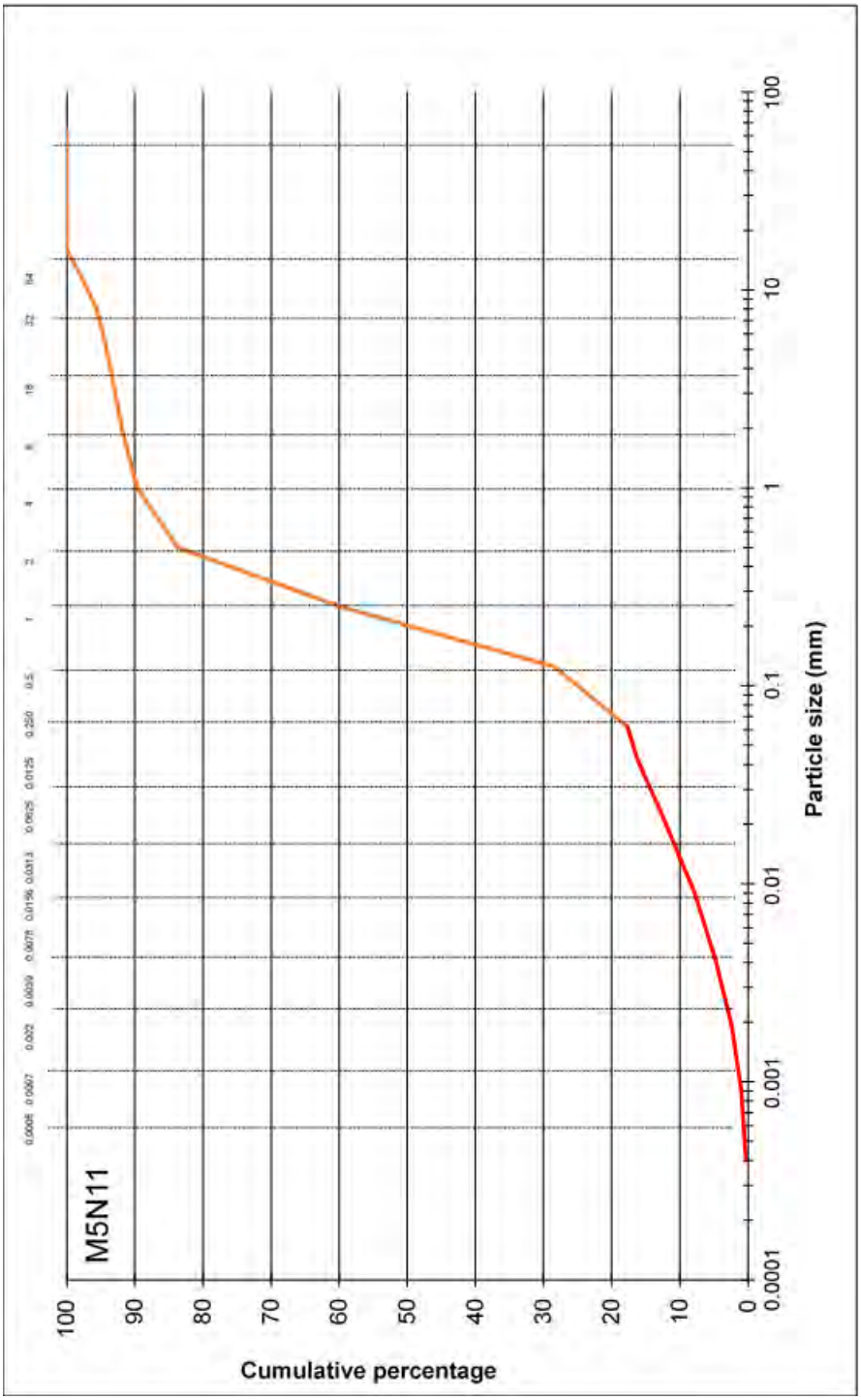
M5N11
Cumulative percentage
100
90
80
70
60
50
40
30
20
10
0
Particle size (mm)
100
10
1
0.1
0.01
0.001
0.0001

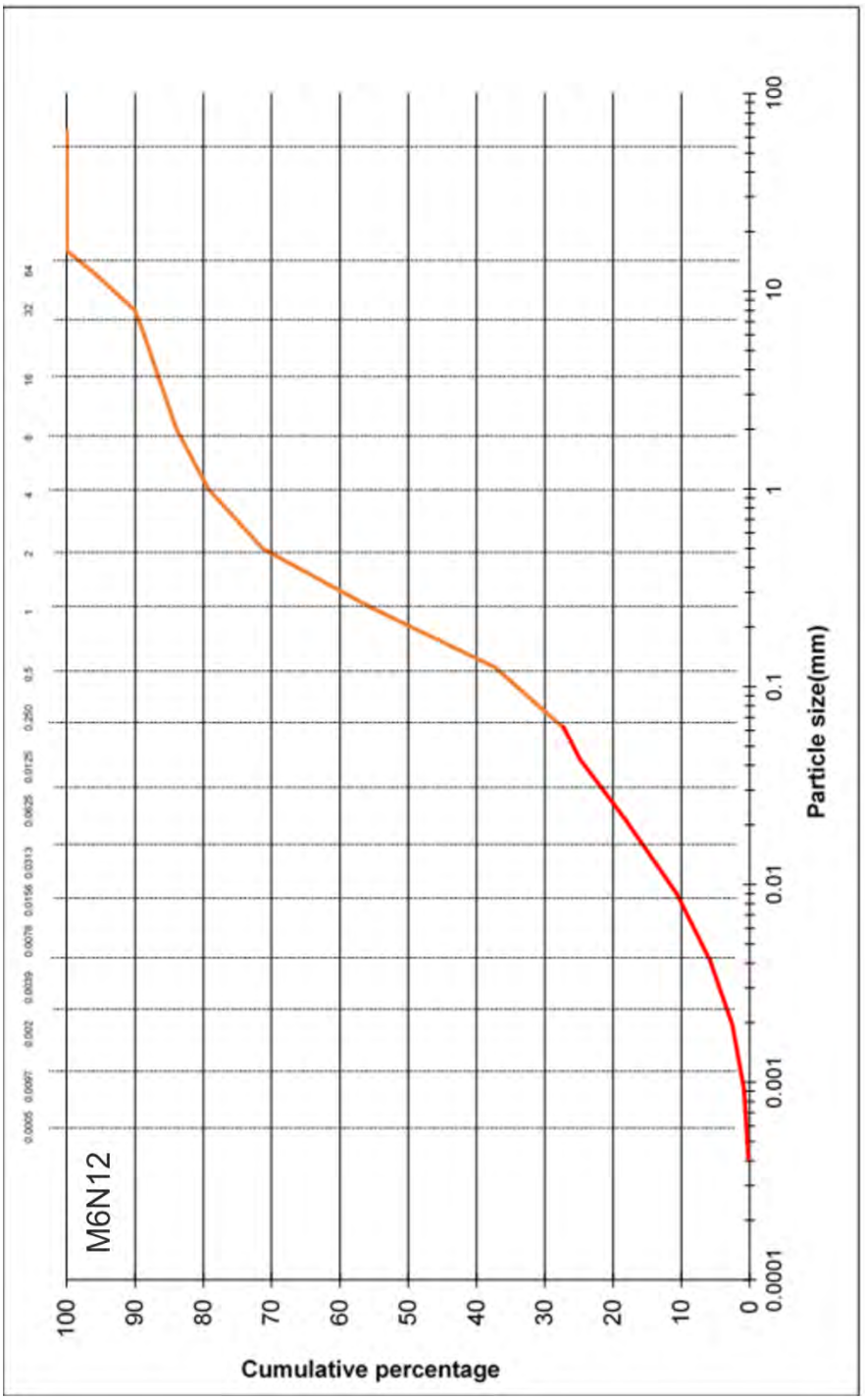
M6N12
Cumulative percentage
Particle size(mm)
100
90
80
70
60
50
40
30
20
10
0
0.0001
0.001
0.01
0.1
1
10
100

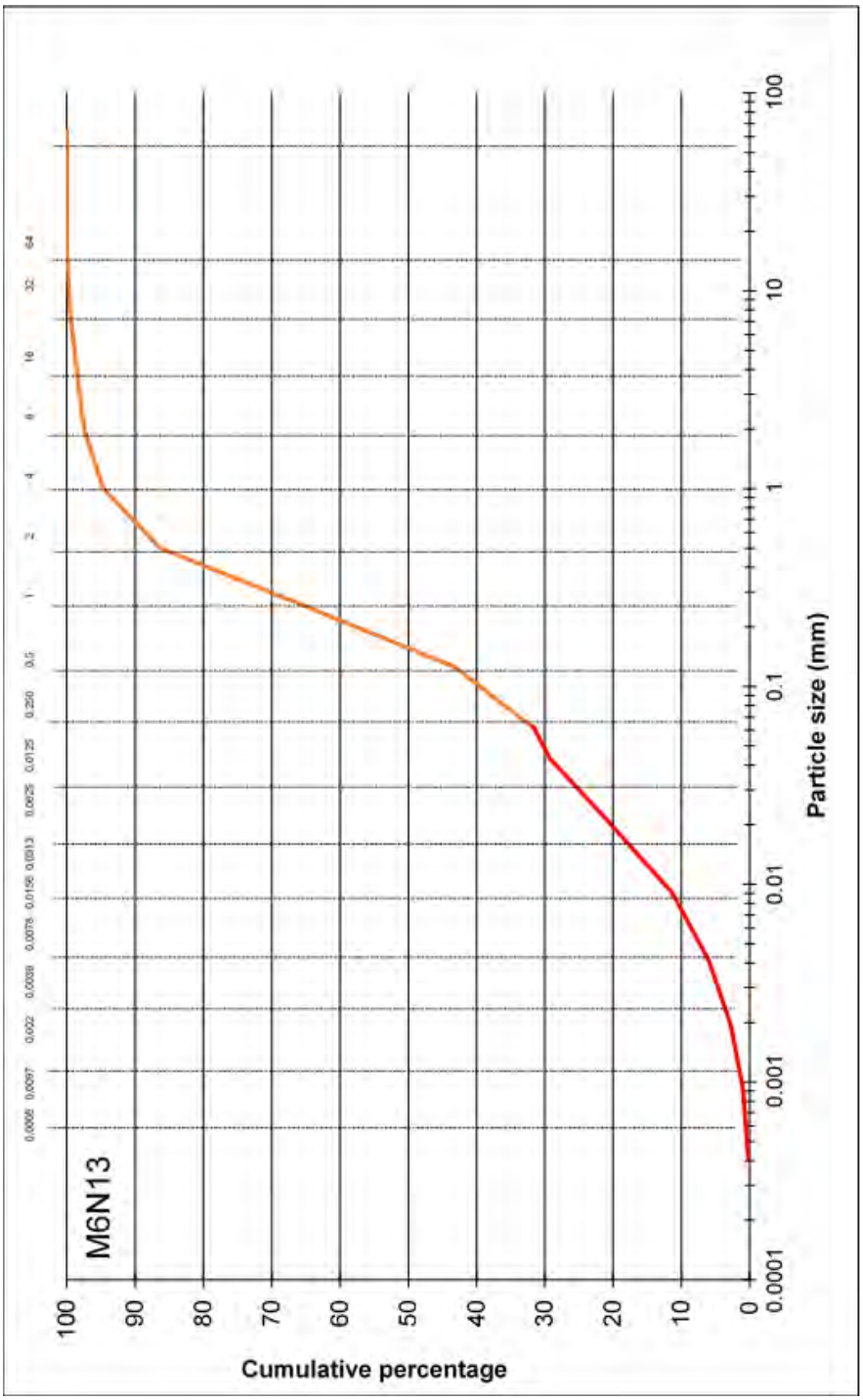
M6N13
Cumulative percentage
Particle size (mm)
100
90
80
70
60
50
40
30
20
10
0
0.0001
0.001
0.01
0.1
1
10
100

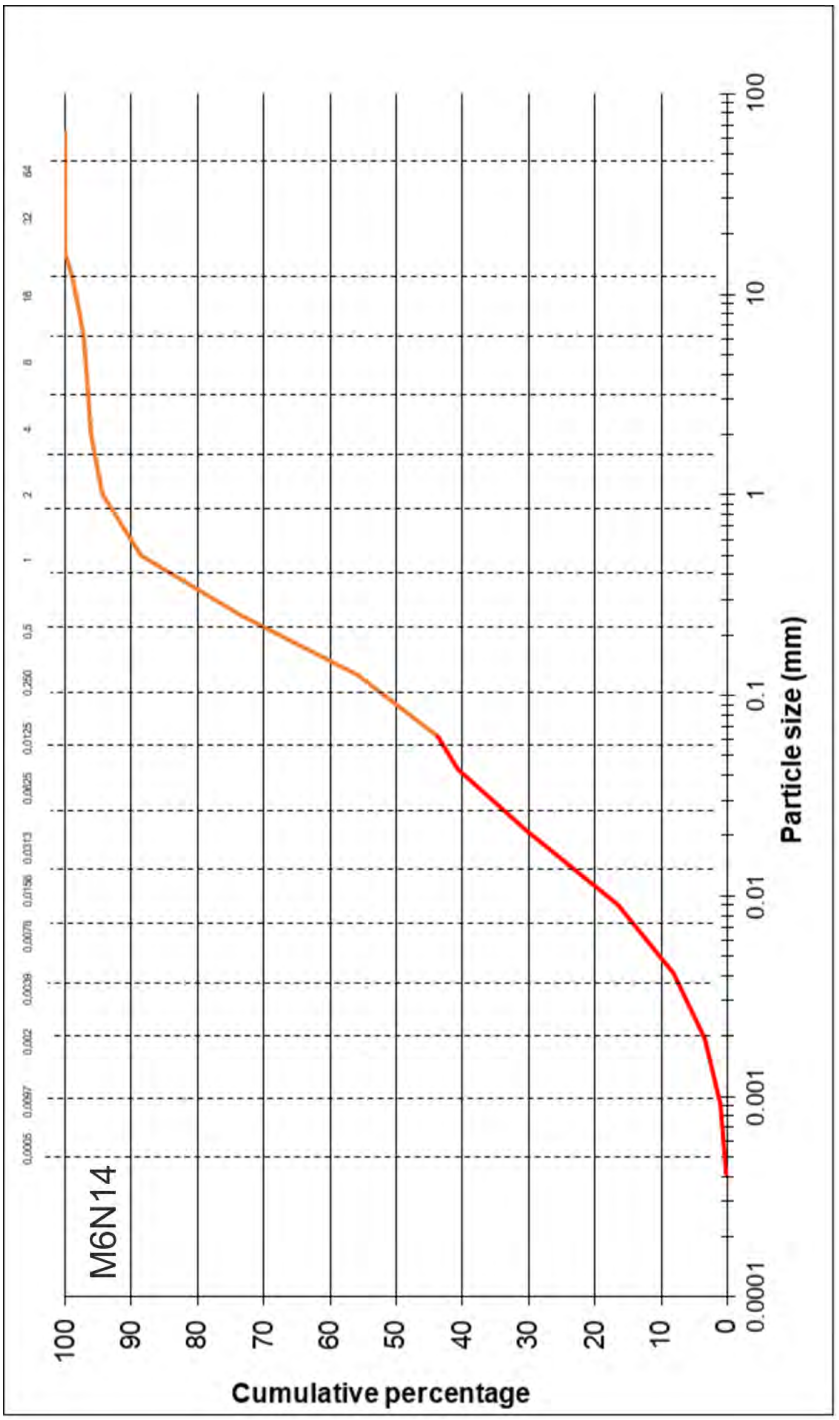
M6N14
Cumulative percentage
Particle size (mm)
100
90
80
70
60
50
40
30
20
10
0
0.0001
0.001
0.01
0.1
1
10
100